

# C1q staining in free-floating brain sections: Morphological appearance and effects of age, Alzheimer pathology and anaesthetics

Christian Georg Rupprecht

Vollständiger Abdruck der von der TUM School of Medicine and Health der Technischen Universität München zur Erlangung eines  
Doktors der Medizin (Dr. med.)  
genehmigten Dissertation.

Vorsitz: Prof. Kathrin Schumann, Ph.D.

Prüfende der Dissertation:

1. apl. Prof. Dr. Gerhard Rammes
2. Prof. Dr. Gabriele Multhoff
3. Prof. Dr. Jochen Herms

Die Dissertation wurde am 08.04.2024 bei der Technischen Universität München eingereicht und durch die TUM School of Medicine and Health am 07.11.2024 angenommen.



# Acknowledgements

I would like to express my gratitude to several individuals who have contributed to the completion of this research project.

First and foremost, I would like to thank my supervisor, Prof. Dr. Gerhard Rammes, for his support and guidance throughout my research work. His encouragement and willingness to provide advice and constructive criticism have been essential in shaping my scientific perspective and have taught me to appreciate the excitement of scientific work.

I am also indebted to Dr. Matthias Kreuzer, who provided valuable statistical support and guidance, which were indispensable for the successful completion of my doctoral thesis.

Furthermore, I would like to thank Andreas Blaschke for his expert knowledge in immunofluorescence and Western blot techniques, which were crucial for the experimental design and data analysis.

I would also like to acknowledge Dr. Sabrina Rim Sarker for her technical support in image analysis, which was essential for the evaluation of our immunofluorescence data.

I would like to express my gratitude to Caroline d'Anglade and Anastasia Alekseev for their active involvement in my research project, providing dedicated and diligent support.

Lastly, I would like to thank my parents and particularly my father for their unwavering support throughout my academic journey and for sharing their scientific insights and knowledge with me.



# Abstract

Inflammatory processes are critical for the pathophysiology of neurodegenerative diseases. Synaptic pruning has been identified as an autoimmune reaction leading to the breakdown of brain synapses. C1q, the initiator protein of the complement system, is a vital molecule during this process. C1q is known to regulate brain development by sorting out dysfunctional synapses. However, studies suggest that this function gets reactivated in older age and contributes to neurodegeneration.

Meanwhile, an increasing number of histological images of cerebral C1q is available using a broad variety of immunofluorescence techniques. However, a literature survey revealed a great diversity and conflicting results concerning the distribution of C1q across the brain. Therefore, we created a free-floating staining protocol which allowed us to reproduce and combine all previous results in one staining. We demonstrated an overall distribution of C1q over the whole brain. C1q deposition could be seen both on neuronal and non-neuronal cells. Furthermore, for the first time we described linear, branched C1q signals in the area between the dentate gyrus and the CA1 region of the hippocampus. Based on their morphological appearance and localization, we considered those signals as C1q-dendritic-like-structures.

As a second step, we quantified C1q levels. Previous literature revealed age as a strong stimulus for C1q expression. We investigated whether this stimulus has a uniform effect within the hippocampus or whether regional differences can be detected. Moreover, because C1q is known to promote neurodegenerative processes, we extended our studies to an animal model of Alzheimer's disease. We did not only confirm age as a strong stimulus for C1q expression, but also demonstrated that this effect shows regional differences. Within the hippocampus a greater increase was seen in the dentate gyrus in comparison to the CA1 region. Furthermore, we identified a two-sided effect of Alzheimer's pathology on cerebral C1q levels. On the one hand, the effect of age was intensified within our transgenic mouse model. On the other hand, an effect independent of age occurred. At an earlier stage of 15 months Alzheimer transgenic animals showed suppressed concentrations of C1q. However, with increasing age, this turned into the opposite, so that a significant increase could be detected at the age of 20 months.

Within anaesthetics xenon has the reputation of an almost ideal narcotic due to its low teratogenicity and toxicity. More and more studies indicate that xenon is even capable of reducing neurodegenerative processes like Alzheimer's disease. Even if xenon shows favorable properties for neuronal cells, it is still unclear whether xenon affects inflammatory synaptic pruning mechanisms. To investigate this topic we developed a modern method for in vitro studies. We created an acute brain slice approach with the possibility of pharmacological interventions. We showed that short time incubation, either with xenon or isoflurane, has no acute effect on brain C1q levels.

In conclusion, our studies underline the importance of C1q for aging and neurodegenerative processes. Moreover, our model offers an opportunity to study pharmacological interventions.

# Kurzzusammenfassung

Entzündungsprozesse sind von wesentlicher Bedeutung für die Pathophysiologie neurodegenerativer Erkrankungen. „Synaptic-pruning“ wurde als eine Autoimmunreaktion identifiziert, welche zum Abbau von Synapsen im Gehirn führt. C1q, das Initiatorprotein des Komplementsystems, ist ein wichtiges Molekül in diesem Prozess. C1q ist dafür bekannt, dass es die Gehirnentwicklung reguliert, indem es dysfunktionale Synapsen aussortiert. Studien legen jedoch nahe, dass diese Funktion im Alter reaktiviert wird und so zur Neurodegeneration beiträgt.

Inzwischen gibt es eine wachsende Zahl histologischer Darstellungen von cerebralem C1q, welche mit einer Vielzahl von Immunfluoreszenztechniken erstellt wurden. Eine Literaturübersicht ergab jedoch eine große Vielfalt und widersprüchliche Ergebnisse hinsichtlich der Verteilung von C1q im Gehirn. Aus diesem Grund haben wir ein „free-floating“ Färbeprotokoll entwickelt, das uns ermöglicht, alle bisherigen Ergebnisse in einer Färbung zu reproduzieren und zu kombinieren. Wir konnten eine Verteilung der C1q Expression über das gesamte Gehirn nachweisen. C1q Ablagerungen fanden sich sowohl auf neuronalen als auch auf nicht-neuronalen Zellen. Außerdem beschrieben wir erstmals lineare, verzweigte C1q Signale im Bereich zwischen dem Gyrus dentatus und der CA1-Region des Hippocampus. Aufgrund ihres morphologischen Erscheinungsbildes und ihrer Lokalisation sehen wir diese Signale als C1q-dendritenähnliche („dendritic-like“) Strukturen an.

In einem zweiten Schritt haben wir die C1q Expression quantifiziert. Die bisherige Literatur hat gezeigt, dass das Alter zu einem starken Anstieg der C1q Expression führt. Wir untersuchten, ob dieser Stimulus einheitlich im Hippocampus zu finden ist oder ob regionale Unterschiede auftreten. Da bekannt ist, dass C1q neurodegenerative Prozesse fördert, haben wir unsere Untersuchungen auf ein Tiermodell der Alzheimer-Krankheit ausgeweitet. Wir konnten nicht nur bestätigen, dass das Alter einen starken Stimulus für die C1q Expression darstellt, sondern auch, dass dieser Effekt regional unterschiedlich ausgeprägt ist. Innerhalb des Hippocampus fand sich ein größerer Anstieg im Gyrus dentatus im direkten Vergleich zur CA1 Region. Darüber hinaus konnten wir einen zweiseitigen Effekt der Alzheimer-Pathologie auf die zerebralen C1q Spiegel feststellen. Einerseits wurde der Effekt des Alters in unserem

transgenen Mausmodell verstärkt, andererseits trat ein vom Alter unabhängiger Effekt auf. In einem frühen Stadium von 15 Monaten zeigten transgene Alzheimer Tiere eher niedrigere C1q Konzentrationen. Mit zunehmendem Alter kehrte sich dies jedoch ins Gegenteil um, so dass im Alter von 20 Monaten ein signifikanter Anstieg festgestellt werden konnte.

Innerhalb der Anästhetika hat Xenon aufgrund seiner geringen Teratogenität und Toxizität den Ruf eines nahezu idealen Betäubungsmittels. Immer mehr Studien weisen ferner darauf hin, dass Xenon in der Lage ist, neurodegenerative Prozesse wie die Alzheimer-Krankheit günstig zu beeinflussen. Auch wenn Xenon protektiv auf neuronale Zellen wirkt, ist noch unklar, ob Xenon entzündliche synaptische „pruning“-Mechanismen beeinflusst. Um diese Fragestellung zu untersuchen, haben wir eine moderne Methode für in-vitro-Studien entwickelt. Unser Ansatz mittels lebender Hirnschnitte eröffnet die Möglichkeit pharmakologischer Applikationen. Wir konnten zeigen, dass eine kurzzeitige Inkubation mit Xenon oder Isofluran keine akuten Auswirkungen auf den C1q Spiegel im Gehirn hat. Zusammenfassend unterstreichen unsere Studien die Bedeutung von C1q für Alterungs- und neurodegenerative Prozesse. Außerdem bietet unser Modell die Möglichkeit, die Auswirkungen pharmakologischer Interventionen zu untersuchen.

# Table of Contents

Acknowledgements	I
Abstract	III
Kurzzusammenfassung	V
List of Figures	XI
List of Tables	XIII
Nomenclature	XV
1 Introduction	1
1.1 Structure of C1q	1
1.2 C1q source in the brain	2
1.3 Morphology of C1q in the brain	3
1.4 Synaptic pruning in the developing brain	4
1.4.1 Synaptic pruning via microglia	4
1.4.2 Synaptic pruning via astrocytes	6
1.5 C1q level changes during normal aging	6
1.6 C1q in Alzheimer animal models	7
1.6.1 C1q increase during Alzheimer's disease (AD)	7
1.6.2 The neuroprotective aspect of the C1q protein	7
1.6.3 The role of C1q in complement activation and synaptic pruning	8
1.7 Anaesthetics and neurotoxicity	8
1.7.1 Neurotoxic effects on the developing brain	8
1.7.1.1 Isoflurane	9
1.7.1.2 Xenon	10
1.7.1.3 Combination of isoflurane and xenon	10
1.7.2 Anaesthetics in Alzheimer's disease	10
1.7.2.1 Isoflurane	11
1.7.2.2 Xenon	12

1.8	Aims of the thesis . . . . .	13
2	Material and Methods . . . . .	15
2.1	Mice . . . . .	15
2.1.1	Aging groups . . . . .	15
2.2	Preparation and Regeneration . . . . .	15
2.3	Incubation with anaesthetics . . . . .	17
2.4	Immunofluorescence . . . . .	18
2.4.1	Double staining of C1q and Glial-Fibrillary-Acidic Protein (GFAP) . . . . .	18
2.4.2	Double staining of C1q and Microtubule-Associated-Protein 2 (MAP2) . . . . .	19
2.4.3	Double staining with two different C1q antibodies . . . . .	19
2.4.4	Antibody-Overview . . . . .	20
2.4.5	Double staining of C1q and methoxy-X04 . . . . .	20
2.5	Imaging . . . . .	21
2.6	Light intensity analysis and plaque load measurement . . . . .	21
2.7	Statistics . . . . .	23
2.7.1	Immunofluorescence imaging . . . . .	23
3	Results . . . . .	25
3.1	Morphology . . . . .	25
3.1.1	C1q is globally distributed across the entire brain . . . . .	25
3.1.2	Morphology of C1q positive somata is dependent on localization . . . . .	26
3.1.3	C1q positive somata can be visualized by different anti-C1q antibodies. . . . .	29
3.1.4	C1q is located paraneuronal as well as perineuronal around DAPI-positive cell nuclei . . . . .	30
3.1.5	C1q dendritic-like structures . . . . .	33
3.1.6	C1q accumulates in mouse models of Alzheimer's disease . . . . .	36
3.2	The effect of age, Alzheimer's disease and anesthetics on brain C1q . . . . .	38
3.2.1	C1q increase during normal aging . . . . .	38
3.2.2	C1q levels are altered in Arc-A $\beta$ -mice . . . . .	42
3.2.3	The effect of xenon and isoflurane on brain C1q levels . . . . .	43
4	Discussion and Conclusion . . . . .	49
4.1	Morphology . . . . .	49
4.2	The influence of age and Alzheimer's disease on C1q brain levels . . . . .	53
4.3	Effects of xenon and isoflurane on brain C1q . . . . .	56
A	Supplementary Material . . . . .	59
B	Publication . . . . .	69

C Bibliography

71



# List of Figures

1.1	Structure of C1q . . . . .	2
1.2	C1q basal level . . . . .	4
1.3	Complement dependent synaptic pruning via microglia . . . . .	5
1.4	Synaptic pruning by astrocytes (direct pathway) . . . . .	6
1.5	Pathology of Alzheimer ´s disease . . . . .	11
2.1	Preparation and Regeneration . . . . .	16
2.2	Xenon treatment scheme with corresponding control . . . . .	17
2.3	Isoflurane treatment scheme with corresponding control . . . . .	17
2.4	GFAP staining . . . . .	18
2.5	MAP2 staining . . . . .	19
2.6	Axio Observer.Z1 . . . . .	21
2.7	Annotations of the dentile gyrus, the CA1 region and the hippocampus . . . . .	22
2.8	Threshold adjustment . . . . .	22
2.9	Examples for ROC curves and AUC values . . . . .	24
3.1	Immunofluorescence staining reveals an overall C1q distribution across the entire brain . . . . .	26
3.2	Densely packed C1q somata in the stratum pyramidale of the CA2 and CA3 region . . . . .	27
3.3	The morphology of C1q somata differs across various brain regions . . . . .	28
3.4	Double staining of anti-C1q ab182451 and anti-C1q ab71940 proves the specificity of the antibodies for C1q somata . . . . .	29
3.5	GFAP positive astrocytes show no overlap or connection to C1q positive somata	30
3.6	Paraneuronal C1q in a triple staining of C1q, MAP2 and DAPI . . . . .	31
3.7	Perineuronal C1q in a triple staining of C1q, MAP2 and DAPI . . . . .	32
3.8	C1q positions around somata of different cell types . . . . .	33
3.9	C1q dendritic-like structure in transgenic Arc-A $\beta$ mice and corresponding wild type control . . . . .	34
3.10	Triple staining of C1q, DAPI, and GFAP . . . . .	35
3.11	Possible antibody interference in the double staining of C1q and MAP2 . . . . .	35

---

3.12 Colocalisation of C1q dendritic like structures and MAP2 positive neuron . .	35
3.13 Morphology of C1q in transgenic arc-A $\beta$ mice, a mouse model for Alzheimer's disease . . . . .	37
3.14 Light intensity values were calculated from Arc-A $\beta$ -mice and corresponding wild-types . . . . .	39
3.15 Light intensity measurement: C1q increase during aging . . . . .	40
3.16 Plaque load detection: C1q plaques increase during aging . . . . .	41
3.17 Light intensity measurement: C1q level changes in Arc-A $\beta$ -mice . . . . .	42
3.18 Light intensity measurements of the dentate gyrus: xenon and isoflurane treated slices . . . . .	43
3.19 Light intensity measurements of the dentate gyrus in xenon and isoflurane treated slices . . . . .	44
3.20 Light intensity measurements of the CA1 region: xenon and isoflurane treated slices . . . . .	45
3.21 Light intensity measurements of the CA1 region: xenon and isoflurane treated slices . . . . .	46
3.22 AUC analysis of light intensity values . . . . .	47
4.1 Molecular receptors for xenon and isoflurane (reproduced from Longone et al. 2011) . . . . .	56
A.1 Georg thieme Verlag KG license terms and conditions . . . . .	60

# List of Tables

2.1	Preparation solution . . . . .	16
2.2	Artificial cerebrospinal fluid . . . . .	16
2.3	Primary antibodies . . . . .	20
2.4	Secondary antibodies . . . . .	20
2.5	Methoxy-X04 stock solution . . . . .	20
2.6	Effect sizes of AUC values . . . . .	24
A.1	Software- and IT-Support . . . . .	59
A.2	Prepublication chapters . . . . .	66
A.3	Prepublication figures . . . . .	67



# Nomenclature

## Abbreviations

---

Abbreviation	Description
A $\beta$	$\beta$ -amyloid
ab	Abcam
aCSF	artificial cerebrospinal fluid
AD	Alzheimer's disease
APP	amyloid precursor protein
AUC	area under the curve
C/EBP- $\delta$	CCAAT/enhancer binding protein delta
CA	Cornu ammonis
CREB	cAMP response element-binding protein
CxCR1	C-X-C motif chemokine receptor 1
DAPI	4,6-diamidino-2-phenylindole
GABA	gamma-aminobutyric acid
GAD67	glutamate-decarboxylase; isotype 67
GFAP	glial fibrillary acidic protein
GFP	green fluorescent protein
GPR6	G-protein coupled receptor 6
let-7c	lethal-7c
LRP1B	low density lipoprotein receptor-related protein 1B
LTP	long term potentiation
MAP2	microtubule associated protein 2
MEGF10	multiple epidermal growth factor like domains protein 1
MERTK	c-mer proto-oncogene tyrosine kinase

---

---

<b>Abbreviation</b>	<b>Description</b>
miRNA	micro ribonucleic acid
mRNA	messenger ribonucleic acid
NGF	nerve growth factor
NGS	normal-goat-serum
NMDA	N-methyl-D-aspartate
P7 rats	postnatal day 7 rats
PBS	phosphate buffered saline
PFA	paraformaldehyde
ROC	receiver operating characteristic
ROI	region of interest
TG	transgenic
TGF $\beta$	tumor-growth-factor- $\beta$
TUM	Technical University Munich
WT	wild-type
YFP	yellow-fluorescence-protein

---

# 1 Introduction

The complement system is a vital constituent of the innate immune system, consisting of over 40 plasma proteins that facilitate pathogen recognition and elicit direct and indirect toxic effects. Complement activation is triggered via three distinct pathways: the lectin pathway begins with the the binding of mannose binding lectin on the surface of pathogens; the alternative pathway commences with the automatic hydrolysis of C3 in the bloodstream leading to the binding of the resulting C3b to adjacent pathogen surfaces; and the classic pathway is involved in the initiation of enzymatic reactions by the initiator protein C1q following antigen-antibody binding (Sjöberg et al. 2008).

”Nowadays, more and more functions of the C1q protein are revealed. It appears that C1q is involved in brain development as well as in neuroprotection but also in synaptic pruning mechanism and the occurrence of neurodegenerative diseases such as Alzheimer’s diseases”. (published in C. Rupprecht, Sarker, et al. (2022)).

## 1.1 Structure of C1q

The C1q protein has a distinctive structure that resembles a ”bunch of flowers” (Thielens et al. 2017) composed of 18 polypeptides (Figure 1.1). Each of the six flower heads consists of the C-terminal domain of one A, B, and C chain, while a collagen-like region forms the rest of each chain. Disulfide bridges at the N-terminal end connect the A and B chains and the C chains with each other (Thielens et al. 2017).

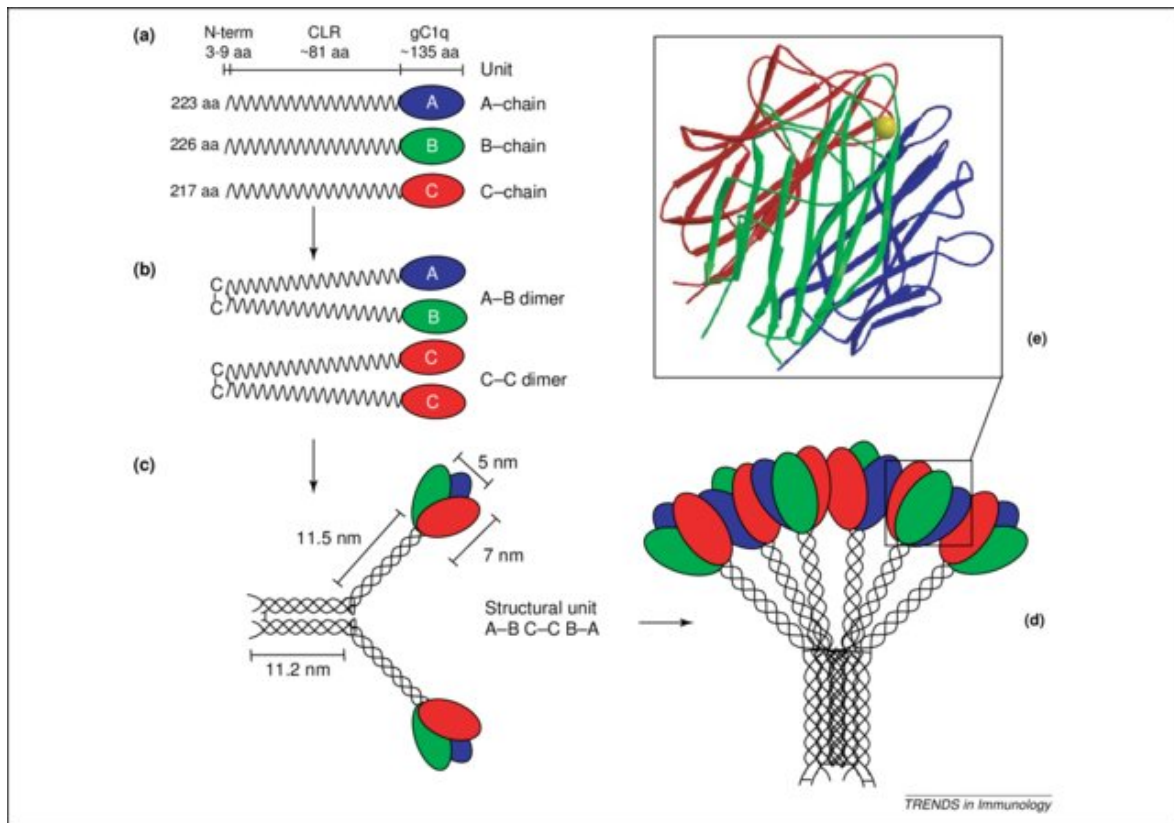


**Figure 1.1:** Structure of C1q (Figure reproduced from Kishore et al. 2004)

## 1.2 C1q source in the brain

Cell-specific deletion of C1qa (Fonseca, Chu, Hernandez, et al. 2017), mRNA analysis in neuronal and glial cell cultures (Diaz-Aparicio and Sierra 2019), immunofluorescence experiments (Schäfer et al. 2000; Stephan et al. 2013) and the combination of immunohistochemistry and in situ hybridization (Schäfer et al. 2000) identified microglia as the dominant source of C1q in the brain.

Nowadays, it seems likely that neurons also express C1q. Usually, the neuronal expression should be low. However, under certain conditions, as they occur in neuronal disease, this pathway gets activated by astrocyte signals. In this context, tumor growth-factor- $\beta$  (TGF $\beta$ ) is an essential chemokine (Bialas and Stevens 2013; Stevens et al. 2007).

### 1.3 Morphology of C1q in the brain

In this section, an overview of the morphology of C1q in the brain is given, which in part was prepublished in C. Rupprecht, Sarker, et al. (2022)

”C1q shows an overall distribution across the entire brain (Figure 1.2), which sharply rises with increasing age.” (published in C. Rupprecht, Sarker, et al. (2022)). In particular, in the area of the dentate gyrus, the hippocampus, the piriform cortex, and the substantia nigra immunofluorescence images have shown powerful signals (Figure 1.2) (Stephan et al. 2013). (adapted from C. Rupprecht, Sarker, et al. (2022)).

At the cellular level, C1q accumulates perinuclearly along the cell bodies of microglia cells (Kawai et al. 2020). On the contrary, astrocytes most likely do not directly interact with C1q molecules (Fan et al. 2007) but indirectly regulate neuronal C1q expression using chemokines (Bialas and Stevens 2013).

In synaptic pruning mechanisms, C1q works as an ”eat me signal” and interferes with pre- and postsynaptic material (Zabel and Kirsch 2013; Hong et al. 2016) (Based on C. Rupprecht, Sarker, et al. (2022)). Electron microscopy images (Stephan et al. 2013; Dejanovic et al. 2018), as well as analysis of synaptosomes fractions (Györfly et al. 2018) revealed a direct attachment of C1q to synaptic connections.

”C1q does not only interact with synaptic material but also with neuronal cell bodies. Whereas Lopez et al. (2012) described a perineuronal extracellular localization of C1q protein in the CA2 region of the hippocampus and the deep cerebellum and Fonseca, Chu, Hernandez, et al. (2017) reported extracellular C1q surrounding YFP-positive neurons in the CA1 hippocampal region, Stephan et al. (2013) observed intracellular C1q located in inhibitory neurons.” (published in C. Rupprecht, Sarker, et al. (2022)). Furthermore GAD67 positive interneurons have been identified to carry the C1q protein (Fonseca, Chu, Hernandez, et al. 2017).

C1q-positive plaques only exist in brains with Alzheimer pathology (C. Rupprecht, Sarker, et al. 2022). These structures, characterized by intense staining, are identical to  $\beta$ -amyloid plaques. ”They are mainly found in the cortex, hippocampus, striatum, and thalamus and stay connected to microglia cells and reactive astrocytes (Rodríguez et al. 2009; Matsuoka et al. 2001; Morgan 2018; Fonseca, Chu, Berci, et al. 2011)”. (published in C. Rupprecht, Sarker, et al. (2022)). Additionally, some studies indicate the accumulation of C1q around apical dendrites in pathological brain tissue of Alzheimer’s disease (Afagh et al. 1996).

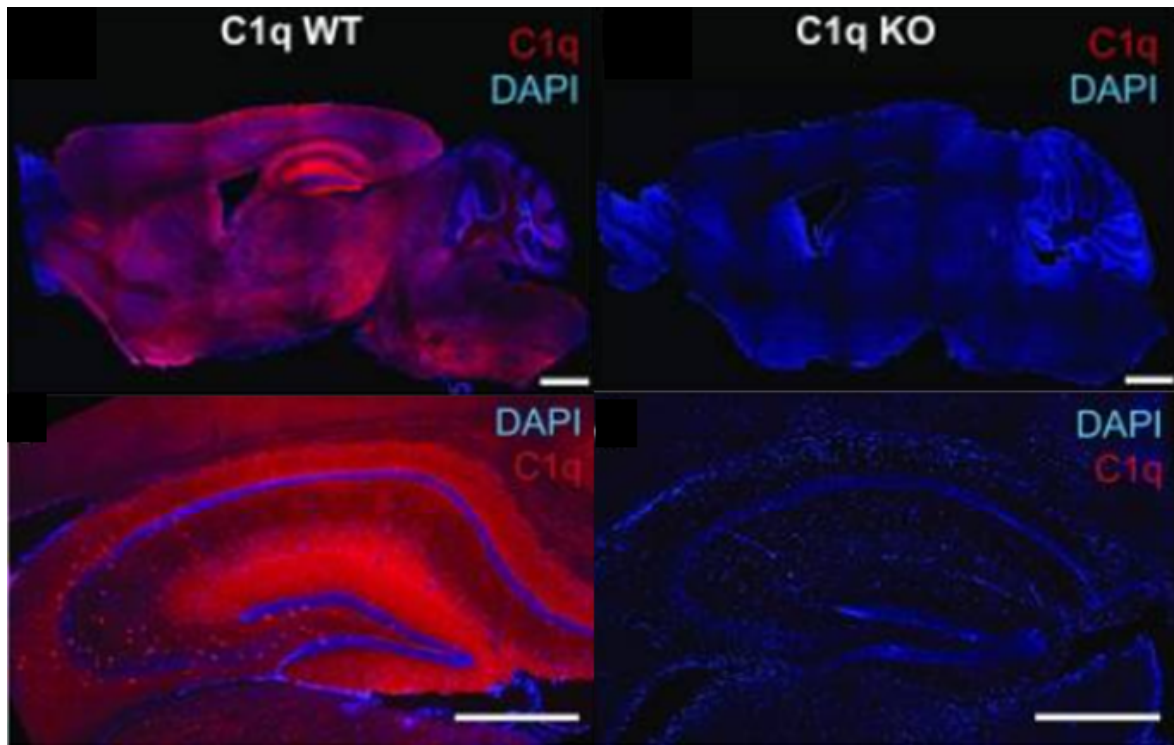


**Figure 1.2:** C1q basal level (right side: Knockout control) (reproduced from Stephan et al. 2013).

## 1.4 Synaptic pruning in the developing brain

Postnatal brains show a diverse range of processes that are critical for future development. While learning induces the training of networks and synaptic interactions, rarely used pathways are reduced or destroyed. Synaptic pruning summarizes the destruction of synapses through the body's own immune system.

### 1.4.1 Synaptic pruning via microglia

In this section an overview of synaptic pruning via microglia is given, which in part was prepublished in C. Rupprecht, R. Rupprecht, et al. (2021).

Microglia-dependent pruning is essential for normal brain development. As shown by Rosa C. Paolicelli et al. (2011) deficiency in pruning leads to an "excess of dendritic spines and immature synapses" and, from there, to "immature brain circuitry" (Rosa C. Paolicelli et al. 2011).

Knockout experiments have revealed that two biochemical pathways are responsible for smooth functioning. The majority of microglia cells highly express the CxCr1-Receptor. This receptor interacts with fractalkines on neuronal membranes and controls pruning mechanism either by direct participation in the phagocytosis process or through indirect effects that affect microglia activity or number (Rosa C. Paolicelli et al. 2011; Rosa Chiara Paolicelli et al. 2014; Wolf et al. 2013). Another pathway that directly contributes to synaptic pruning uses the complement system. "The active form of the C3 protein, C3b, can opsonize neurons and is recognized by microglia by means of its C3 receptor". (published in C. Rupprecht, Sarker, et al. (2022)). Furthermore, the C1q protein is important in two ways. On the one hand, C1q can tag synapses on its own and connects them to the C1q receptor of microglia cells. On the other hand, C1q increases the C3b/C3-receptor pathway by activating C3 protein (Zabel and Kirsch 2013; Schafer et al. 2012; Presumey et al. 2017). (adapted from C. Rupprecht, R. Rupprecht, et al. (2021)).

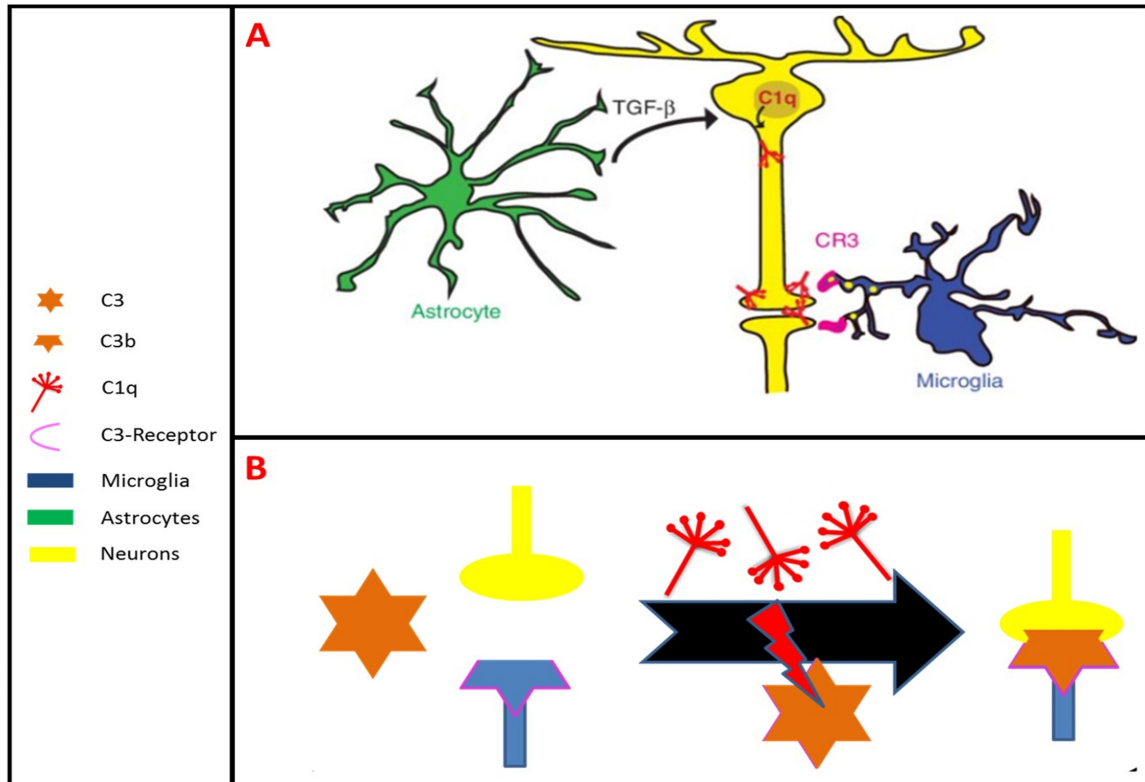


**Figure 1.3:** Complement dependent synaptic pruning via microglia

A) Astrocytes induce neuronal C1q expression via TGF $\beta$ , followed by complement dependent synaptic pruning. (Figure reproduced from Chung, Allen, et al. 2015).

B) C1q converts C3 into its active form. The resulting C3b connects synaptic material with phagocytosis receptors of microglia.

### 1.4.2 Synaptic pruning via astrocytes

Astrocytes exhibit a direct and indirect effect on synaptic pruning. In the indirect route, microglia execute phagocytosis processes. However, astrocytes increase their activity by causing an increase in C1q protein via TGF $\beta$  expression. In the direct route, synaptic material gets directly phagocytosed by astrocytes (Figure 1.4). Therefore, the receptors MERTK and MEGF10 recognize certain "eat-me-signals" (e.g., C1q, phosphatidylserine) on the surface of synapses (Chung, Allen, et al. 2015; Chung, Clarke, et al. 2013; Iram et al. 2016).

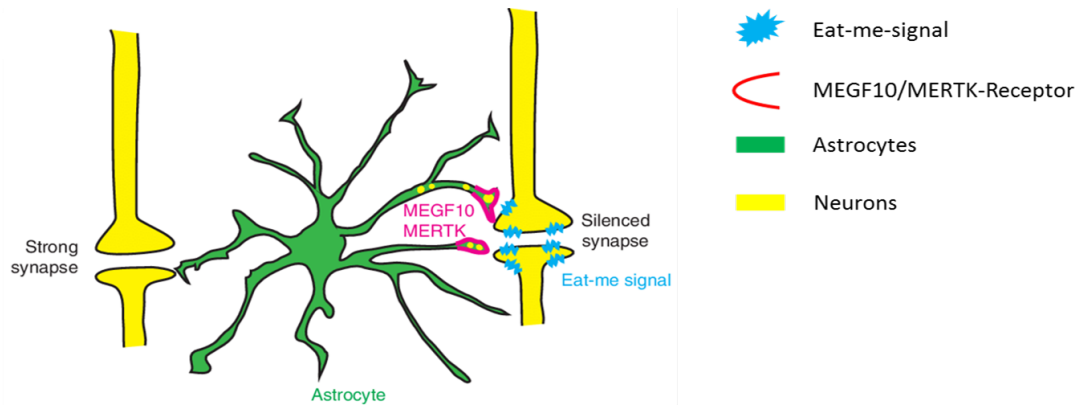


**Figure 1.4:** Synaptic pruning by astrocytes (direct pathway): Astrocytes recognize certain "eat me signals" by MEGF10 and MERTK receptors. (Figure reproduced from Chung, Allen, et al. 2015) (legend added by author).

## 1.5 C1q level changes during normal aging

Immunofluorescence imaging (Stephan et al. 2013), mRNA analytics (Reichwald et al. 2009) and Western blot analysis (Stephan et al. 2013; Naito et al. 2012; Reichwald et al. 2009) demonstrated an age-related increase in cerebral C1q, with a particularly pronounced effect in the synaptic layer of the hippocampus, certain areas of the CA2 neuropils, the stratum lacunorum moleculare, and the neuropil of the central nervous system (Stephan et al. 2013). Furthermore "C1q-patches" (Stephan et al. 2013) seem to occur at high age. According to Stephan et al. (2013) "these C1q patches, mainly detected in the cortex, thalamus, midbrain, and striatum, are not amyloid plaques but represent a novel structure of unknown significance and function".

Animal behavioral experiments indicated that increased C1q levels may have a negative impact on cognitive function during aging. Specifically, mice with C1q deficiency showed protection from aging-related cognitive decline (Stephan et al. 2013).

## 1.6 C1q in Alzheimer animal models

### 1.6.1 C1q increase during Alzheimer's disease (AD)

Using mRNA detection and Western blot analysis, Reichwald et al. (2009) demonstrated a progressive increase in C1q levels between APP23 transgenic mice and control groups. This elevation became significant at 15 months of age for mRNA detection and at 24 months for Western blotting. In a separate study, Hong et al. (2016) described elevated C1q levels in Alzheimer's brains at an earlier stage and linked this increase to  $\beta$ -amyloid deposition. While monomeric  $\beta$ -amyloid did not influence C1q expression, oligomeric  $\beta$ -amyloid represented a potent stimulus.

### 1.6.2 The neuroprotective aspect of the C1q protein

For a long time, C1q has been considered a harmful molecule that drives neurodegeneration. In contrast to these adverse reports, more and more studies reveal its role in neuroprotection. Pisalyaput and Tenner (2008) discovered improved viability of neuronal cell cultures after treatment with purified C1q protein. Subsequent in vitro experiments showed a significant reduction in  $\beta$ -amyloid induced neurotoxicity in mature and immature neuronal cells (Pisalyaput and Tenner 2008; Benoit, Hernandez, et al. 2013).

To explore the molecular background of this type of neuroprotection classical apoptosis pathways have been investigated. C1q altered neither caspase nor calpain activation nor mitochondrial potentials (Benoit and Tenner 2011). According to Benoit and Tenner (2011) C1q has direct effects on neuronal gene expression and miRNA modulation. During neuroprotection, C1q downregulates let-7c miRNA and increases the expression of C/EBP- $\delta$  and activation of CREB. These three items work together in releasing neurotrophic factors like nerve growth factor (NGF). Especially in  $\beta$ -amyloid injured neurons, C1q drives the expression of low-density lipoprotein receptor-related protein 1B (LRP1B) and G-protein coupled receptor 6 (GPR6) and overcomes their inhibition by fibrillary  $\beta$ -amyloid. Due to their neuroprotective function and upregulation in vitro and even in vivo, they are the central mediators of C1q-induced neuroprotective effects (Benoit, Hernandez, et al. 2013; Benoit and Tenner 2011).

C1q also, directly and indirectly, reduces the interaction between toxic  $\beta$ -amyloid and neuronal structures. On the one hand, C1q activates LRP1B, as previously described. This membrane receptor is most likely involved in regulating  $\beta$ -amyloid uptake and production.

On the other hand, C1q directly interferes with  $\beta$ -amyloid and enhances protein aggregation into a less toxic form (Bialas and Stevens 2013).

### 1.6.3 The role of C1q in complement activation and synaptic pruning

In contrast to its potential neuroprotective effects (1.6.2), neurodegenerative properties seem to dominate the situation in AD.

The relationship between  $\beta$ -amyloid and C1q protein is ambiguous. On the one hand, C1q protein increases the aggregation of  $\beta$ -amyloid and reduces its toxicity (Bialas and Stevens 2013). On the other hand,  $\beta$ -amyloid stimulates C1q expression (Hong et al. 2016) and activates the classical complement pathway by direct interaction with C1q (H. Jiang et al. 1994; Sim et al. 2007; Tacnet-Delorme et al. 2001). Several studies demonstrated increased accumulation of C1q in synaptosomal fractions (Hong et al. 2016; Györfy et al. 2018; Dejanovic et al. 2018), as well as extended colocalization between C1q and synaptic markers in AD brains (Dejanovic et al. 2018; Hong et al. 2016). Hong et al. (2016) showed that early synapse loss in Alzheimer's models is complement-dependent, indicating that C1q may be involved in various ways. On the one hand, C1q extends the inflammatory activity of glial cells and increases C3-dependent synaptic engulfment by microglia. On the other hand, C1q may act as an "eat me" signal and directly contribute to synaptic pruning (Iram et al. 2016; Hong et al. 2016; Luchena et al. 2018; S. Jiang and Bhaskar 2017).

These findings suggest that mechanisms of synaptic pruning during brain development (as described in section 1.4) may be negatively reactivated during AD, leading to neurodegeneration.

## 1.7 Aneasthetics and neurotoxicity

### 1.7.1 Neurotoxic effects on the developing brain

In 2018, 235130 surgeries were performed on inpatient children under the age of 5 in Germany (Rainer Radtke 2019). Volatile anesthetics are commonly in use for such surgical interventions. While these substances are indispensable in today's medicine, their potential danger should always be considered, particularly for young patients.

Population-based (Wilder et al. 2009) and sibling birth cohorts (DiMaggio et al. 2011)

revealed a connection between early childhood exposure to anesthetics and the occurrence of learning disabilities and behavioral and developmental disorders.

### 1.7.1.1 Isoflurane

Isoflurane application may lead to neurodegeneration, whereas neuronal apoptosis after isoflurane application is undisputed. Istaphanous et al. (2013) showed cell death of cortical neurons after exposing 7-day-old mice to 1.5% isoflurane for 6 hours. Similarly, G. Liang et al. (2010) revealed that only six hours of incubation with 0.75% isoflurane is sufficient to induce significant neuronal apoptosis (G. Liang et al. 2010).

The effect of isoflurane on long-term memory is more inconsistent and seems to be concentration or exposure time-dependent. Whereas in the previously described experiment by G. Liang et al. (2010) no influence was detectable, Tao et al. (2016) found that repeated exposure to 2% isoflurane for 2 hours per day for three consecutive days resulted in significant cognitive impairment, particularly on memory tasks that rely on the hippocampus. These findings are consistent with those of Murphy and Baxter (2013), who reported greater cognitive impairment in mice exposed to isoflurane repeatedly compared to those with a single exposure.

The neurotoxic effects of isoflurane on neuronal cell cultures and human neuronal progenitor cells depend on exposure time and concentration. Consistent with the previous *in vivo* experiments, *in vitro* experiments have also shown that isoflurane induces neurotoxicity. Research by Wei et al. (2005) and Xie, Dong, Maeda, R. Moir, et al. (2006) has indicated that this effect only occurs at concentrations above 2%, and the neurotoxicity increases with the duration of exposure, suggesting that an incubation period of at least six hours is necessary to produce a measurable effect.

However, outside of the dangerous concentration and incubation time range, isoflurane has been shown to have some neuroprotective effects. For example, Sall et al. (2009) demonstrated that a four-hour incubation with 3.4% isoflurane inhibits growth but has no neurotoxic effects on neuronal progenitor cells. Similarly, Zhao et al. (2013) found that one-hour incubation with 0.6% isoflurane increased progenitor cell proliferation. Interestingly, the opposite effect occurred after increasing the dose.

### 1.7.1.2 Xenon

Xenon is currently of interest as an anesthetic with fewer neurotoxic side effects than previous ones (e.g., isoflurane, sevoflurane). However, it does not have advantages in the developing brain.

In 2008, Davide Cattano et al. (2008) showed a significant increase of neuronal apoptosis in the brains of seven-day-old mice after four hours of incubation with 70% xenon. Three years later, another study reported increased apoptotic gene expression in P7 (postnatal day 7) rat brains following two hours of exposure to 75% xenon (D. Cattano et al. 2011). In 2013, Brosnan and Bickler (2013) compared the toxicity of different anesthetics using hippocampal slice cultures from P7 rats at similar potent anesthetic concentrations. The study found that xenon, isoflurane, and sevoflurane had identical neurotoxic effects on the developing brain.

### 1.7.1.3 Combination of isoflurane and xenon

Although both isoflurane and xenon can have detrimental effects on the developing brain when used alone, their combination can yield different results. Studies have shown that when used together, the two anesthetics enhance the depth of anesthesia and exhibit reduced toxic effects. Both in vitro and in vivo experiments demonstrated that "Xenon mitigates isoflurane-induced neuronal apoptosis in the developing rodent brain" (Ma et al. 2007). Additionally, the combination of both anesthetics reduced the neurotoxicity of isoflurane and retained the neuroprotective effects of xenon (Davide Cattano et al. 2008).

## 1.7.2 Anaesthetics in Alzheimer's disease

Among the various types of dementia Alzheimer's disease is the most common form in the elderly population (Henstridge et al. 2019). The disease initially manifests as isolated memory lapses and progressively leads to severe cognitive decline, including deficits in memory recall, orientation, mental function, and autonomic nervous system dysfunction (*Stages of Alzheimer's* 2019).

At the beginning of the 20th century, Alois Alzheimer identified two pathological structures that underlie these symptoms (Vishal et al. 2011). One is the aggregation of  $\beta$ -amyloid to form plaques; the other is the degeneration of cytoskeleton elements into neurofibrillary tangles (Figure 1.5). Recent studies in the field of anesthesia suggest that anesthetics can affect both pathologies and potentially exacerbate the development of the disease.

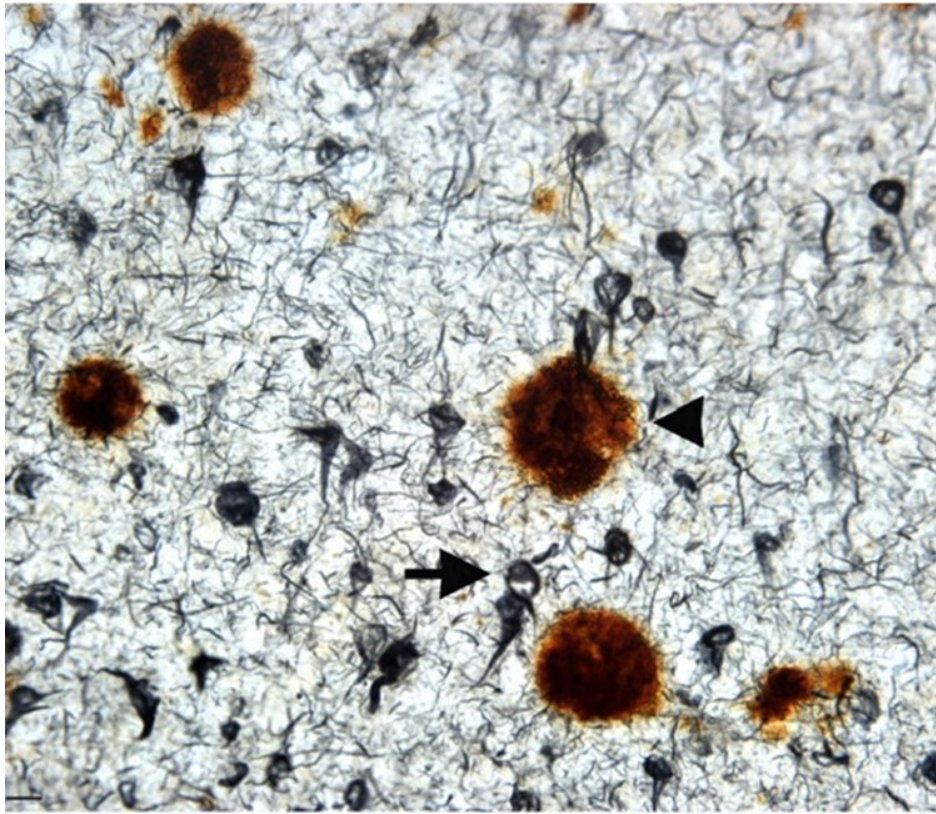


**Figure 1.5:** Pathology of Alzheimer's disease (reproduced from Rohn 2013)  
(arrow: neurofibrillary tangle; arrowhead:  $\beta$ -amyloid plaque)

### 1.7.2.1 Isoflurane

Neurotoxicity following the application of isoflurane is not only evident in the developing brain (subsubsection 1.7.1.1) but also in adulthood. According to Xie, Culley, et al. (2008), a clinically used concentration of 1.4% isoflurane for two hours increases caspase activation significantly. When considering the immunofluorescence and the Western blot analysis by Perucho, Rubio, et al. (2010), isoflurane-induced apoptosis is slightly stronger in transgenic Alzheimer's animals than their corresponding control. Through these direct toxic effects, isoflurane could contribute to neurodegeneration in general.

Furthermore, isoflurane interferes directly with Alzheimer's pathology. As a result of caspase activation, isoflurane alters amyloid precursor protein (APP) processing and increases  $\beta$ -amyloid levels in the brain (Xie, Dong, Maeda, R. D. Moir, et al. 2007; Xie, Culley, et al. 2008; Xie and Xu 2013; Zhang et al. 2017). This, in turn, enhances caspase activity

retroactively, creating a potential vicious cycle (Xie, Dong, Maeda, R. D. Moir, et al. 2007; Xie and Xu 2013; Dong, Xu, et al. 2011).

Furthermore, isoflurane can modulate the composition of  $\beta$ -amyloid by promoting its aggregation and accumulation. Studies have reported increased oligomeric  $\beta$ -amyloid levels ranging from 20 to 30kDa following isoflurane incubation (Perucho, Rubio, et al. 2010; Zhang et al. 2017; Perucho, Casarejos, et al. 2012; Eckenhoff et al. 2004). Notably, while high concentrations of isoflurane led to the formation of  $\beta$ -amyloid plaques in aged rats (Zhang et al. 2017), no changes were observed in the morphology of plaques in symptomatic Alzheimer's mice (Perucho, Rubio, et al. 2010).

Isoflurane does not only affect  $\beta$ -amyloid but also tau proteins. Numerous studies have reported increased levels of phosphorylated tau protein following isoflurane treatment. Both control groups and transgenic Alzheimer's mice exhibited alterations in tau protein levels, as indicated by Li et al. (2014) and Dong, X. Wu, et al. (2012), with a more pronounced effect observed in the Alzheimer's models. According to Li et al. (2014), Alzheimer's animals demonstrated a more potent and longer-lasting increase in phosphorylated tau proteins, while Dong, X. Wu, et al. (2012) showed an early rise in these proteins. The observed link between  $\beta$ -amyloid and tau phosphorylation, as demonstrated by Jin et al. (2011), may be a contributing factor.

### 1.7.2.2 Xenon

Xenon is often described as an ideal anesthetic due to its low toxicity, lack of teratogenicity, and potential neuroprotective properties (Hecker, Baumert, et al. 2004). Several neurodegenerative diseases, including Alzheimer's dementia, are associated with overstimulation of NMDA (N-Methyl-D-Aspartate) receptors (Loopuijt and Schmidt 1998; Lavaur et al. 2016). As an antagonist of NMDA and AMPA receptors (Haseneder, Kratzer, Kochs, Höfelmann, et al. 2009; Haseneder, Kratzer, Kochs, Mattusch, et al. 2009), xenon can counteract increased excitatory receptor activity and protect cells from excitotoxic stress (Lavaur et al. 2016; Hecker and Rossaint 2001). Xenon has been shown to protect against injury from hypoxia (Banks et al. 2010) and traumatic events (M. Liang et al. 2022; Harris et al. 2013) by this mechanism.

$\beta$ -Amyloid alters glutamatergic neurotransmission in multiple ways, resulting in low-level excitotoxicity and subsequent neuronal cell death (Lavaur et al. 2016; Wang et al. 2013; Liu et al. 2019). Treatment with 75% xenon counteracts this damage and even increases trophic effects in specific cell types (Lavaur et al. 2016). Thus, xenon can potentially protect against

NMDA receptor-mediated toxicity in acute brain damage and potentially in insidious diseases like Alzheimer's dementia.

Both Bürge et al. (2019) and Hofmann et al. (2021) have suggested that xenon's neuroprotective properties extend beyond its antagonistic effects on NMDA receptors. In particular, they have found that xenon can improve impaired synaptic plasticity, as demonstrated by the restoration of long-term potentiation (LTP) in the presence of  $\beta$ -amyloid at subclinical concentrations of xenon (Bürge et al. 2019; Hofmann et al. 2021).

Xenon also affects the gene expression of MEGF10 receptors and therefore reverse the neurotoxic effect on astrocytic synapse elimination (Shi et al. 2023).

Questions remain unanswered regarding xenon's effects on modulated NMDA receptors in Alzheimer's disease. For example, it is unclear how xenon affects the NMDA-promoted production of  $\beta$ -amyloid (Lesné et al. 2005).

Despite these uncertainties, the existing research suggests that xenon may hold promise as a therapeutic intervention for neurodegenerative diseases. Further investigation is needed to fully elucidate the mechanisms of xenon's neuroprotective effects and potential clinical applications.

## 1.8 Aims of the thesis

"Free Floating" is a special staining method that does not require cryopreservation. This facilitates the staining of delicate and sensitive structures in an intact structural environment and even enables the opportunity for pharmacological interventions.

With this experimental setup, we aimed to label C1q to confirm previous results on frozen sections and describe new morphological features.

The second part of the thesis deals with C1q expression. In order to investigate the influence of age on C1q levels, slices from hippocampus were studied by means of immunofluorescence. To address the impact of Alzheimer pathology transgenic Arc- $A\beta$  mice were used as a mouse model for Alzheimer's disease.

In the third part, we studied the putative influence of anesthetics on C1q expression. For this purpose, we treated slices either with isoflurane or xenon and compared the results to their corresponding controls.

These studies aim to elucidate relevant mechanisms underlying C1q expression in the brain and to characterize the impact of anaesthetics in relation to their side effect profile.

## 2 Material and Methods

Material and Methods haven been prepublished in an adapted version in C. Rupprecht, Sarker, et al. (2022).

### 2.1 Mice

”Transgenic arc- $A\beta$  mice (C57BL7/6 strain) and corresponding wild-type littermates were bred in the animal core facility of the Technical University Munich (TUM). The animal housing and sacrificing was done in strict compliance with the regulations of the European Union (2010/63/EU), the laws of Upper Bavaria, and the restrictions of the Technical University Munich. Animals had been supplied with water and food ad libitum. They grew up in a pathogen-free controlled environment and comfortably lived under a day and night cycle of 12 hours.” (published in C. Rupprecht, Sarker, et al. (2022)).

#### 2.1.1 Aging groups

In this study, we utilized transgenic Arc- $A\beta$  mice as a model for Alzheimer’s disease. These mice overexpress the human APP 695 gene, which leads to the development of pathological features similar to those observed in Alzheimer’s disease. Genetic analysis was conducted at three weeks of age to confirm the transgenic status, while negative results confirmed the wild-type status of the control group. We selected two age groups to investigate the effects of physiological aging and chronic  $\beta$ -amyloid exposure on C1q levels. The first group consisted of animals with an average age of 15 months, while the second group comprised only animals aged between 20-21 months.

## 2.2 Preparation and Regeneration

Mice including wild-types (n=9) aged 15 and 20 months and transgenic arc- $A\beta$  (n=6) aged 15 and 20 months were narcotized with isoflurane and euthanized by neck dislocation.

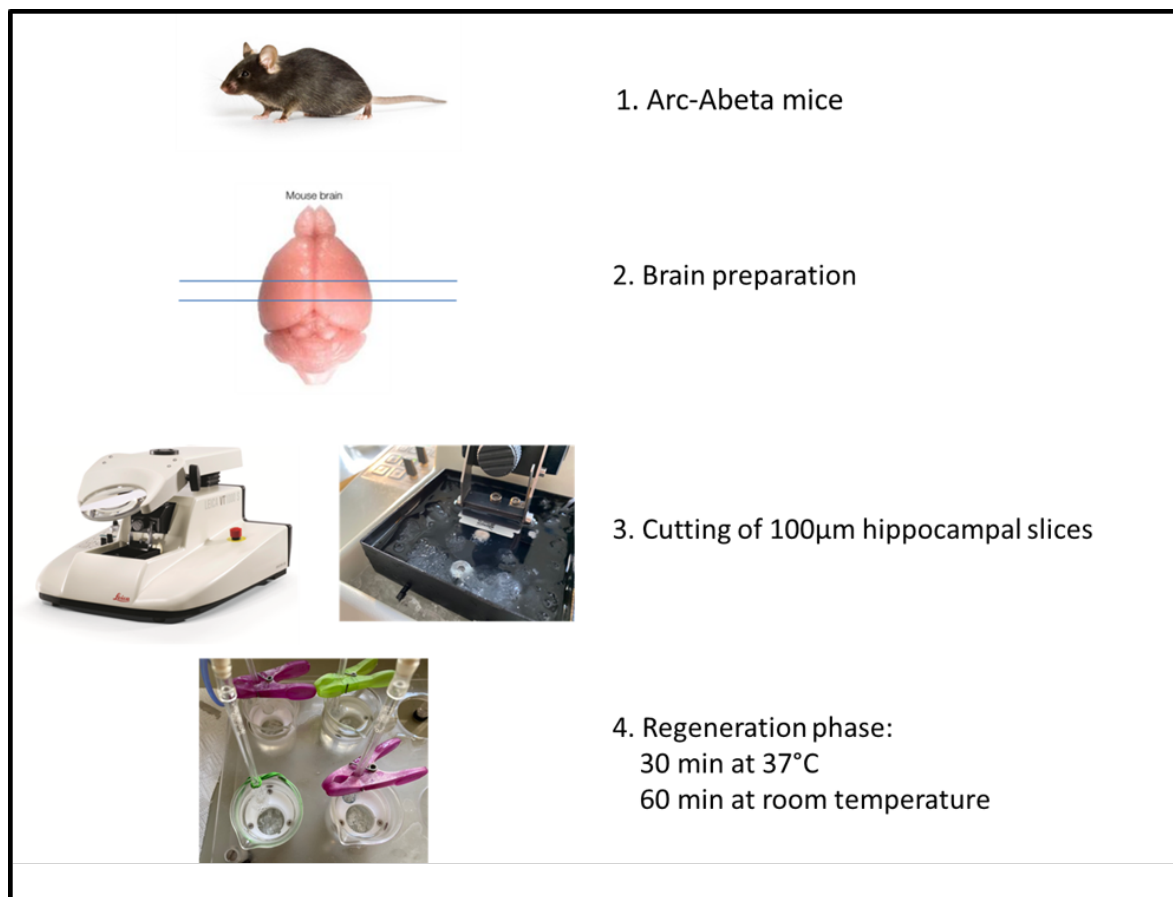
After whole brain extraction 100  $\mu\text{m}$  thick slices were prepared using a Leica VT 1000S vibratome. The brain was maintained in an ice-cold and oxygenated preparation solution (Table 2.1) throughout the preparation and cutting process. "To enable cell recovery, slices were transferred into artificial cerebrospinal fluid (aCSF) (Table 2.2) and were kept under continuous carbogen incubation for 30 minutes in a water bath at 37  $^{\circ}\text{C}$  and for 60 minutes under room temperature." (published in C. Rupprecht, Sarker, et al. (2022).)

**Table 2.1:** Preparation solution

substances	ammount	molarity
NaCl	7.305 g/l	125 mM
KaCl	0.186 g/l	2.50 mM
NaH <sub>2</sub> PO <sub>4</sub>	0.172 g/l	1.25 mM
D-(+)Glucose-Monohydrate	4.954 g/l	25.0 mM
NaHCO <sub>3</sub>	2.100 g/l	25.0 mM
MgCL <sub>2</sub> -Hexahydrate	1.220 g/l	6.00 mM
CaCl <sub>2</sub> -Dihydrate	0.037 g/l	0.25 mM

**Table 2.2:** Artificial cerebrospinal fluid

substances	ammount	molarity
NaCl	7.305 g/l	125 mM
KaCl	0.186 g/l	2.50 mM
NaH <sub>2</sub> PO <sub>4</sub>	0.172 g/l	1.25 mM
D-(+)Glucose-Monohydrate	4.954 g/l	25,0 mM
NaHCO <sub>3</sub>	2.100 g/l	25.0 mM
MgCL <sub>2</sub> -Hexahydrate	0.203 g/l	1.00 mM
CaCl <sub>2</sub> -Dihydrate	0.294 g/l	2.00 mM

**Figure 2.1:** Preparation and Regeneration

## 2.3 Incubation with anaesthetics

To investigate the effects of xenon and isoflurane slices were divided into four equal groups. Following recovery, slices were incubated with the respective compounds according to the scheme below. All treatments were done at room temperature and continuous carbogen flow.

**Xenon:** After pretreatment with  $N_2$  for 90 minutes 65% xenon was applied for 60 minutes. The remaining anesthetic was removed with a subsequent wash step using  $N_2$ .

**Isoflurane:** After incubation in carbonated aCSF for an additional hour slices were exposed to 0.6% isoflurane for 90 minutes, followed by a 60-minute wash step under carbogen.

**Control groups:** To serve as corresponding controls, slices were continuously treated with  $N_2$  or left untreated.

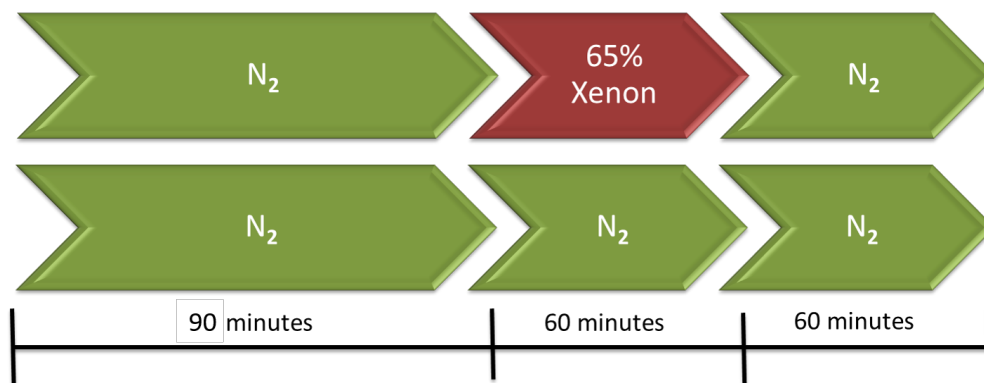


Figure 2.2: Xenon treatment scheme with corresponding control

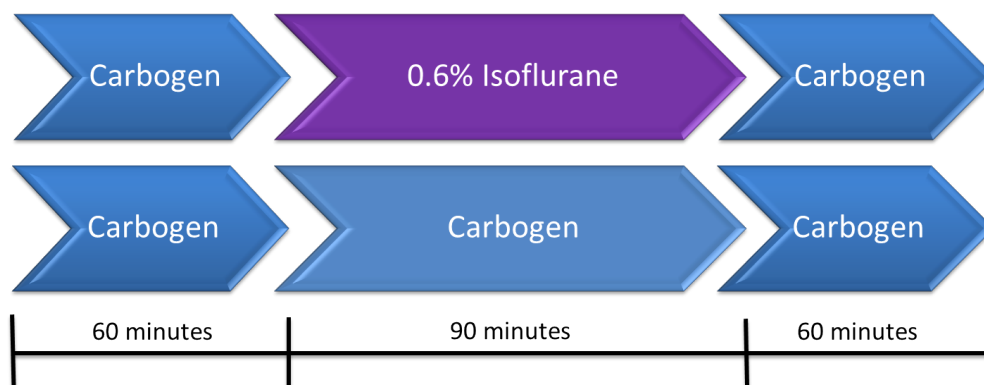


Figure 2.3: Isoflurane treatment scheme with corresponding control

## 2.4 Immunofluorescence

Following incubation slices were stored overnight in 4% paraformaldehyde (PFA) at 4°C. Thress washing steps with phosphate-buffered saline (PBS) for 10 minutes each and the Transfer into a new well removed excessive PFA. Subsequently, slices were blocked for one hour at room temperature with a mixture of 10% normal goat serum (NGS), 0.5% Triton X-100, and 89.5% PBS. (Adapted from C. Rupprecht, Sarker, et al. (2022)).

### 2.4.1 Double staining of C1q and Glial-Fibrillary-Acidic Protein (GFAP)

Primary antibody solution containing rabbit anti-C1q (Abcam(ab) 182451) at a dilution of 1:250 and mouse anti-GFAP (Cell Signalling 3670) at a dilution of 1:100 was used overnight at 4°C. After three washing processes with 1x PBS, slices were incubated for 2 hours with secondary antibodies against rabbit (Thermo Fischer A 11034; 1:250) and mouse (ab150119; 1:250 / ab150115; 1:100). Subsequently, slices were washed three times with PBS (each for 10 minutes) and dried on microscope slides before being covered with "ProLong Glass Antifade Mountant with NucBlue" (Invitrogen P36985). (Adapted from C. Rupprecht, Sarker, et al. (2022)).

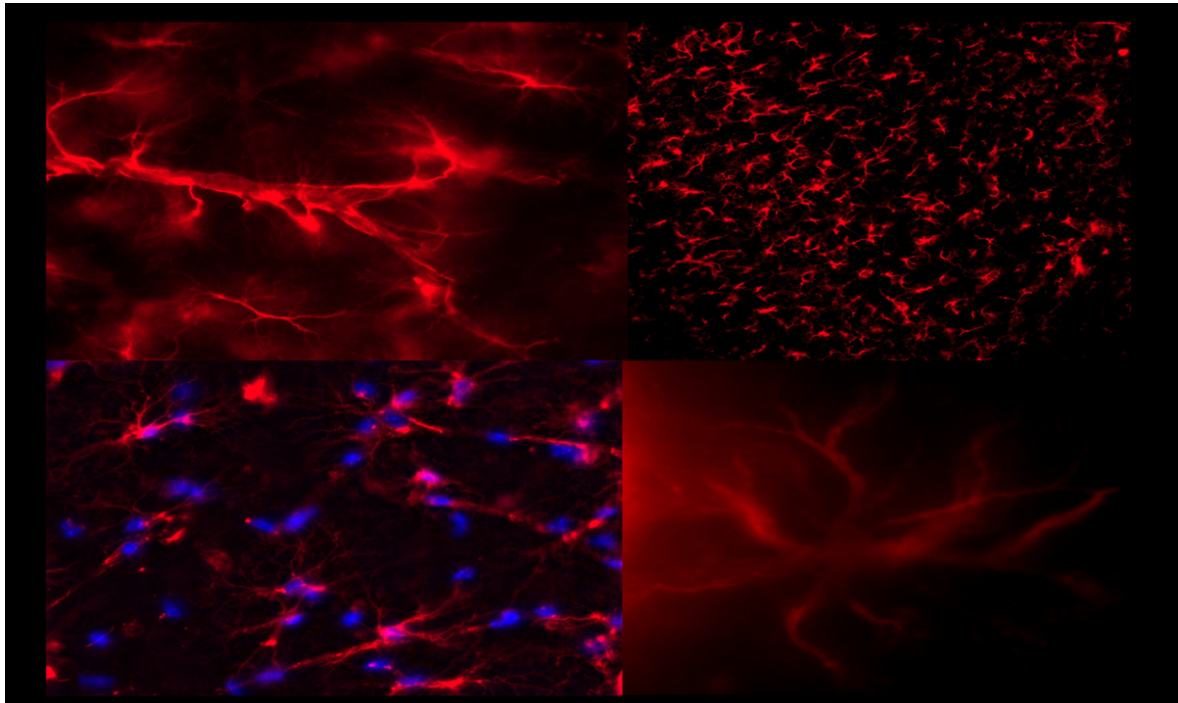
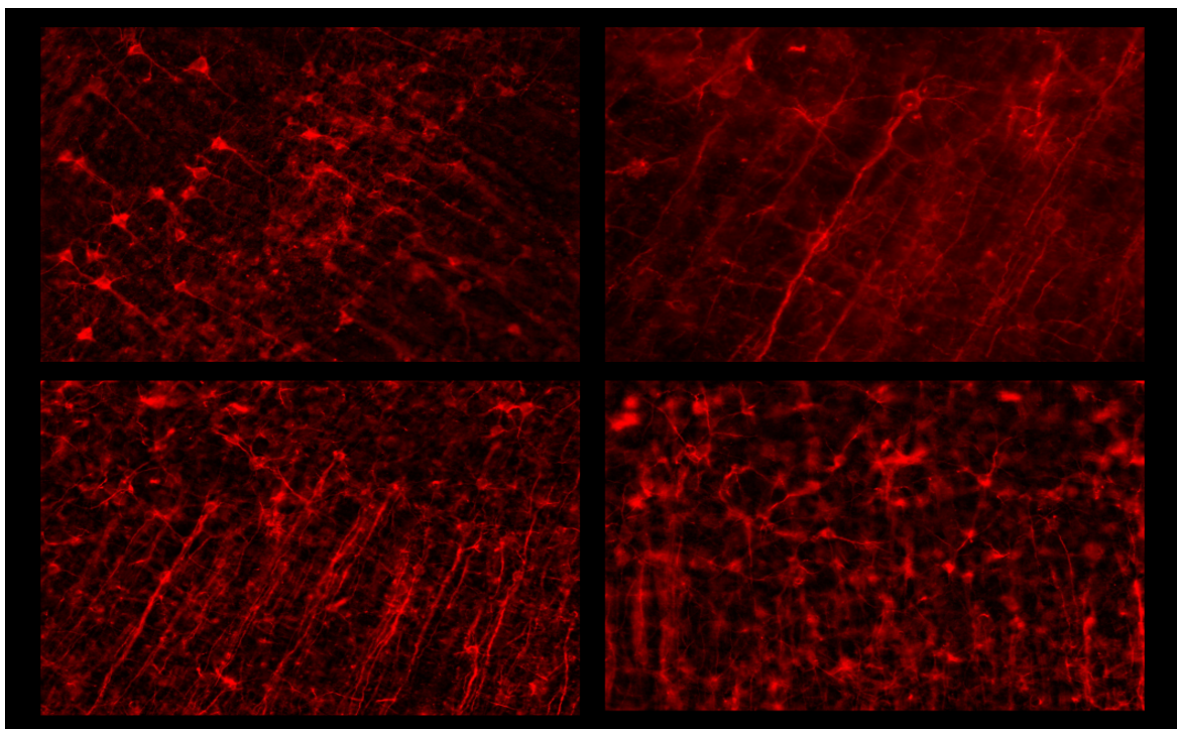


Figure 2.4: GFAP staining

### 2.4.2 Double staining of C1q and Microtubule-Associated-Protein 2 (MAP2)

The C1q staining was performed following the protocol outlined in subsection 2.4.1. Therefore, the MAP2 staining was added. The last washing steps of the C1q staining were shortened to two washes with 1xPBS for 10 minutes each before incubating the slices with chicken MAP2 (ab92434 or ab5392; 1:1000). Abcam 150119 (1:500) was used as the secondary antibody for 2 hours at room temperature. After three more washing steps with PBS (each for 10 minutes). Slices were dried on microscope slides and covered using "ProLong Glass Antifade Mountant with NucBlue" (Invitrogen P36985).



**Figure 2.5:** MAP2 staining

### 2.4.3 Double staining with two different C1q antibodies

The protocol followed the methodology outlined in subsection 2.4.2. However, instead of targeting MAP2, we used another anti-C1q antibody (ab71940; dilution 1:50) along with the secondary anti-mouse antibody ab172326 (dilution 1:25).

### 2.4.4 Antibody-Overview

**Table 2.3:** Primary antibodies

Company	Antibody-Number	Host	Target	Dilution
Abcam	182451	Rabbit	C1q	1:250
Abcam	71940	Mouse	C1q	1:50
Cell Signalling	3670	Mouse	GFAP	1:100
Abcam	92434	Chicken	MAP2	1:1000
Abcam	5392	Chicken	MAP2	1:1000

**Table 2.4:** Secondary antibodies

Company	Antibody-Number	Host	Target	Dilution	Conjugation
Thermo Fischer	A11034	Goat	Rabbit	1:250	Alexa Fluor 488
Abcam	150119	Goat	Mouse	1:500	Alexa Fluor 647
Abcam	150115	Goat	Mouse	1:100	Alexa Fluor 647
Abcam	150172	Goat	Chicken	1:250	Alexa Fluor 594

### 2.4.5 Double staining of C1q and methoxy-X04

"C1q staining was completed as described above. (...). Next, slices were incubated for 60 minutes in a solution of 0.4% methoxy stock solution (Table 2.5), 49.8% PBS and 49.8% ethanol without methylethylketone).

**Table 2.5:** Methoxy-X04 stock solution

substances	ammount
Methoxy-X04	10 mg
DMSO	100 µl
Iso-Propanol	450 µl
1x PBS	450 µl
1M NaOH	50 µl

After three washing steps with PBS-ETOH solution (50% PBS; 50% Ethanol with methylethylketone) and three washing steps with distilled water, slices were dried on microscope slides and covered by using "Dako Fluorescence Mounting Medium" (Dako S3023)." (published in C. Rupprecht, Sarker, et al. (2022)).

## 2.5 Imaging

"All images were taken by Axio Observer.Z1 from ZEISS microscopy equipped with six objectives (2,5x, 10x, 20x, 40x, 63x(oil) and 100x(oil) and four filters (96HE for blue wavelength; 46HE and 38HE for green wavelength; 63HE for red wavelength). ZEN 3.0 blue edition was used as software for image processing.



**Figure 2.6:** Axio Observer.Z1 (Zeiss microscopy 2020)

As part of the light intensity measurement, strict care was taken to record all images under the same conditions. Therefore, the microscope settings were adjusted to a binning of 1:1 and an exposure time of 1000 ms. Using the advanced tile function, regions of interest were defined. At least four reference points were set in each region to verify the focus area. By alternating imaging both the DAPI and the C1q staining, all pictures were taken using the 10x objective." (Published in C. Rupprecht, Sarker, et al. (2022)).

## 2.6 Light intensity analysis and plaque load measurement

To ensure the integrity of the data all image labels were automatically replaced with randomized numerical values to eliminate potential detection bias. Two independent researchers conducted the analysis in a blinded manner. The analysis was assisted by "Qupath". Light intensity measurements were captured in two distinct regions of interest, namely the dentate gyrus and the CA1 region. These areas were manually identified and annotated, which allowed for the exclusion of any disruptive artifacts such as ruptures, bubbles, or folds. For

all annotated area, Qupath measured the median and mean light intensity. (Adapted from C. Rupprecht, Sarker, et al. (2022).)

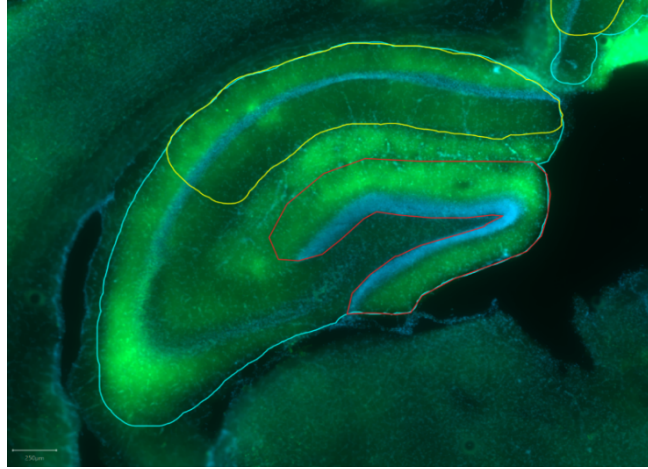


**Figure 2.7:** Annotations of the dentate gyrus (red), the CA1 region (yellow) and the hippocampus (cyan)

Since most plaques are localized in the cortex, we limited the plaque load measurement to this region. "Inside our specified regions, we used a uniform threshold to detect the plaque area. In this context a threshold of 7500 in combination with a smoothing sigma of 0.5 was determined. (compare Figure 2.8). Using these values, Qupath calculated the percentage of area that the plaques occupy of the total area". (Published in C. Rupprecht, Sarker, et al. (2022)).

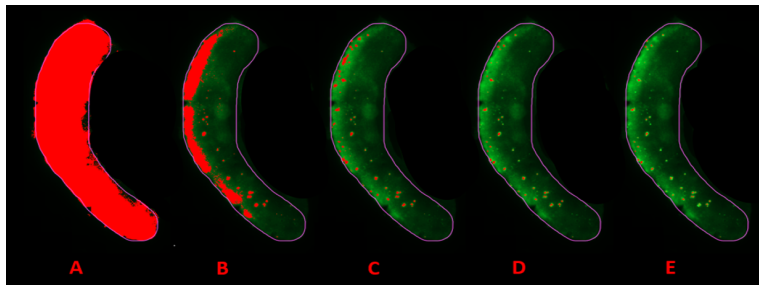


**Figure 2.8:** Adjustment of the threshold with

- (A) Threshold = 1000, no plaques are identified.
- (B) Threshold = 3000, isolated plaques are identified.
- (C) Threshold = 5000, almost all plaques are identified.
- (D) Threshold = 7500, all plaques are identified and filled in.
- (E) Threshold = 9000, all plaques are identified but not filled in.

## 2.7 Statistics

### 2.7.1 Immunofluorescence imaging

”In order to control for confounding effects of staining variability, we normalized data to a respective reference point derived from the respective individual mice. For this purpose, light intensities of the whole hippocampus were measured and assigned to the respective day of staining for each mouse brain. Within each group the median was determined and assigned to the respective aging group and genetic status (subsection 2.1.1). Within these homogenous experimental groups, the median was again determined. After that, the respective median was divided by the individual data to obtain the normalization factor, which was multiplied with individual experimental data from the same staining condition.

Normalized light intensity measurements and the unprocessed plaque load detection data were allocated to their respective group of age and their transgene status. The Mann-Whitney-U test was used as a test for significance.” (Published in C. Rupprecht, Sarker, et al. (2022)). Based on the rank-sum and the sample size  $U_1$  (Equation 2.1) and  $U_2$  (Equation 2.2) or  $z$ -values (Equation 2.3) were calculated. Both groups’ results were chosen and compared to a predetermined reference value on a significance level of  $\leq 5\%$ .

$$U_1 = n_1 * n_2 + \frac{n_1 * (n_1 + 1)}{2} - R_1 \quad (2.1)$$

$$U_2 = n_1 * n_2 + \frac{n_2 * (n_2 + 1)}{2} - R_2 \quad (2.2)$$

$$z = \frac{U - \frac{n_1 * n_2}{2}}{\sqrt{\frac{n_1 * n_2 * (n_1 + n_2 + 1)}{12}}} \quad (2.3)$$

Receiver-Operating-Characteristics (ROC) curves combined with area under the curve (AUC) values were used to quantify effect sizes. The AUC value is the area under the ROC curve and represents the accuracy of a diagnostical test. A value close to 0 or 1 indicates that two groups can be distinguished by measuring this parameter (indicating high test accuracy). In contrast, a value close to 0.5 indicates that no differentiation can be made (indicating poor test accuracy). This approach can be extended to evaluate effect sizes, whereby a drug’s

efficacy is considered superior if it can effectively discriminate between treated and untreated groups.

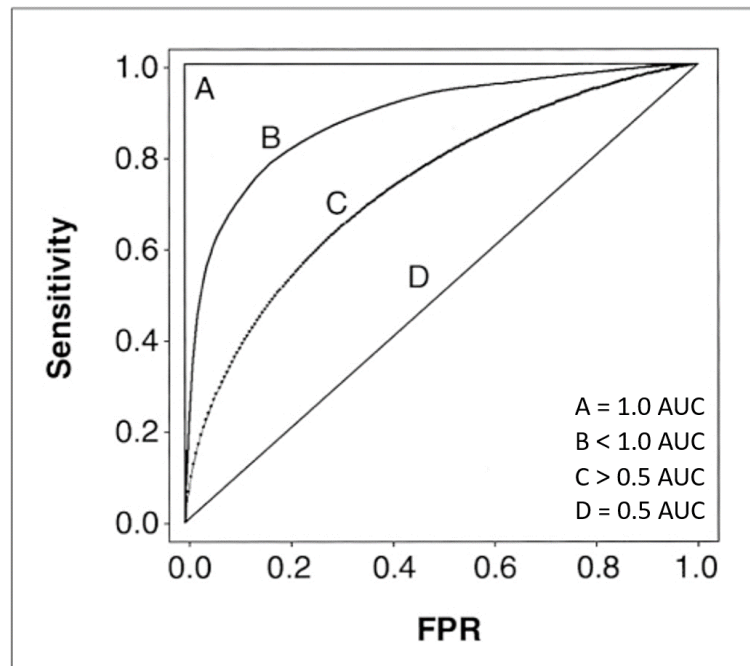


**Figure 2.9:** Examples for ROC curves and AUC values (Park et al. 2004)  
(FPR= false positive rate)

According to Mandrekar (2010) and to Hosmer et al. (2013) an AUC value of 0.5 suggests „no difference/effect“, 0.9 equals a „very strong difference/effect“, 0.8 equals a „strong difference/effect“ and 0.7 equals a „moderate difference/effect“. The interval from 0.5 to 0.7 was defined as „no discernible difference/effect“. The results gain significance if the confidence interval limits lie entirely within one of these defined areas.

AUC value	effect size
0.9-1.0	very strong effect
0.8-0.9	strong effect
0.7-0.8	moderate effect
0.5-0.7	no discernible effect
0.5	no effect

**Table 2.6:** Effect sizes of AUC values

## 3 Results

### 3.1 Morphology

In this section our results and images about the morphological representation of C1q in the brain are described, which have been published in C. Rupprecht, Sarker, et al. (2022).

”Frozen staining methods have the advantage of easy handling, thin tissue sections, and low force on the slices. However, freezing bears the risk of changing or even destroying morphology. In order to gain more clarity about morphological characteristics, we successfully used a newly developed free-floating staining method avoiding freezing.” (published in C. Rupprecht, Sarker, et al. (2022)).

#### 3.1.1 C1q is globally distributed across the entire brain

”Overview images of mouse brain tissue sections revealed a general distribution of C1q across the entire brain (Figure 3.1). Although every part of the brain seems to express C1q to a certain extent, regional differences became apparent. Regions such as the dentate gyrus and some parts of the hippocampal cornu ammonis (CA) layers always showed high expression levels, in contrast to the dendritic region of the hippocampus or certain parts of the brain stem.” (published in C. Rupprecht, Sarker, et al. (2022)).

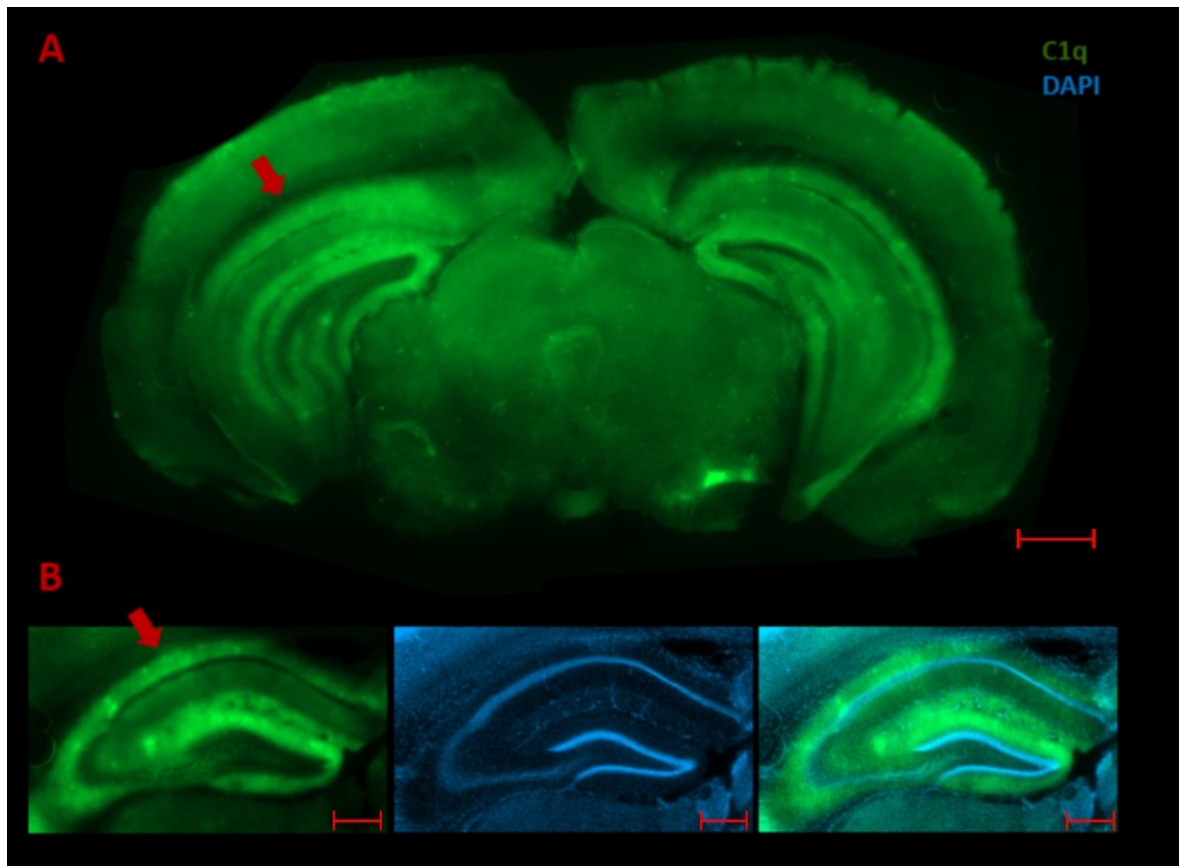


**Figure 3.1:** Immunofluorescence staining reveals an overall C1q distribution across the entire brain. A) Overview image of a whole mouse brain tissue slice stained with abcam 182541 anti-C1q antibody (green). C1q is present across the entire brain with pronounced signals at the dentate gyrus and CA1 region (red arrow). (Scale bar: 1000 $\mu$ m) B) High magnification image of the hippocampus reveals regional differences of C1q deposition. The molecular layer of the dentate gyrus and the stratum oriens of the CA1 regions (red arrow) reveal pronounced signals. In contrast, the stratum pyramidale, stratum radiatum, and the granule cell layer of the dentate gyrus show almost no signal. DAPI (blue) visualizes cell nuclei. (Scale bar: 500  $\mu$ m) (reproduced from C. Rupprecht, Sarker, et al. 2022).

### 3.1.2 Morphology of C1q positive somata is dependent on localization

"Circular C1q signals could be detected using a higher magnification, which always had a DAPI-positive cell nucleus in the center. After excluding interactions with the DAPI staining, we considered those signals "C1q positive somata". These C1q-positive somata are present in every part of the brain. Whereas these are numerous with a circular appearance in the cortex (Figure 3.3B; Cortex), they are elongated and occur more rarely in the CA1 region of the hippocampus (Figure 3.3B; CA1). In addition, the CA4 region (Figure 3.3B; CA4)

was characterized by strong staining of somata with apparent connections between the single somata signals.

Occasionally, we observed densely packed groups of C1q somata, mainly in the CA2 and CA3 regions of the hippocampus (Figure 3.2). These fields are limited to the CA cell body layer and show prominent staining signals. Whereas those signals in the CA2 layer appear well ordered and with small extensions in the direction of the dendritic zone, the signals in the CA3 area seem to stay in closer connections with each other, comparable to the network system observed in the CA4 region.” (published in C. Rupprecht, Sarker, et al. (2022)).

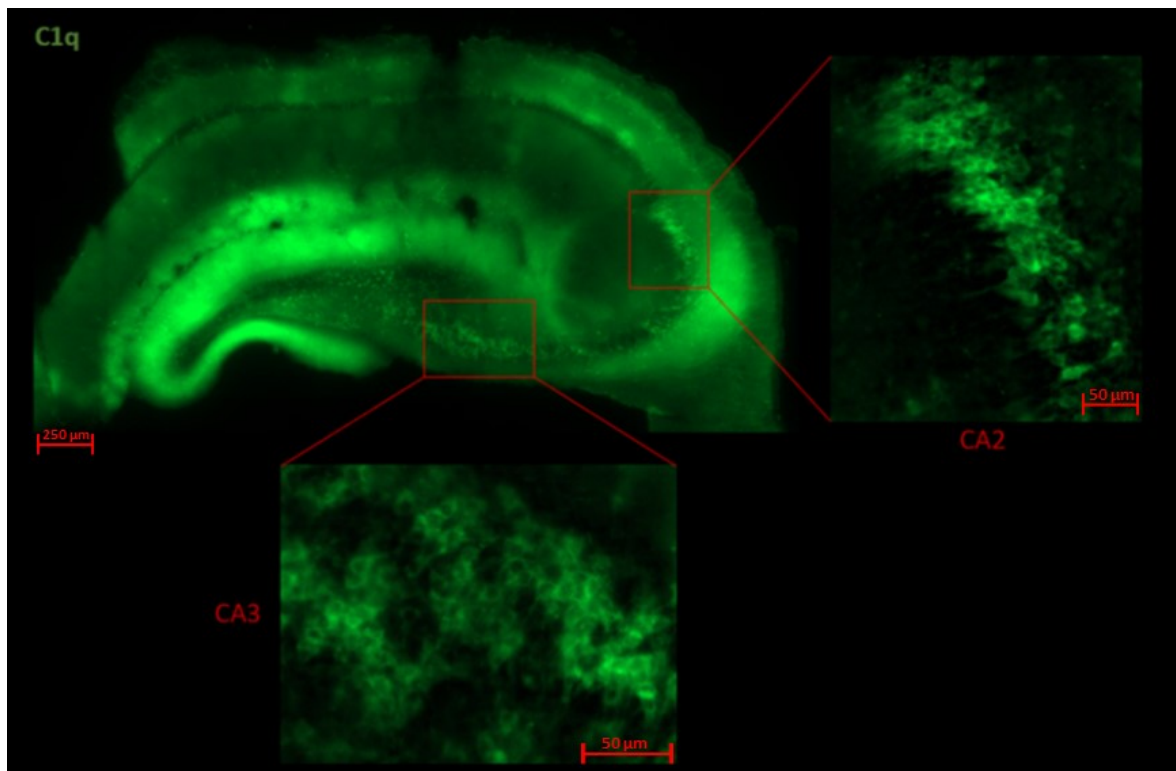


**Figure 3.2:** Densely packed C1q somata in the stratum pyramidale of the CA2 and CA3 region: left-upper picture: Overview image of the C1q distribution across the hippocampus. right-upper picture: High magnification image of C1q somata fields in the CA2 region left-lower picture: High magnification image of C1q somata fields in the CA3 region (Figure reproduced from C. Rupprecht, Sarker, et al. 2022).

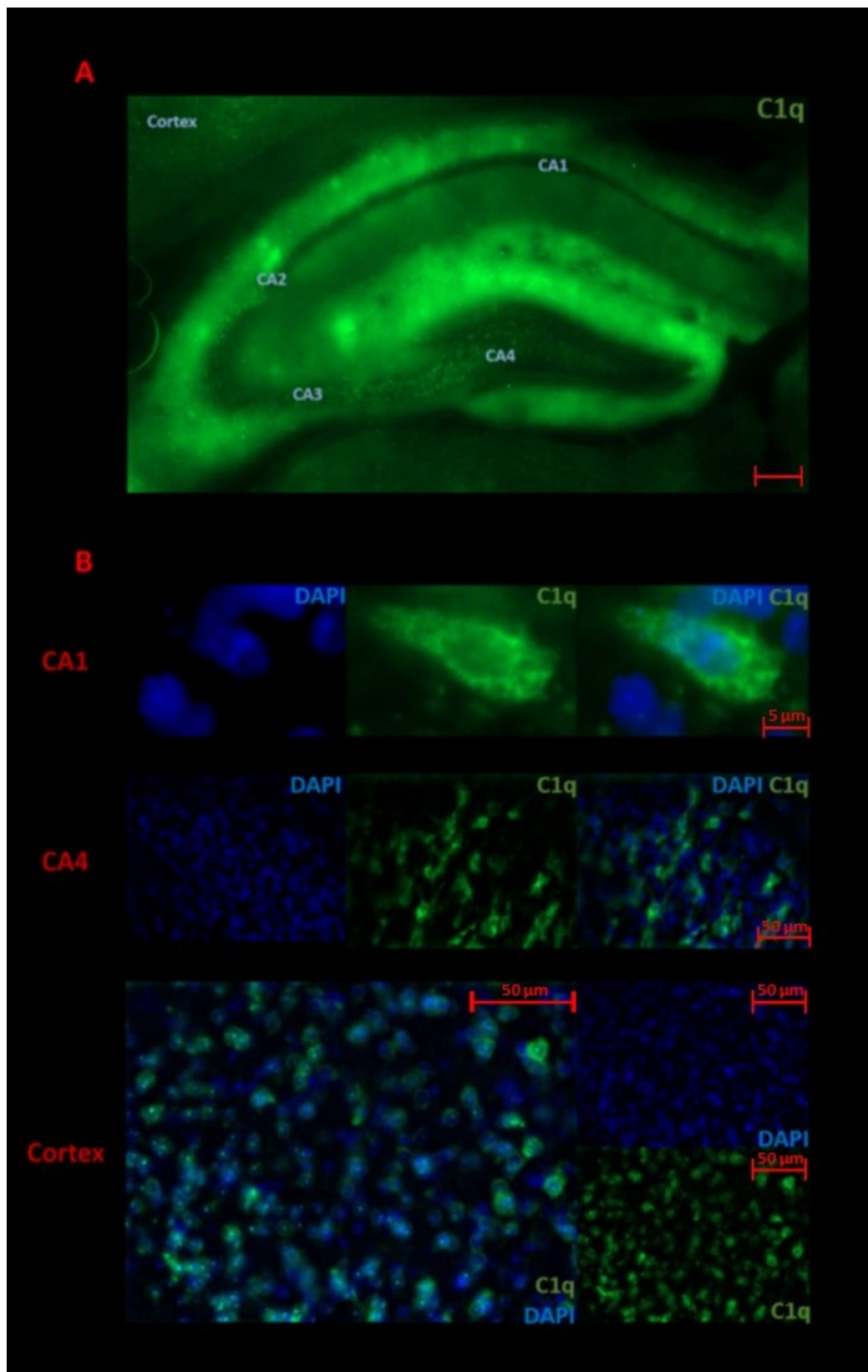


**Figure 3.3:** The morphology of C1q somata (green) differs across various brain regions. A) Overview of a C1q stained mouse brain slice showing all hippocampus regions. C1q somata are visual in the CA3 and CA4 regions. (Scale bar: 250  $\mu\text{m}$ ) B) The morphological appearance of C1q somata depends on their anatomical localisation. C1q somata appear rare and elongated in the CA1 region, numerous and interconnected in the CA4 region and numerous, sharp limited and circular in the cortex. (reproduced from C. Rupprecht, Sarker, et al. 2022).

### 3.1.3 C1q positive somata can be visualized by different anti-C1q antibodies.

”To confirm antibody specificity for C1q somata, we performed double staining with two different C1q antibodies (ab 182451; ab 71940). Since the staining with both antibodies showed a clear colocalization (Figure 3.4), our next steps aimed to differentiate the cell type underlying C1q positive somata.” (published in C. Rupprecht, Sarker, et al. (2022)).

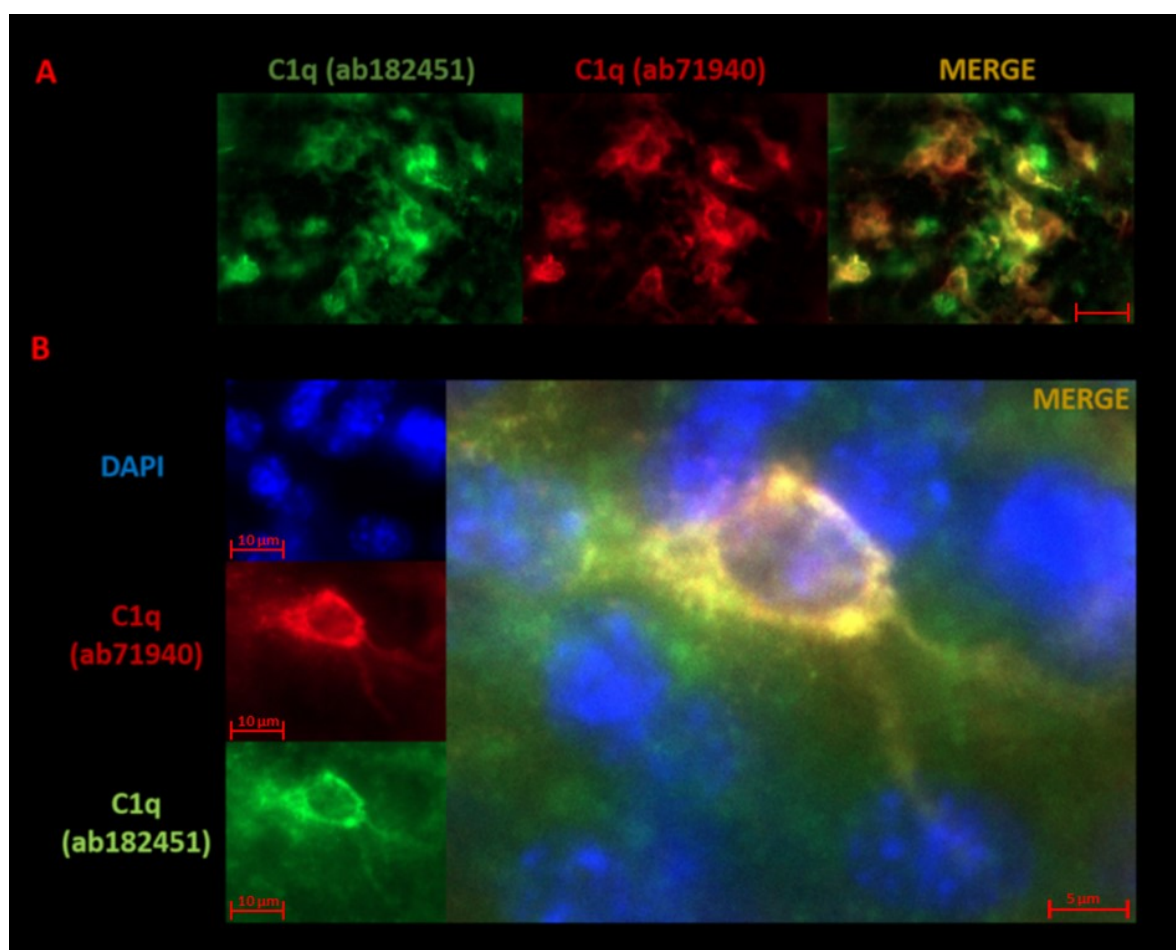


**Figure 3.4:** Double staining of anti-C1q ab182451 and anti-C1q ab71940 proves the specificity of the antibodies for C1q somata (reproduced from C. Rupprecht, Sarker, et al. 2022). A) Overview image of the hippocampal CA4 region showing the confluence of both staining signals. (Scale bar: 25 μm) B) Higher magnification image reveals the distribution of C1q around a DAPI-stained cell nucleus in both C1q stainings. Anti-C1q antibodies show a complete overlap.

### 3.1.4 C1q is located paraneuronal as well as perineuronal around DAPI-positive cell nuclei

”Based on their appearances and localization, we questioned whether neurons are the cellular origin of C1q-positive somata. To test this hypothesis, we performed double staining of MAP2 as a neuronal marker in combination with ab182451 as a marker for C1q. On the one hand, Figure 3.6 demonstrates that C1q somata occur close to MAP2 positive neurons without any connection or interaction, suggesting a paraneuronal glial origin. As an additional double staining of C1q and GFAP excluded astrocytes involvement (Figure 3.5), we hypothesize microglia to be the origin of paraneuronal C1q somata. On the other hand, Figure 3.7 reveals the deposition of C1q along the cell membrane of neuronal cell bodies. As there was a direct morphological correlation but no clear overlap, we suggested a perineuronal deposition (Figure 3.8). Moreover, our results showed that C1q signals cover neuronal cell bodies and extend in the direction of dendrites (Figure 3.7: yellow arrows).” (published in C. Rupprecht, Sarker, et al. (2022)).

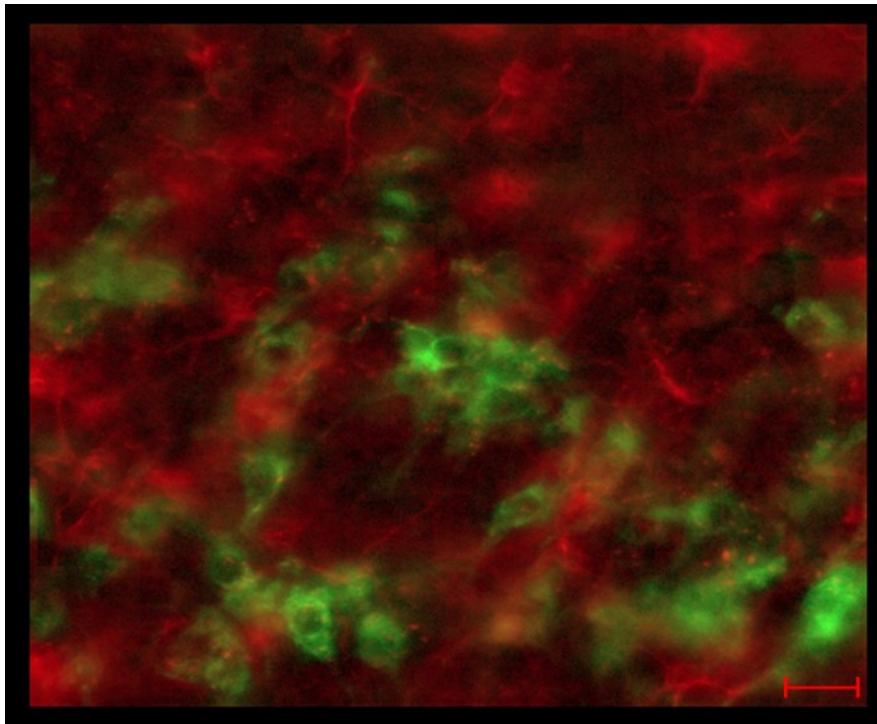


**Figure 3.5:** GFAP positive astrocytes (red) show no overlap or connection to C1q positive somata (green). The image was taken in the hippocampus CA4 region. (Scale bar: 15  $\mu$ m) (reproduced from C. Rupprecht, Sarker, et al. 2022).

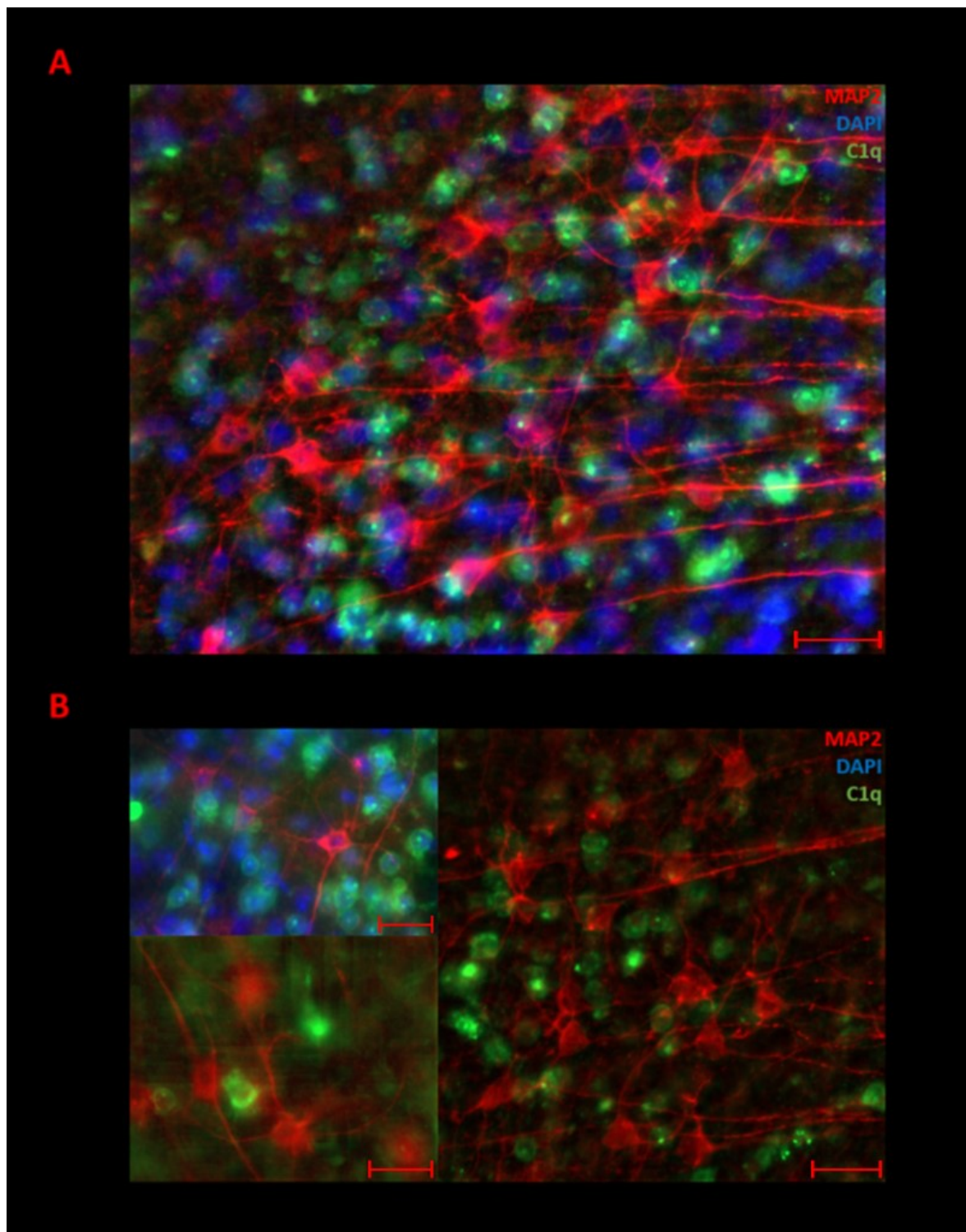


**Figure 3.6:** Paraneuronal C1q in a triple staining of C1q (green), MAP2 (red) and DAPI (blue). C1q somata do not colocalize with MAP2 neurons (reproduced from C. Rupprecht, Sarker, et al. 2022).

A) Overview image showing cortical DAPI stained cell nuclei, C1q somata, and MAP2 positive neurons. C1q somata are located close to MAP2-positive neurons in a paraneuronal position. (Scale bar: 25  $\mu\text{m}$ )

B) Signals of C1q, as well as MAP2, surround DAPI-stained cell nuclei in the cortex as well as in the hippocampus. There was no interaction between MAP2-stained neuronal cell bodies and C1q somata. (Scale bars: 25  $\mu\text{m}$ )

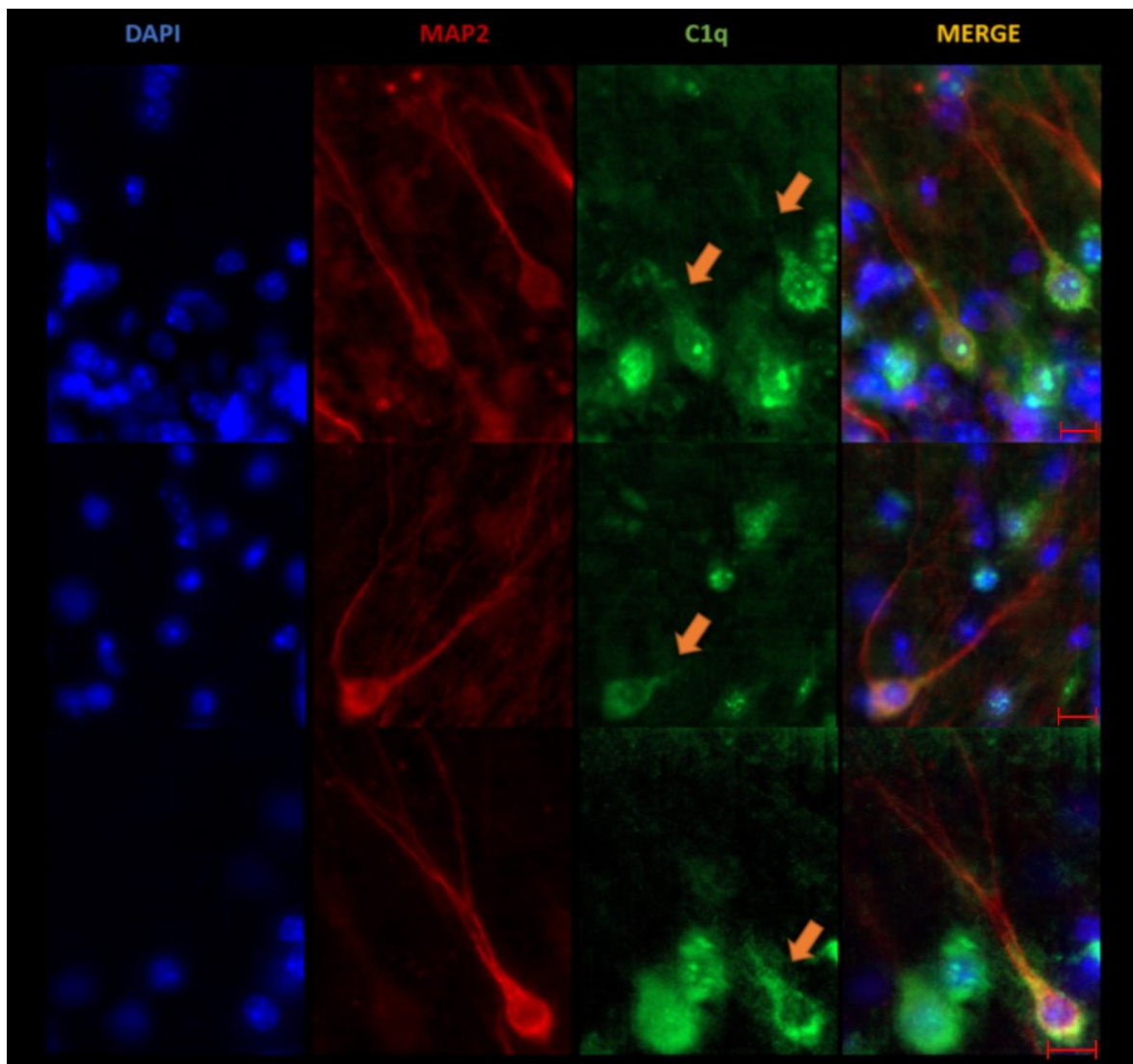


**Figure 3.7:** Triple staining of C1q (green), MAP2 (red) and DAPI (blue) (reproduced from C. Rupprecht, Sarker, et al. 2022):  
C1q somata show a perineuronal position around MAP2 positive neurons. Small protrusions of C1q appear along neuronal dendrites (yellow arrows). Images were taken in the hippocampus. (Scale bars: 10  $\mu$ m)

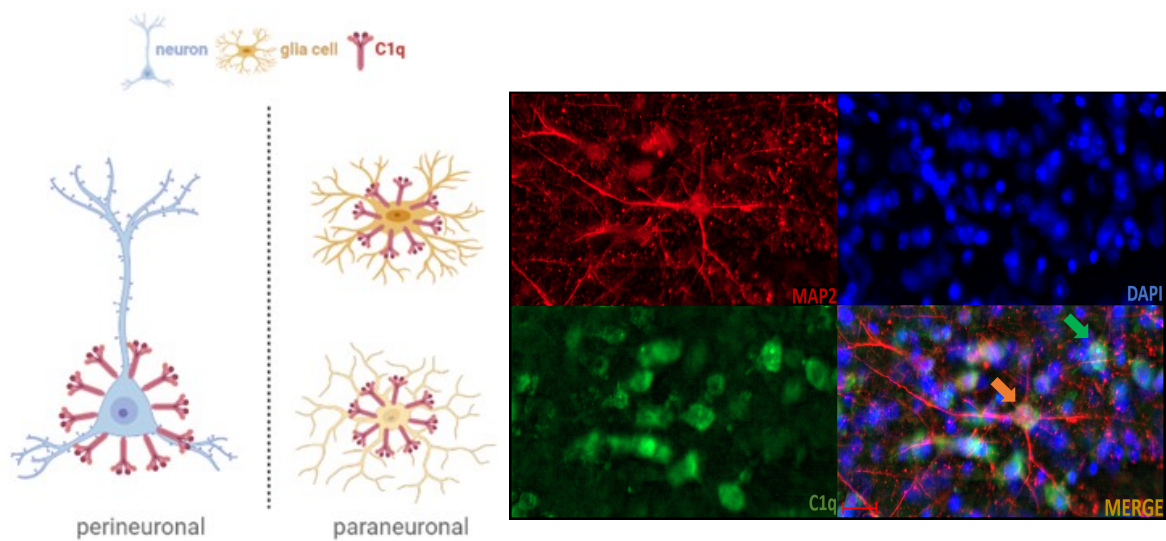


**Figure 3.8:** C1q positions around somata of different cell types. The accumulation around neuronal cell bodies is defined as a perineuronal position (orange arrow), while we use the term paraneuronal for non-neuronal (glial) C1q somata (green arrow). (Scale bar: 20 $\mu$ m) Graph created with BioRender.com (reproduced from C. Rupprecht, Sarker, et al. 2022).

### 3.1.5 C1q dendritic-like structures

”Our results indicate that C1q is not only located perineuronal along neuronal cell bodies but also extends in the direction of dendritic structures. Based on these findings, we investigated whether this phenomenon is only present near the cell body or whether it is also evident around peripheral dendritic structures. Therefore, we defined the stratum radiatum of the CA1 and CA2 region, enriched in basal dendrites and glial cells, as a region of interest and focused on this area with high magnification objectives. Within this ROI, we detected dendritic-like structures (Figure 3.9). These structures primarily arise from C1q-positive somata in the CA layer and extend toward the dentate gyrus. On their way, the signals split up into multiple branches. To exclude any involvement of extensions of astrocytes, we performed double staining of C1q and GFAP (Figure 3.10). Based on the combination of localization, origin, branching, and the exclusion of astrocytic involvement, these signals most likely represent the accumulation of C1q on neuronal dendrites. Their neuronal origin could be substantiated to some extent (Figure 3.12/Figure 3.11), which, however, should be fully elucidated in further studies. Intriguingly, there was no qualitative difference between C1q dendritic-like structures in the transgenic mouse model of Alzheimer’s disease Arc-A $\beta$  and the corresponding wild-type control (Figure 3.9) or between young animals of 6 weeks (data not shown) and older brain sections.” (published in C. Rupprecht, Sarker, et al. (2022)).

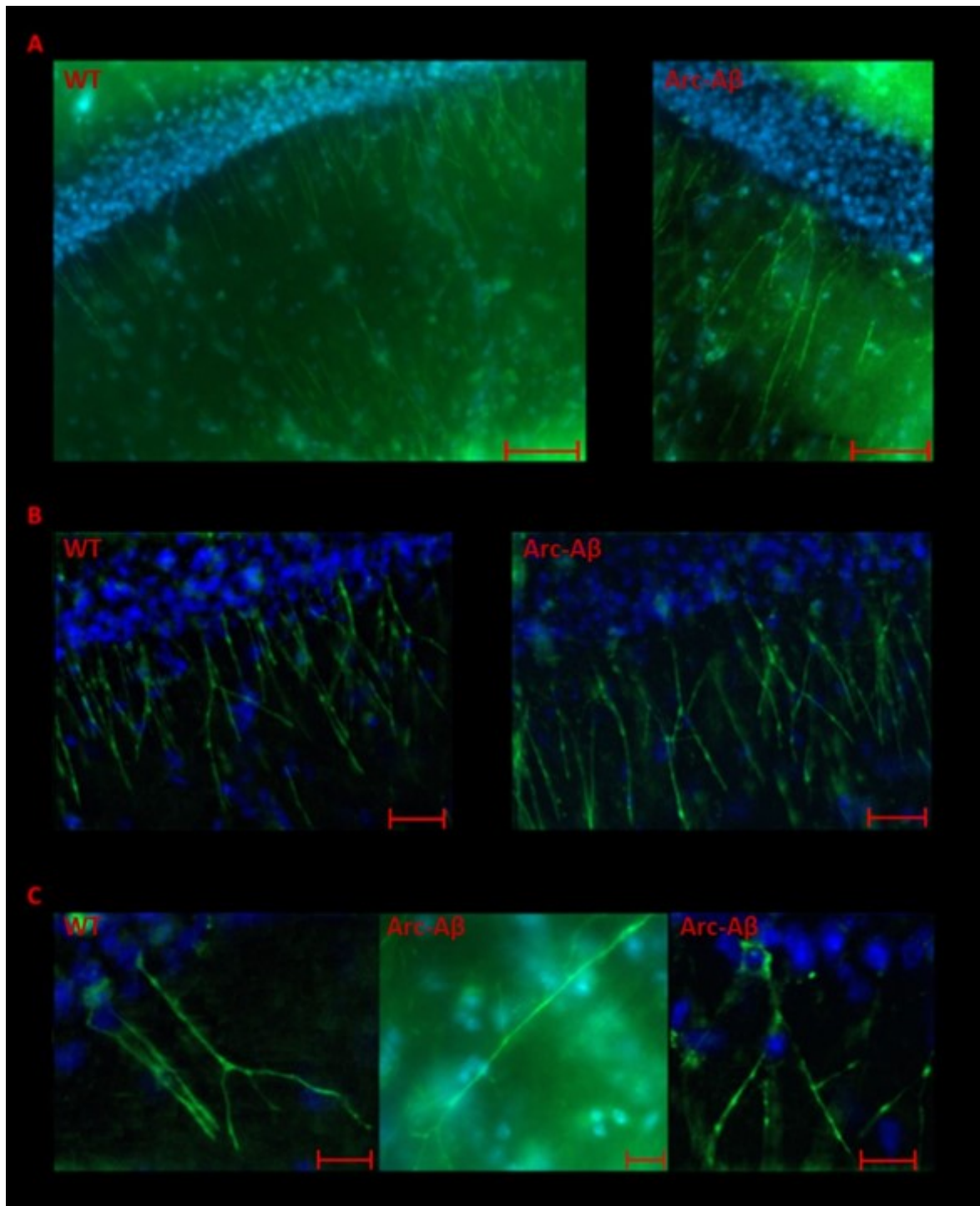


**Figure 3.9:** C1q dendritic-like structure in transgenic *Arc-A $\beta$*  mice and corresponding wild type control (reproduced from C. Rupprecht, Sarker, et al. 2022).  
 A) Staining of C1q (green) and DAPI (blue) showing overview images of the stratum pyramidale (demonstrated by the ring of numerous DAPI-cell nuclei) and stratum radiatum. C1q dendritic-like structures arise from the stratum pyramidale and extend through the stratum radiatum toward the dentate gyrus. (Scale bars: 60  $\mu$ m)  
 B) 40x images showing numerous C1q dendritic-like structures in the stratum pyramidale and upper stratum radiatum. A division of the signals into first-side branches is apparent. (Scale bars: 30  $\mu$ m)  
 C) Single C1q dendritic-like structures demonstrated by images with 100x and 63x magnification. C1q dendritic-like structures rise from C1q somata and extend toward the dentate gyrus. On its way the signals splits into up to three side branches. (Scale bars: 15  $\mu$ m)

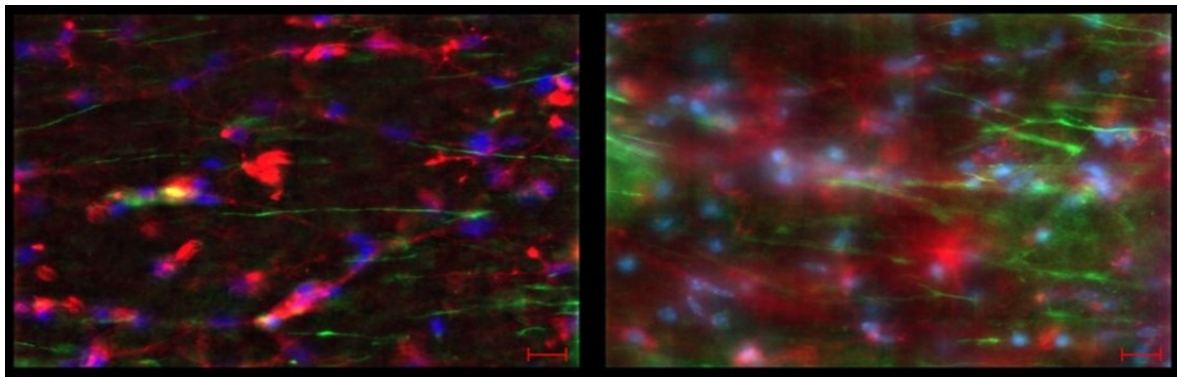


**Figure 3.10:** Triple staining of C1q (green), DAPI (blue) and GFAP (red): C1q dendritic-like structures are shown in a field of astrocytes without any interaction, correlation or overlap. (Scale bars: 15  $\mu$ m) (reproduced from C. Rupprecht, Sarker, et al. 2022).

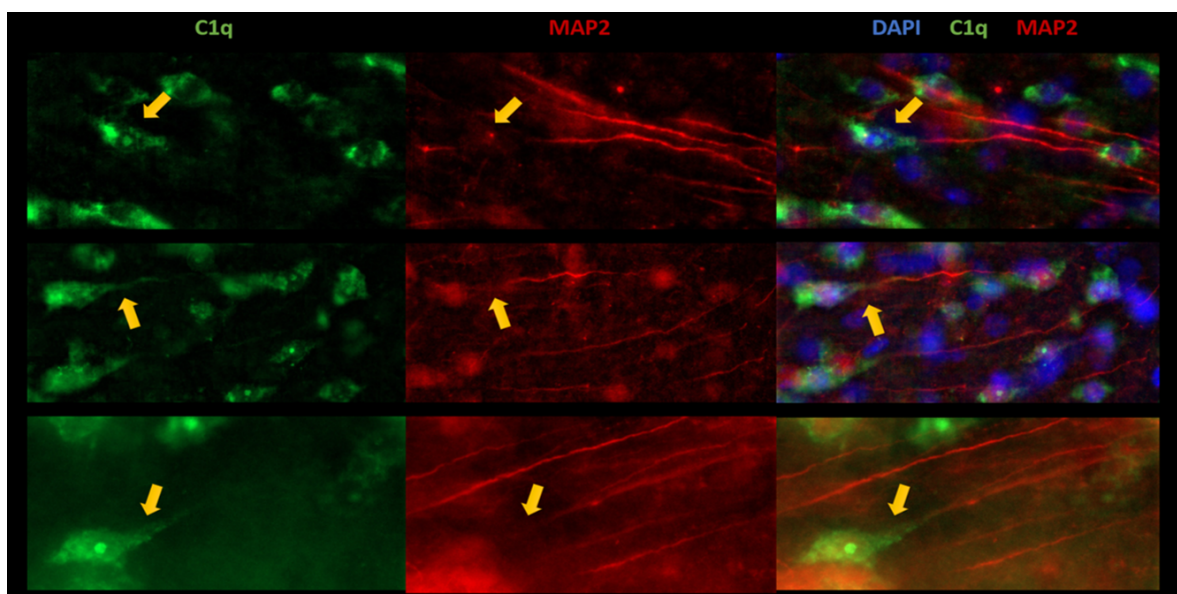


**Figure 3.11:** Possible antibody interference in the double staining of C1q (green) and MAP2 (red). The C1q staining is weak or even missing in areas of intense MAP2 staining (yellow arrows) and vice versa. Since both signals flow into one another, a neural origin is still likely. Images were taken in the hippocampus CA1 region.

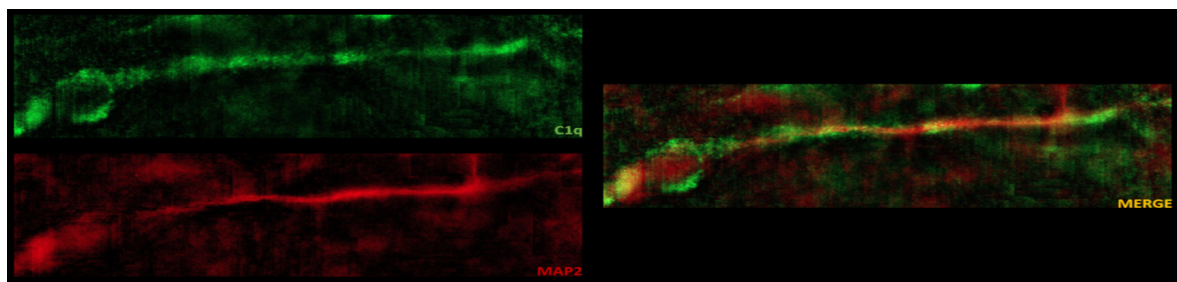


**Figure 3.12:** Colocalisation of C1q dendritic like structures and MAP2 positive neuron. Images were taken in the hippocampus CA1 region.

### 3.1.6 C1q accumulates in mouse models of Alzheimer's disease

”Depositions and accumulations of C1q in the form of plaques are only present in mouse models of Alzheimer's disease and are mainly localized in the cortex and the hippocampus (Figure 3.13A). Based on their formation and location, we assumed a relationship between C1q and  $\beta$ -amyloid plaques based on their formation and location. To investigate this assumption more closely, we performed double staining of C1q and methoxy-X04, a marker for amyloid plaques. The results presented in Figure 3.13C showed a continuous overlap of both markers. (...). Additional double staining of GFAP and C1q revealed that astrocytes surround C1q plaques and their processes were in contact with them suggesting a functional interaction (Figure 3.13D).” (published in C. Rupprecht, Sarker, et al. (2022)).

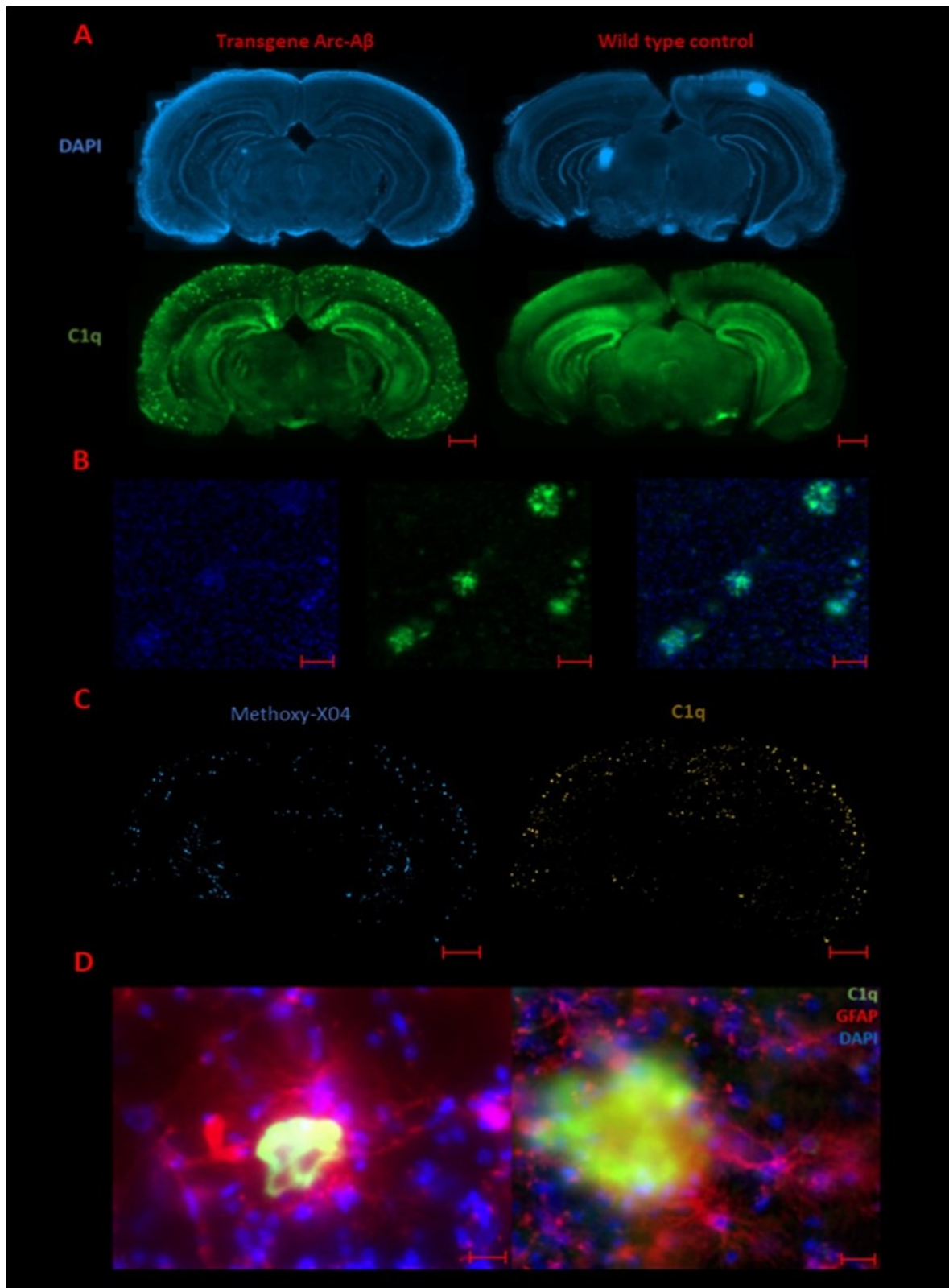


**Figure 3.13:** Morphology of C1q (green) in transgenic arc-A $\beta$  mice, a mouse model for Alzheimer's disease (A) reproduced from C. Rupprecht, R. Rupprecht, et al. 2021 and B-D) from C. Rupprecht, Sarker, et al. 2022):

A) Overview images of transgenic arc-A $\beta$  mice in comparison to the corresponding wild-type control. C1q plaques only occur in the transgenic animal line and are mainly located in the cortex and the hippocampus. (Scale bars: 1000  $\mu$ m)

B) C1q plaques in a field of cortical neurons. Some plaques revealed an increased concentration of cell nuclei (blue). (Scale bars: 100  $\mu$ m)

C) C1q plaques completely overlap with methoxy-X04, a marker for  $\beta$ -amyloid deposition. (Scale bars: 1000  $\mu$ m)

D) Astrocytes do not only surround C1q plaques but also reach out into the plaque area with their processes. (Scale bars: 15  $\mu$ m)

## 3.2 The effect of age, AD and anesthetics on brain C1q

This section in part was prepublished in C. Rupprecht, R. Rupprecht, et al. (2021) and C. Rupprecht, Sarker, et al. (2022).

The second component aims to investigate variations in C1q expression during physiological aging, the prevalence of AD, and after anesthetic exposure. We quantified C1q levels through two distinct modalities. Firstly, light intensity measurement was employed to assess the overall C1q level, explicitly targeting the CA1 region and the dentate gyrus. Secondly, plaque load detection monitored changes in C1q aggregates within the cortical area.

### 3.2.1 C1q increase during normal aging

Figure 3.15 demonstrates an age related effect on hippocampal C1q expression. Mice at the age of 20 months showed significantly elevated levels of C1q both in the dentate gyrus (Figure 3.14/Figure 3.15a) and the CA1 region (Figure 3.14/Figure 3.15c) relative to 15 months old animals. Notably, regional differences were evident within the hippocampus, with a more substantial increase detected in the dentate gyrus than in the CA1 region. Additionally, the age-related effect was more pronounced in the transgenic mouse model for Alzheimer's disease (Figure 3.15b,d). (Adapted from C. Rupprecht, R. Rupprecht, et al. (2021) and C. Rupprecht, Sarker, et al. (2022)).

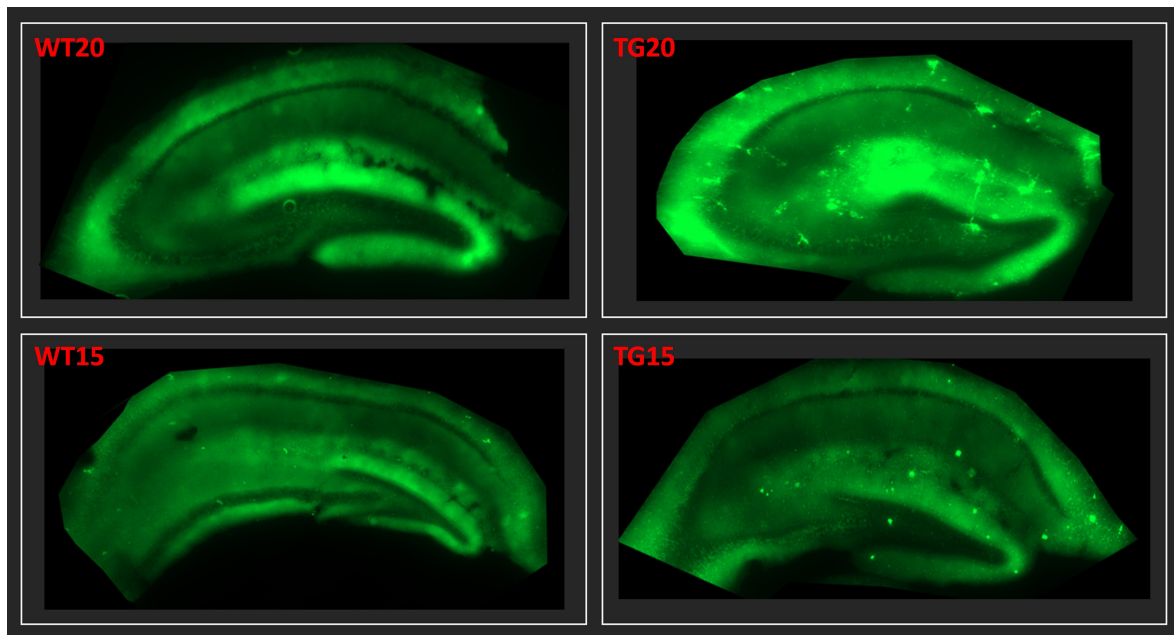


**Figure 3.14:** Light intensity values were calculated from Arc-A $\beta$ -mice (15 and 20 months) and corresponding wild-types (15 and 20 months). (TG: transgenic, WT: wild type) (reproduced from C. Rupprecht, Sarker, et al. 2022).

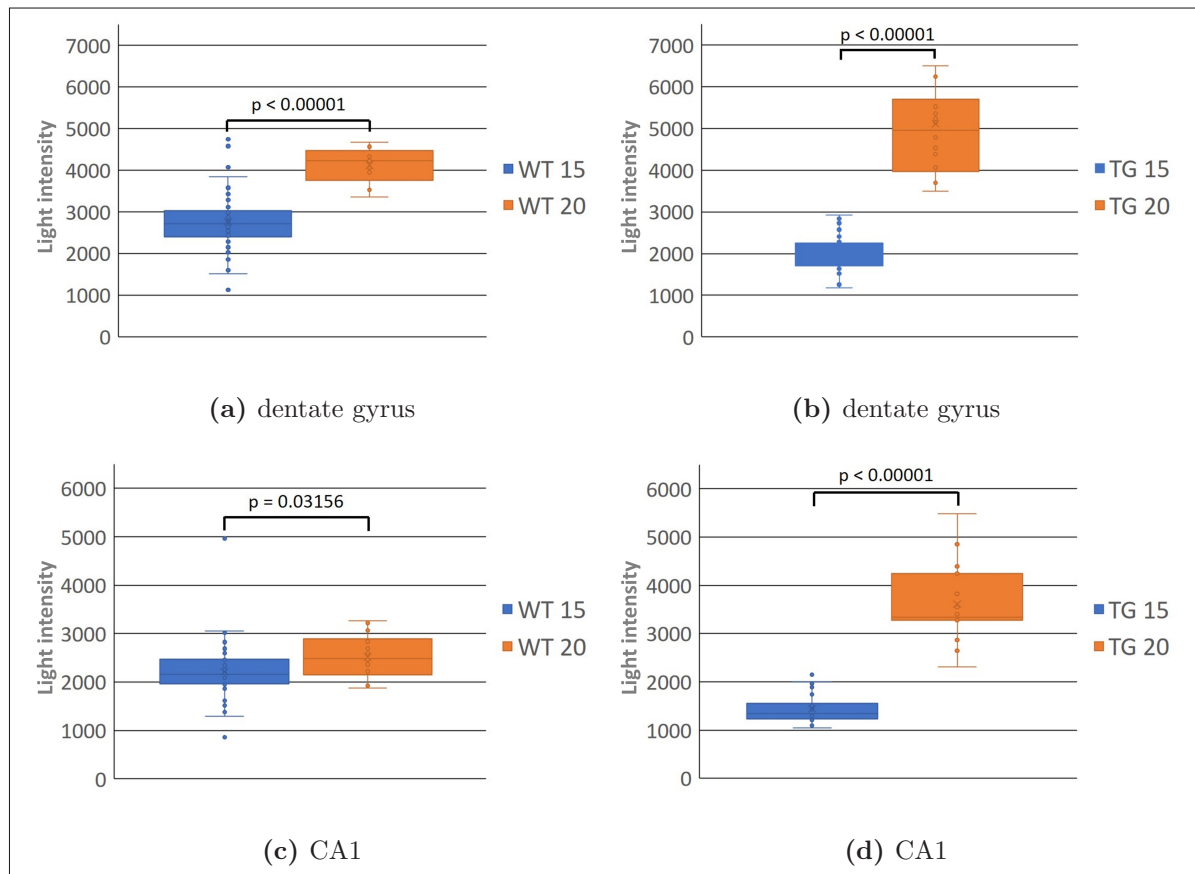


**Figure 3.15:** C1q expression within the dentate gyrus differs significantly between 15- and 20-month-old animals (Mann–Whitney U test:  $p < 0.00001$ ). This effect is even more pronounced in the transgenic mouse model (TG: transgenic, WT: wild type) ( a) and b) reproduced from C. Rupprecht, R. Rupprecht, et al. 2021).

This investigation revealed that aging exerts a significant impact not only on basal C1q levels but also on C1q plaque formation. Cortical plaque concentrations markedly increased in our transgenic Alzheimer mouse model within the five-month test period (Figure 3.16). In contrast no plaques were observed in the corresponding wild-type group, regardless of age. (Adapted from C. Rupprecht, R. Rupprecht, et al. (2021) and C. Rupprecht, Sarker, et al. (2022)).

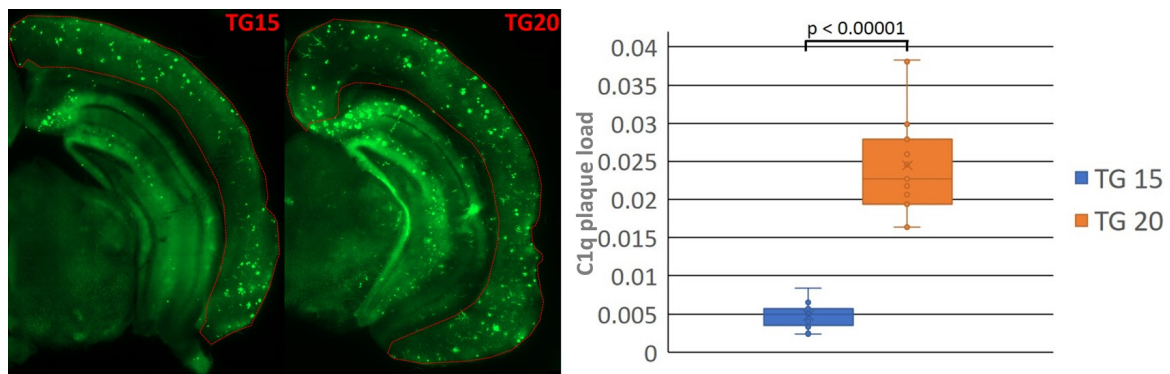


**Figure 3.16:** Plaque load detection reveals a significant increase of C1q plaques in transgenic Arc-A $\beta$ -mice between the age of 15 and 20 months. (Mann–Whitney U test:  $p < 0.00001$ ) (TG: transgenic, WT: wild type) (reproduced from C. Rupprecht, Sarker, et al. 2022).

### 3.2.2 C1q levels are altered in Arc-A $\beta$ -mice

15 months old transgenic arc-A $\beta$  mice displayed significantly lower concentrations of C1q in both the dentate gyrus (Figure 3.17a) and CA1 region (Figure 3.17c) of the hippocampus. This effect reversed at the age of 20 months, with transgenic mice exhibiting significantly higher C1q levels in both regions (Figure 3.17b,d). (Adapted from C. Rupprecht, R. Rupprecht, et al. (2021) and C. Rupprecht, Sarker, et al. (2022)).

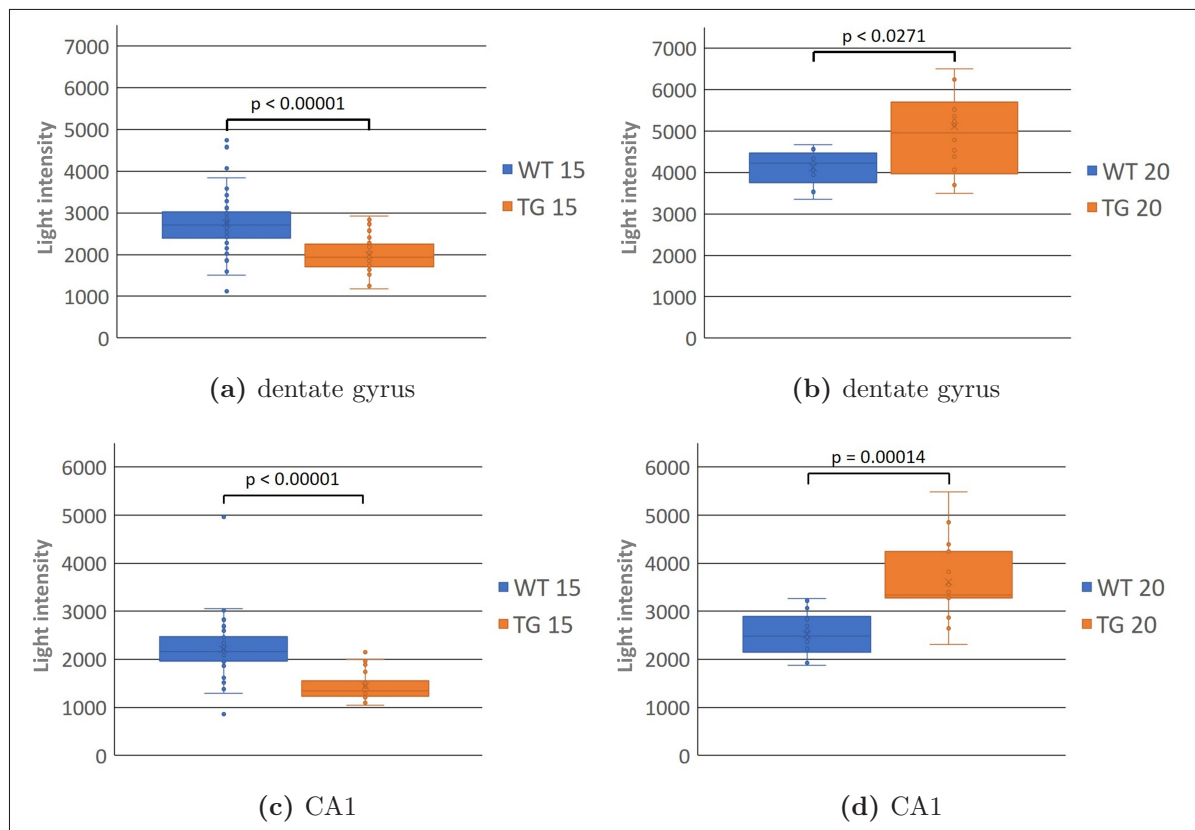


**Figure 3.17:** Light intensity measurements show suppressed C1q levels both in the CA1 region and the dentate gyrus in Arc-A $\beta$  mice at the age of 15 months (Mann–Whitney U test:  $p < 0.00001$ ). However, at 20 months, there was a significant increase in C1q light intensity in both groups (Mann–Whitney U test:  $p < 0.03$ ). (TG: transgenic, WT: wild type) (reproduced from C. Rupprecht, Sarker, et al. 2022).

### 3.2.3 The effect of xenon and isoflurane on brain C1q levels

Following an incubation period of mouse brain slices with xenon and isoflurane we analyzed C1q levels through light intensity measurements in two discrete hippocampus regions. The collected data were then stratified into four distinct categories based on region, age, and transgenic status, as depicted in Figure 3.18, Figure 3.19, Figure 3.20 and Figure 3.21.

In both the dentate gyrus and CA1 region, administration of anesthetics did not result in a statistically significant increase in C1q levels. Furthermore, the apparent observed significant decrease in C1q levels induced by isoflurane (Figure 3.18b) could not be detected within the wild-type control (Figure 3.18a), within the CA1 region data (Figure 3.20a,b) as well as in the other age group (Figure 3.19a,b, Figure 3.21a,b).

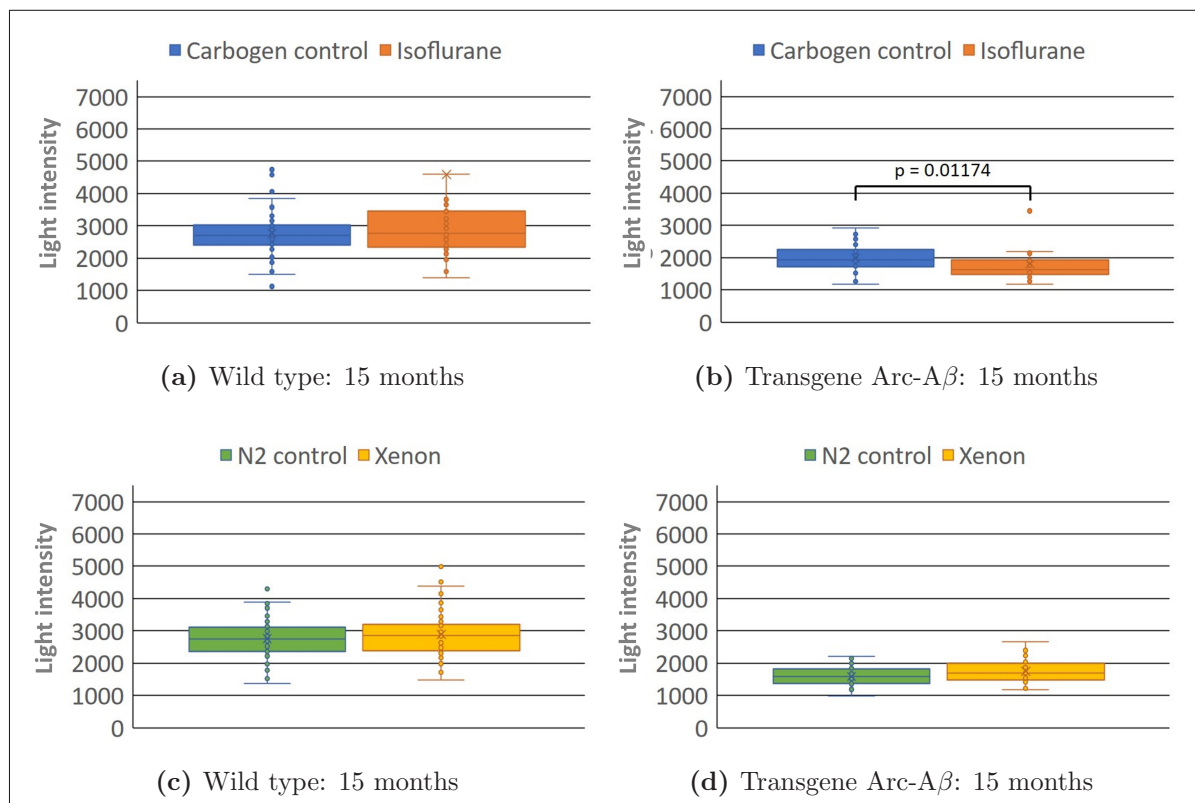


**Figure 3.18:** Light intensity measurements of the dentate gyrus do not show significant elevations of C1q in either the transgenic Arc-A $\beta$  group or the corresponding wild type control (Mann-Whitney U test:  $p > 0.05$ ). There was a significant decrease in the transgenic group after isoflurane incubation (Mann-Whitney U test:  $p < 0.012$ ).

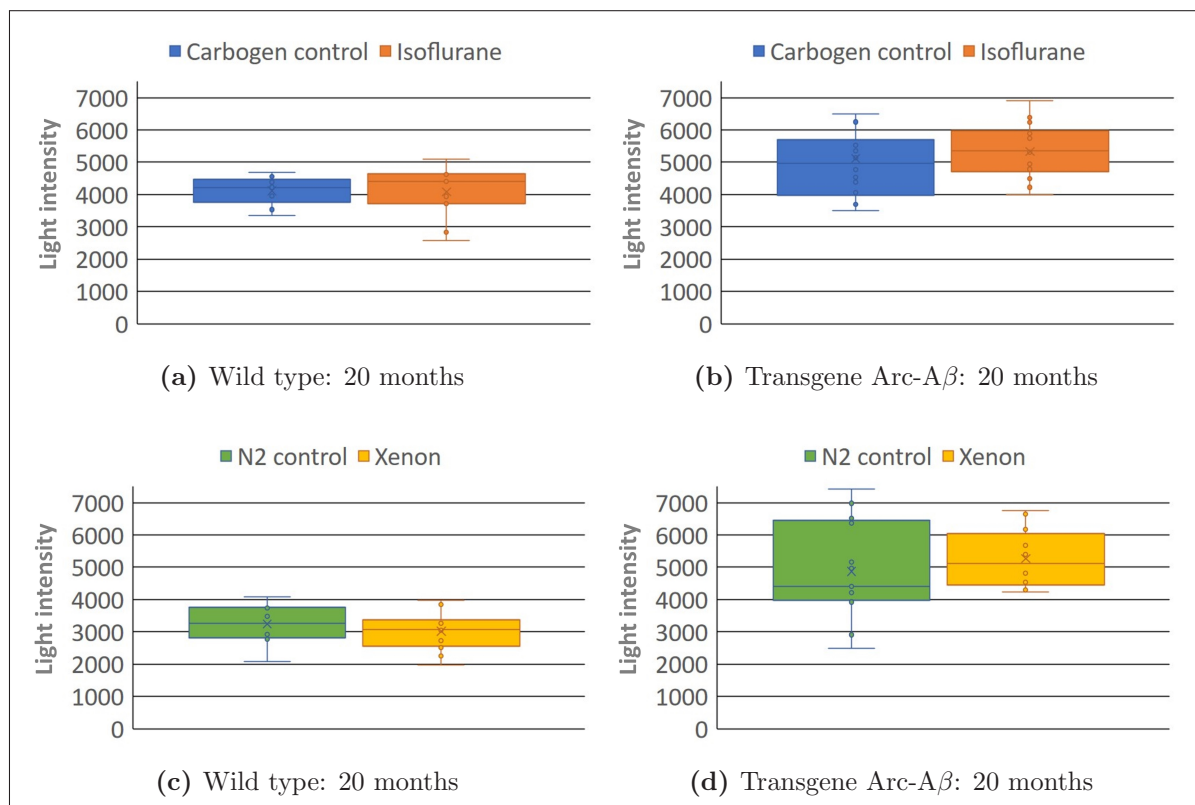


**Figure 3.19:** Light intensity measurements of the dentate gyrus do not show significant elevations of C1q after xenon or isoflurane incubation in either the transgenic Arc-A $\beta$  group or the corresponding wild-type control (Mann-Whitney U test:  $p > 0.05$ ).

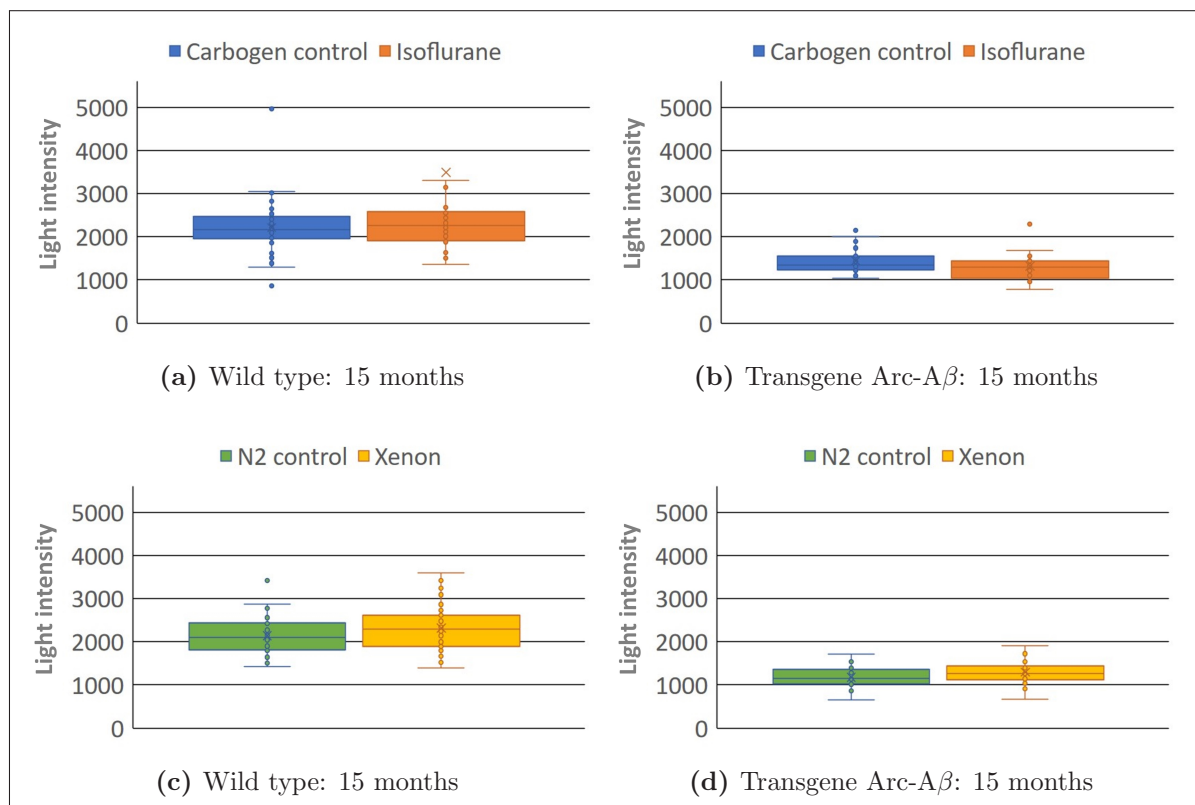


**Figure 3.20:** Light intensity measurements of the CA1 region do not show significant elevations of C1q after xenon or isoflurane incubation in either the transgenic Arc-A $\beta$  group or the corresponding wild type control (Mann-Whitney U test:  $p > 0.05$ ).

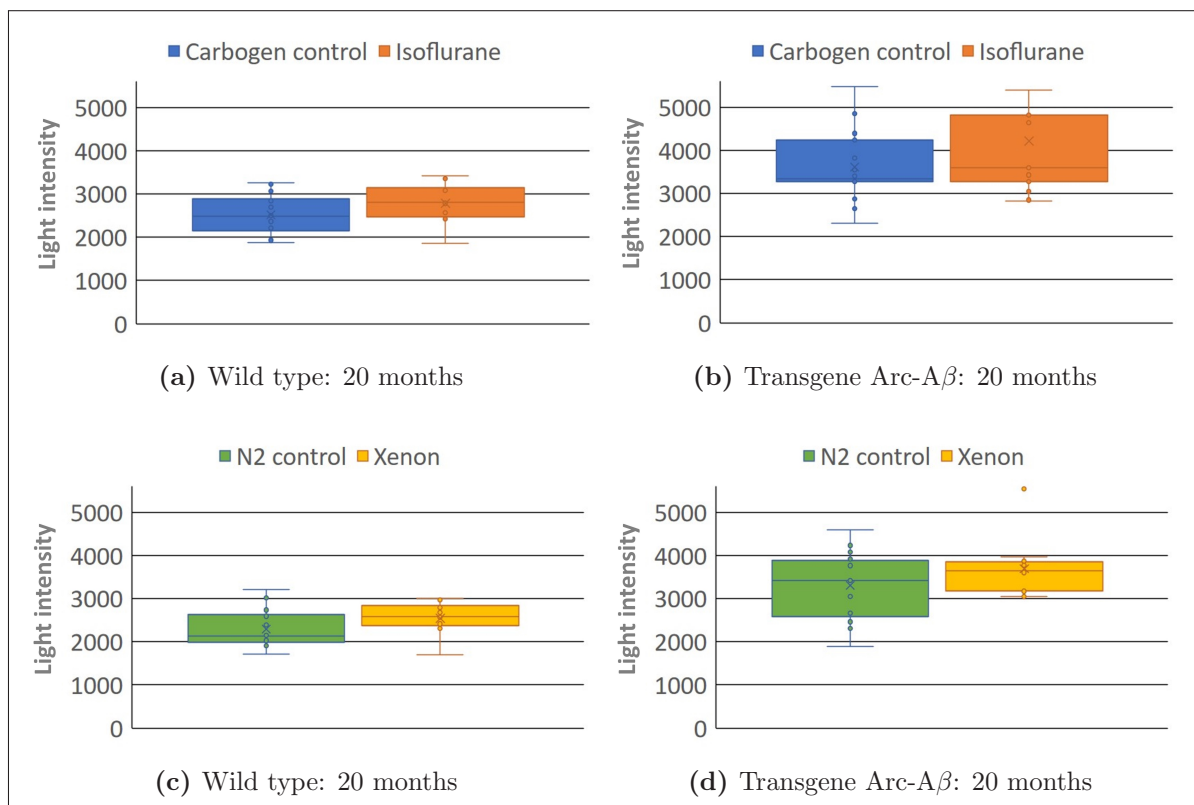


**Figure 3.21:** Light intensity measurements of the CA1 region do not show significant elevations of C1q after xenon or isoflurane incubation in either the transgenic Arc-A $\beta$  group or the corresponding wild type control (Mann-Whitney U test:  $p > 0.05$ ).

To facilitate statistical handling and to test for equality, we calculated AUC values (subsection 2.7.1) for each anatomic region and age group (Figure 3.22). The AUC values for both xenon and isoflurane-treated slices, depicted in Figure 3.22b, Figure 3.22d, Figure 3.22a and Figure 3.22c, showed an average value that is close to 0.5, indicating that the compounds did not have a significant acute effect on C1q levels in this experimental setup. However, the data exhibits a wide range and large standard deviation, which prevents a definitive conclusion and warrants further investigation.

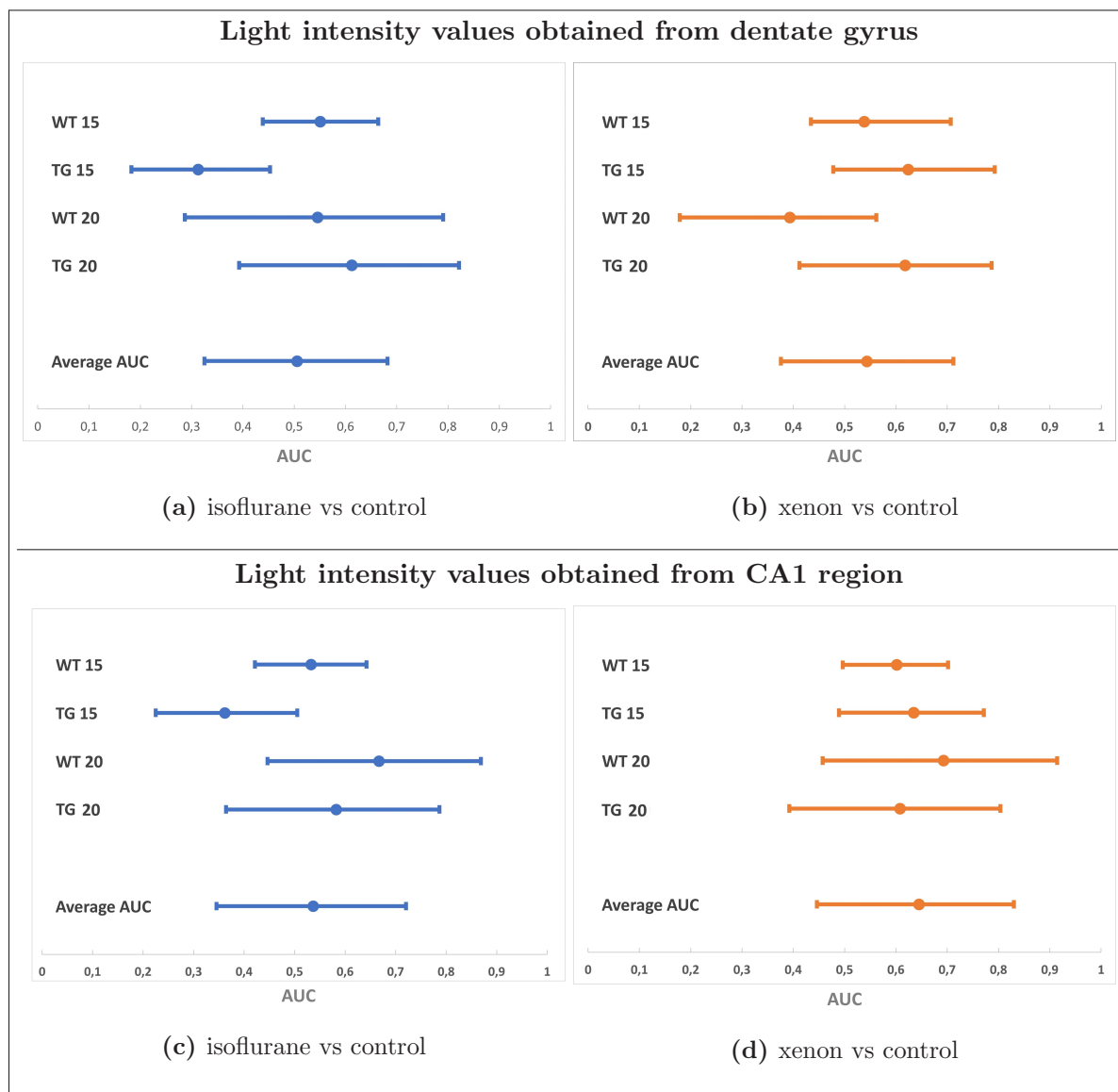


**Figure 3.22:** AUC values are calculated by offsetting a treatment group against the corresponding control and can be used to determine effect sizes (Table 2.6). The following graph shows the average AUC of 0.32-0.72 in the isoflurane and 0.38-0.83 in the xenon group. Even if the mean values do not indicate an acute effect, there is no significance in any group due to the large standard deviation.

Nevertheless, regarding the previously described data, which validated the setup by showing a significant elevation of C1q with increasing age (Figure 3.15), it can be concluded that both xenon and isoflurane affect C1q levels less than the normal aging of 5 months.

## 4 Discussion and Conclusion

Free-floating tissue samples prevent freezing-induced damage, resulting in improved retention of cell structures and antigens, ultimately leading to better tissue morphology and antigenicity preservation. Additionally, free-floating can be used for pharmacological interventions to study the effects of drugs on brain tissue. In this unique technique slices of brain tissue are cut and allowed to float freely in a solution containing nutrients and oxygen. This procedure allows the tissue to remain viable and functional for a short period, typically a few hours.

### 4.1 Morphology

In this section the morphological representation of C1q in the brain is discussed, which has been published in C. Rupprecht, Sarker, et al. (2022).

Our experimental free-floating setup provided the possibility to investigate the morphology of C1q in the brain. We replicated all previously described morphological features and combined them in one staining. Moreover, we detected C1q dendritic-like structures. A more detailed understanding of the morphology helps us to better understand the functioning of the immune system and how it responds to different pathogens and diseases. (Adapted from C. Rupprecht, Sarker, et al. (2022).)

"In overview images of cerebral sections and the hippocampus, we confirmed basal C1q levels distributed over the whole brain (Figure 3.1). Within this overall distribution, we detected an accumulation of C1q on cell bodies and described their morphological features dependent on their respective localization (Figure 3.2, Figure 3.3). The interaction of C1q with somata was two-fold (Figure 3.8). On the one hand, C1q has a perineuronal position around MAP2-positive somata (Figure 3.7). On the other hand, paraneuronal C1q seems to colocalize with glia cells (Figure 3.6). Intriguingly, our setup revealed "C1q positive dendritic-like structures" within the dendritic zone of the hippocampus (Figure 3.9). Even though its neuronal origin could be substantiated to some extent, a detailed elucidation is

needed in further studies. Finally, we were able to demonstrate the deposition of C1q within plaques. (...). Complementary stainings revealed an overlap with  $\beta$ -amyloid accumulation and interaction with astrocytes (Figure 3.13).” (published in C. Rupprecht, Sarker, et al. (2022))

”In overview images of cerebral sections and the hippocampus, we confirmed basal C1q levels distributed over the entire brain (Figure 3.1). Studies in neuroinflammation often used this type of C1q distribution as a starting point for different quantification methods (Hammond et al. 2020; T. Wu et al. 2019), but only a few studies dealt with morphology itself. Stephan et al. (2013) showed that basal C1q is already present in mouse pups of 6 weeks but dramatically increases with normal aging. The expression at young age can be related to the function of C1q during brain development. As an ”eat me signal,” C1q recognizes excessive synapses and leads to complement-dependent synaptic pruning, thereby avoiding immature brain circuitries (Rosa C. Paolicelli et al. 2011). However, this does not explain the increasing levels of C1q during normal aging since these processes show a significant reduction in adulthood (Petanjek et al. 2011). We hypothesize that in older age, C1q is involved in different cellular processes. On the one hand, C1q might be present in an inactive form to provide readiness for the execution of inflammatory processes, as they occur in defense of streptococcus infections (T. A. Rupprecht et al. 2007). On the other hand, C1q can also exert neuroprotective properties (Benoit and Tenner 2011). Further studies should address the physiological role of C1q at a higher age. Besides its essential physiological functions, C1q is most likely part of the pathophysiology behind neurodegenerative disorders. Hong et al. (2016) demonstrated that the early synapse loss in Alzheimer’s disease is complement-dependent, indicating a pathological reactivation of synaptic pruning mechanisms.” (published in C. Rupprecht, Sarker, et al. (2022)). These facts align with our previous results showing increased basal C1q in a mouse model of Alzheimer’s disease (C. Rupprecht, R. Rupprecht, et al. 2021; Reichwald et al. 2009). (Adapted from C. Rupprecht, Sarker, et al. (2022)).

”In the next step, we focused on the putative cellular target structures of C1q. Previous literature revealed some inconsistency about the interaction of C1q with neuronal cell bodies. Lopez et al. (2012) described perineuronal extracellular C1q in the CA2 region of the hippocampus, Fonseca, Chu, Hernandez, et al. (2017) C1q surrounding YFP positive neurons in the CA1 region, and Stephan et al. (2013) C1q inside of GABAergic neurons. In the literature, however, these accumulations seem to be rather relatively rare. It is of note that our slices show a greatly increased number of C1q positive somata as well as the formation of connected systems and organized fields (Figure 3.2, Figure 3.3). Despite the difference in the amount of expression, our results align with the findings of Lopez et al. (2012) reporting a perineuronal position of C1q around MAP2 positive neurons (Figure 3.7).” (published in C. Rupprecht, Sarker, et al. (2022)).

”Consistent with the previously reported structures, we identified a considerable amount of C1q somata in a paraneuronal position without any correlation or interaction to MAP2 positive neurons (Figure 3.6). Since microglia are the dominant sources of C1q in the brain (Fonseca, Chu, Hernandez, et al. 2017), we assume that paraneuronal C1q somata result from an increased microglial C1q expression. This thesis is in line with previous results, which showed an overlap of perinuclear C1q with microglia (Kawai et al. 2020).” (published in C. Rupprecht, Sarker, et al. (2022)).

”In our experiments, we noticed linear, branched C1q signals between the CA1 and CA2 somata layer and the dentate gyrus of the hippocampus (Figure 3.9). Based on the localization, branching, and origin, we supposed an accumulation of C1q on dendrites. These dendritic-like structures stood out from their surroundings due to their solid signals and concise morphology. Although there were hints of dendritic-like C1q structures in various brain regions, they could only be clearly detected in the hippocampus. Previous literature mentions the deposition of C1q only on apical dendrites in pathological brain tissue (Afagh et al. 1996; Head et al. 2001). In contrast, our data show that C1q surrounds dendrites in total length in healthy brains as well as in the Alzheimer’s mouse model Arc-A $\beta$  (Figure 3.9). On the one hand, those structures might take over a role in neuroprotective processes. On the other hand, potential involvement in neurodegenerative synaptic pruning mechanism should be of interest in further studies. In this context, the source of the dendritic C1q is of high importance, as those structures might point to TGF- $\beta$  induced neuronal C1q expression (Bialas and Stevens 2013).” (published in C. Rupprecht, Sarker, et al. (2022)).

”For many years, genetic mouse models have been used to research Alzheimer’s disease (AD). A histological feature of AD is the deposition of  $\beta$ -amyloid plaques in the brain. However, several studies showed that  $\beta$ -amyloid is not the only protein prevalent in those plaques. Reichwald et al. (2009) demonstrated the accumulation of multiple complement proteins in these areas. Moreover, Fonseca, Chu, Hernandez, et al. (2017) showed that the ”contribution of complement activation” (...) ”differs among various mouse models of Alzheimer’s disease”. For example, C1q plaques were not present in 3xTg mice but in arc-A $\beta$  and TG 2576 mouse models. We investigated whether we could reproduce the data from Fonseca, Chu, Berci, et al. (2011) focusing on the morphological representation of C1q. In our study, we selected methoxy-X04 as a marker for  $\beta$ -amyloid accumulation. Our previous studies showed that the formation of C1q plaques occurs in transgenic ArcA $\beta$  mice and is absent in wild type control animals (Figure 3.13A/(C. Rupprecht, R. Rupprecht, et al. 2021)). Furthermore, we demonstrated that C1q plaques consistently overlap with  $\beta$ -amyloid deposits (Figure 3.13C) (...). Rodríguez et al. (2009) mentioned reactive astrocytes located around  $\beta$ -amyloid plaques. Since our results showed a complete overlap of C1q and  $\beta$ -amyloid plaques, it is not surprising that astrocytes also surround C1q plaques (Figure 3.13D). As C1q

and astrocytes are involved in synaptic pruning mechanisms, those plaques could be a sign of  $\beta$ -amyloid-induced concentrated synapse loss. Further research should address whether the accumulation of microglia and astrocytes around  $\beta$ -amyloid plaques is complement-dependent and whether those cells show increased synaptic pruning activity compared to  $\beta$ -amyloid independent glia cells.” (published in C. Rupprecht, Sarker, et al. (2022)).

”In conclusion, our study revealed a differential morphological representation of C1q in the brain concerning cellular and subcellular target structures, which might contribute to the complex role of this small molecule in physiology and disease.” (published in C. Rupprecht, Sarker, et al. (2022)).

## 4.2 The influence of age and AD on brain C1q

In this section the influence of age and AD on brain C1q is discussed which has been published in part in C. Rupprecht, R. Rupprecht, et al. (2021) and C. Rupprecht, Sarker, et al. (2022).

In order to deepen our understanding of the function of C1q in both physiological and pathological conditions, it is essential to quantify its levels. We adjusted our free-floating setup to enable the measurement of C1q levels through light intensity measurements.

Our experiments confirmed the effect of age on C1q expression described in the literature (Reichwald et al. 2009; Stephan et al. 2013). Furthermore, we could analyze individual regions of the hippocampus. The C1q concentration increased more within the dentate gyrus than in the CA1 region (Figure 3.15). In the further course, two effects of Alzheimer's pathology on C1q levels (Figure 3.17) occurred. Firstly, the effect of age was intensified in the transgenic arc-A $\beta$  mice (Figure 3.15). Secondly, Alzheimer's pathology showed an effect independent of age. At 15 months, the transgenic status led to significant inhibition of C1q expression (Figure 3.17a/c), while at the age of 20 months, a stimulation occurred (Figure 3.17b/d). Finally, we showed that not only soluble C1q increases with age but also the deposition of C1q within plaques (Figure 3.16). (Adapted from C. Rupprecht, R. Rupprecht, et al. (2021)).

As mentioned in section 1.4, synaptic pruning mechanisms are indispensable for normal brain development. However, studies revealed that C1q levels are initially low in the developing brain but exhibit a steep exponential increase in older age (Reichwald et al. 2009; Stephan et al. 2013). This phenomenon raises the question of why the body increases C1q production during life, given that synaptic pruning is far less pronounced in adulthood (Petanjek et al. 2011). To address this question, we investigated whether age has regional effects on hippocampal C1q levels. Our findings indicate that regions with high levels of C1q expression, such as the hippocampus and the dentate gyrus, are highly susceptible to age-dependent increases in C1q expression (Figure 3.15). Utilizing these data, future investigations may explore molecular distinctions between regions with high and low levels of age-induced C1q stimulation. (Adapted from C. Rupprecht, R. Rupprecht, et al. (2021)).

Since age constitutes a major risk factor for neurodegenerative disorders like Alzheimer's dementia and studies indicate the pathological reactivation of synaptic pruning mechanisms in such insidious diseases, we investigated how transgenic mice models for Alzheimer's pathology affect cerebral C1q levels. On the one hand, we detected an enhancement in age-dependent C1q expression. APP23 mice at nine months showed significantly higher C1q mRNA levels

than the wild-type control, which was even more pronounced in higher age (Reichwald et al. 2009). These results align with our light intensity measurement data (Figure 3.15). "Transgenic Arc-A $\beta$  mice, which are characterized by overexpressing human APP695 with Swedish (K670N/M671L) and Arctic (E693G) mutations and constitute a valid model for pathological  $\beta$ -amyloid deposition (Knobloch et al. 2007), showed a markedly greater increase of C1q during aging in comparison to wild type control animals. On the other hand, Alzheimer's pathology itself may influence C1q expression. For example, mice treated intraventricularly with  $\beta$ -amyloid (A $\beta$ ) showed a significant increase in C1q levels (Hong et al. 2016)." (published in C. Rupprecht, Sarker, et al. (2022)). Our results and those of Reichwald et al. (2009) strongly support an age-dependent C1q expression pattern. At younger age, mouse models for Alzheimer's disease show relatively low C1q levels (Figure 3.17a/c). However, this expression pattern in aged animals is entirely different and shows characteristics of rather elevated brain C1q levels (Figure 3.17b/d). "Further investigations are needed to resolve this age-dependent shift in expression patterns in AD models" (published in C. Rupprecht, Sarker, et al. (2022)) and might provide a therapeutic approach. (Adapted from C. Rupprecht, R. Rupprecht, et al. (2021) and C. Rupprecht, Sarker, et al. (2022)).

"C1q plaques only occur in animal models of AD and are mainly located in the cortex and the hippocampus (Figure 3.13A). Interestingly, those C1q aggregates overlap entirely with A $\beta$  plaques unraveled in respective colocalization experiments (Figure 3.13C). Moreover, also in human postmortem brain tissue of patients suffering from AD it has been shown that increased C1q expression is positively correlated with A $\beta$  plaques (Tooyama et al. 2001)." (published in C. Rupprecht, Sarker, et al. (2022)). Our subsequent quantification experiments revealed that C1q cortical plaque concentration markedly increased in our transgenic Alzheimer mouse model within the five-month test period (Figure 3.16) (adapted from C. Rupprecht, Sarker, et al. (2022)). Comparable studies can only be found on  $\beta$ -amyloid deposition (Hashimoto et al. 2020) (adapted from C. Rupprecht, Sarker, et al. (2022)).

"In conclusion, it can be assumed that synaptic pruning mechanisms can be aberrantly reactivated particularly during older age and thereby contribute to neurodegeneration. This is in line with the well-known phenomenon that age constitutes a major risk factor for neurodegenerative disorders such as AD. Complement proteins such as C1q may play a role as "eat me" signals in this context and opsonize synapses for microglia-mediated phagocytosis. These mechanisms constitute a good example of the cooperation of the cellular and non-cellular immune responses in the context of inflammatory processes. Future research should address the following questions: What is the exact role of C1q during age and neurodegeneration in the human brain? Is an increase of C1q triggering neurodegeneration or is it simply a consequence of other ongoing neurodegenerative processes? May C1q serve as a general marker for neurodegeneration or is there a difference between various forms of dementia? Can

C1q serve as a putative biomarker either by quantification in CSF alone or in conjunction with other complement markers or is it accessible in molecular neuroimaging studies, e.g., by positron emission tomography (PET)? May C1q even constitute a putative therapeutic target? In conclusion, C1q and the complement system will add new avenues to the already complicated puzzle underlying aging and neurodegenerative disorders such as Alzheimer's disease. ” (published in C. Rupprecht, R. Rupprecht, et al. (2021)).

### 4.3 Effects of xenon and isoflurane on brain C1q

Although anesthetics have become indispensable in contemporary medicine, their use must be carefully considered due to the possibility of inducing long-term changes in the molecular and cellular structure of the brain. As discussed in subsection 1.7.1, isoflurane and xenon exhibited neurotoxic effects on developing brains. However, in older brains afflicted with Alzheimer's disease, xenon has demonstrated neuroprotective properties (Lavaur et al. 2016), whereas isoflurane has shown neurotoxic features (Xie, Culley, et al. 2008) and amplified  $\beta$ -amyloid (Zhang et al. 2017; Xie, Dong, Maeda, R. D. Moir, et al. 2007) and tau pathology (Li et al. 2014; Dong, X. Wu, et al. 2012). Differences in molecular target structures may underlie these adverse effects. Xenon, acting as an NMDA antagonist, counters neurotoxic excitatory stress (Lavaur et al. 2016; Hecker and Rossaint 2001), whereas isoflurane, as a GABA agonist, exerts the opposite effect (Perucho, Rubio, et al. 2010).

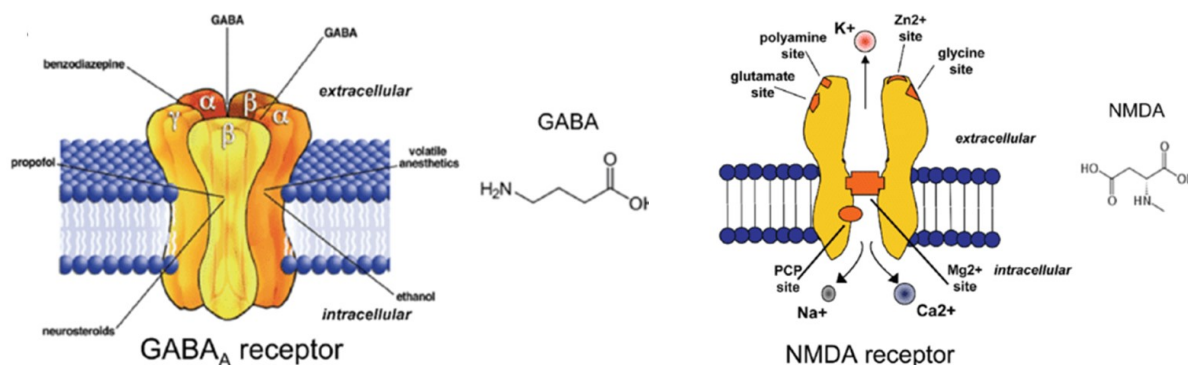


**Figure 4.1:** Molecular receptors for xenon and isoflurane (reproduced from Longone et al. 2011)

By quantifying C1q protein levels in living brain slices after exposing them to clinically relevant concentrations of xenon and isoflurane, we investigated the potential impact of these anesthetics on the inflammatory component of Alzheimer's disease. The findings of this investigation hold significance for the scientific community as they can help enhance our understanding of the underlying mechanisms of the disease and the possible contribution of anesthetics to its progression.

This thesis showed no significant changes in brain C1q levels following the application of isoflurane or xenon. However, the large standard deviations in our results suggest that our setup was only semiquantitative, which means that small but distinct changes might have been missed. Additionally, the lifespan of our brain sections was limited to a few hours, which

may have further limited the ability to detect potential changes in C1q levels over a longer period.

While our results suggest that isoflurane and xenon may not have immediate effects on C1q levels in the brain, it is important to acknowledge the experimental limitations of our study. Specifically, we can not exclude the possibility of a delayed effect due to the limited lifespan of our brain sections. Furthermore, we conducted our study in brain slices rather than living animals, which may have different physiological responses to anesthetics.

To gain a more comprehensive understanding of the potential effects of anesthetics on C1q levels in the brain, future studies should address these limitations by exploring the putative effects of anesthetics in living animals over a longer time frame, from a few hours up to a few days following anesthesia. If future studies could reveal that anesthetics indeed have a significant impact on C1q levels and subsequent inflammatory responses in the brain, this could have implications for the administration of anesthetics in patients with Alzheimer's disease or other neuroinflammatory conditions. As such, there is a pressing need for continued research to ensure that the use of anesthetics in clinical settings is optimized to minimize potential long-term risks.

In conclusion, we have developed a new experimental approach for investigating physiological and pathophysiological processes in living brain tissue. Using electrophysiological techniques, we created living brain slices that provide a valuable platform for studying the molecular mechanisms underlying various neurological conditions. Furthermore, this experimental setup allows for quantifying specific proteins and investigating rapid modulatory effects following the incubation with certain substances. However, the usefulness of these brain slices is limited by their relatively short life span, which is an important consideration when developing research questions related to pharmacology.

Despite these limitations, this approach can potentially reduce the number of laboratory animals used for specific research questions. Additionally, our free-floating approach provides a valuable tool for assessing the role of C1q and other proteins in the brain concerning health and disease. With further optimization and refinement, this experimental setup can help to explore the complex mechanisms underlying neurological disorders and provide valuable insights into potential treatments and therapies.



# A Supplementary Material

**Table A.1:** Software- and IT-Support

<b>Usage area</b>	<b>Software</b>
Image making	ZEN 3.0 blue edition by Carl Zeiss Microscopy GmbH
Image processing	ZEN 3.0 blue edition by Carl Zeiss Microscopy GmbH
Image analysis	ZEN 3.0 blue edition by Carl Zeiss Microscopy GmbH <a href="https://qupath.github.io">https://qupath.github.io</a> (licensed under GNU General Public License)
Statistical analysis	<a href="https://www.socscistatistics.com">https://www.socscistatistics.com</a> (copyright by Jeremy Stangroom) Excel by Microsoft cooperation
Graphics	Powerpoint by Microsoft cooperation Excel by Microsoft cooperation <a href="https://www.biorender.com/">https://www.biorender.com/</a> (copyright by 2023 Biorender)
Grammatics/ Language support	<a href="https://app.grammarly.com">https://app.grammarly.com</a> (copyright by 2023 Grammarly Inc.) <a href="https://chat.openai.com">https://chat.openai.com</a> (rights owned by Open Ai) Word by Microsoft cooperation
Layout and writing	<a href="https://sharelatex.tum.de">https://sharelatex.tum.de</a> (copyright by 2023 Overleaf)

**Figure A.1:** Georg thieme Verlag KG license terms and conditions

RightsLink Printable License <https://s100.copyright.com/CustomerAdmin/PLF.jsp?ref=c04c031f-e69...>

**GEORG THIEME VERLAG KG LICENSE  
TERMS AND CONDITIONS**

Jun 24, 2023

---

This Agreement between Christian Rupprecht ("You") and Georg Thieme Verlag KG ("Georg Thieme Verlag KG") consists of your license details and the terms and conditions provided by Georg Thieme Verlag KG and Copyright Clearance Center.

The publisher has provided special terms related to this request that can be found at the end of the Publisher's Terms and Conditions.

License Number	5571380957394
License date	Jun 17, 2023
Licensed Content Publisher	Georg Thieme Verlag KG
Licensed Content Publication	Pharmacopsychiatry
Licensed Content Title	Morphological Representation of C1q in the Aging Central Nervous System
Licensed Content Author	Christian Rupprecht, Rim S. J. Sarker, Gerhard Rammes
Licensed Content Date	Jan 1, 2022
Licensed Content Volume	55
Licensed Content Issue	04

1 von 6 24.06.2023, 09:37

Type of Use	Dissertation/Thesis
Requestor type	author of the original Thieme publication
Format	print and electronic
Portion	full article/document
Will you be translating?	no
Distribution quantity	5
Title	CIq staining in free-floating brain sections: Morphological appearance and effects of age, Alzheimer pathology and anaesthetics
Institution name	Technichal University Munich
Expected presentation date	Jan 2024
Portions	I would like to reuse the parts of figures, captions, result and discussion cited in my doctoral thesis
	<u>Christian Rupprecht</u> [REDACTED]
Requestor Location	[REDACTED] Germany Attn: Christian Rupprecht
Publisher Tax ID	DE 147638607
Billing Type	Invoice
Billing Address	<u>Christian Rupprecht</u> [REDACTED]

München, [REDACTED]  
Attn: Christian Rupprecht

Total 0.00 EUR

Terms and Conditions

### Terms and Conditions

#### Introduction

The publisher for this copyrighted material is **Georg Thieme Verlag KG**, in the following referred to as **Publisher**. By clicking "accept" in connection with completing this licensing transaction, you agree that the following terms and conditions apply to this transaction (along with the Billing and Payment terms and conditions established by Copyright Clearance Center, Inc. ("CCC"), at the time that you opened your CCC account and that are available at any time at <<http://myaccount.copyright.com>>).

#### Limited License

Publisher hereby grants to you a non-exclusive license to use this material. Licenses are for one-time use only with a maximum distribution equal to the number specified in the license. The first instance of republication or reuse granted by this license must be completed within 12 months of the date this license was granted (although copies prepared before the end date may be distributed thereafter).

**Any and all third party content is expressly excluded from this permission. If the figure/table you wish to reproduce is credited to a source other than the publication (i. e. third party material) you will need to obtain permission from that copyright holder before making any use of the material.**

Licences for reuse in a **dissertation/thesis** are limited to the depositary copies (non-profit and password-protected) that have to be delivered within the university system. Any further use and follow-up publications require separate permission.

**Dissertations/theses delivered in Germany:** permission may not be needed if reuse of the content is made in accordance with §60c UrhWissG ("<https://www.bmjv.de/SharedDocs/Gesetzgebungsverfahren/Dokumente/BGBI-UrhWissG.html?nn=6712350>"). If in doubt, please turn to [permission@thieme.de](mailto:permission@thieme.de)

If you are **the author requesting full use of your article** in an Institutional Repository, **be it**

**as a separate document or when your article is part of your thesis**, special rules apply.

For more detailed information, please check

(German version:)

<https://www.thieme.de/de/autorenounge/Autorenounge-Zeitschriftenautoren-Autorenrechte-95029.htm>

(English version:)

<https://www.thieme.de/de/autorenounge/artikel-teilen-107797.htm>

If you have identified yourself as a signatory to the **STM Permissions Guidelines**, permission is given according to the current version of these Guidelines (<https://www.stm-assoc.org/copyright-legal-affairs/permissions/permissions-guidelines/>).

If you are **publishing your work under an Open Access license**, it has to be made very clear next to the licensed content that the copyright stays with Publisher, and that any further reuse will need explicit permission from Publisher.

Any **photographs showing a recognizable person** cannot be licensed via RightsLink. For permission requests for any such photograph, please contact [permission@thieme.de](mailto:permission@thieme.de) directly.

#### **Geographic Rights: Scope**

Licenses may be exercised anywhere in the world.

**Any anatomical drawings by Karl Wesker or Markus Voll as contained in the Thieme Atlas of Anatomy** authored by Schuenke et al., Gilroy, or Baker, etc. cannot be licensed via RightsLink. For permission requests for any such figure, please contact [permission@thieme.de](mailto:permission@thieme.de) directly.

#### **Altering/Modifying Material: Not Permitted**

You may not alter or modify the material in any manner (except that you may use, within the scope of the license granted, one or more excerpts from the copyrighted material, provided that the process of excerpting does not alter the meaning of the material or in any way reflect negatively on the publisher or any writer of the material), nor may you translate the material into another language.

#### **Reservation of Rights**

Publisher reserves all rights not specifically granted in the combination of (i) the license details provided by you and accepted in the course of this licensing transaction, (ii) these terms and conditions and (iii) CCC's Billing and Payment terms and conditions.

#### **License Contingent on Payment**

While you may exercise the rights licensed immediately upon issuance of the license at the

end of the licensing process for the transaction, provided that you have disclosed complete and accurate details of your proposed use, no license is finally effective unless and until full payment is received from you (either by publisher or by CCC) as provided in CCC's Billing and Payment terms and conditions. If full payment is not received on a timely basis, then any license preliminarily granted shall be deemed automatically revoked and shall be void as if never granted. Further, in the event that you breach any of these terms and conditions or any of CCC's Billing and Payment terms and conditions, the license is automatically revoked and shall be void as if never granted. Use of materials as described in a revoked license, as well as any use of the materials beyond the scope of an unrevoked license, may constitute copyright infringement and publisher reserves the right to take any and all action to protect its copyright in the materials.

**Copyright Notice: Disclaimer**

Must include the following copyright and permission notice in connection with any reproduction of the licensed material: "© Georg Thieme Verlag KG."

**Warranties: None**

Publisher makes no representations or warranties with respect to the licensed material and adopts on its own behalf the limitations and disclaimers established by CCC on its behalf in its Billing and Payment terms and conditions for this licensing transaction.

**Indemnity**

You hereby indemnify and agree to hold harmless publisher and CCC, and their respective officers, directors, employees and agents, from and against any and all claims arising out of your use of the licensed material other than as specifically authorized pursuant to this license.

**No Transfer of License**

This license is personal to you, but may be assigned or transferred by you to a business associate (or to your employer) if you give prompt written notice of the assignment or transfer to the publisher. No such assignment or transfer shall relieve you of the obligation to pay the designated license fee on a timely basis (although payment by the identified assignee can fulfill your obligation).

**No Amendment Except in Writing**

This license may not be amended except in a writing signed by both parties (or, in the case of publisher, by CCC on publisher's behalf).

**Objection to Contrary Terms**

Publisher hereby objects to any terms contained in any purchase order, acknowledgment, check endorsement or other writing prepared by you, which terms are inconsistent with these terms and conditions or CCC's Billing and Payment terms and conditions. These terms and conditions, together with CCC's Billing and Payment terms and conditions (which are incorporated herein), comprise the entire agreement between you and publisher (and CCC) concerning this licensing transaction. In the event of any conflict between your obligations established by these terms and conditions and those established by CCC's Billing and Payment terms and conditions, these terms and conditions shall control.

**Jurisdiction:**

This license transaction shall be governed by and construed in accordance with the laws of the Federal Republic of Germany. You hereby agree to submit to the jurisdiction of the federal and state courts located in Berlin, Germany for purposes of resolving any disputes that may arise in connection with this licensing transaction.

**Special Terms:** This permission only applies for use in printed and electronic, password-protected form in the depository copies of your scientific work. If your thesis is made freely available on the internet via the University's server within the first 12 months after publication by the Thieme Group, the article's full text version has to be removed. 12 months after the article was first published by the Thieme Group, you may make the accepted manuscript version, i. e. the accepted WORD version, also used for print, without the Thieme layout, available on a non-commercial academic Institutional Repository under a CC-BY-NC-ND license. In this case, the article is to be used in the accepted and published WORD version without layout, while use of the final PDF version, and Thieme layout, is explicitly excluded.

(v1.8, Nov 2022)

**Questions?** [customercare@copyright.com](mailto:customercare@copyright.com).

---

---

<b>Prepublication</b>	<b>chapters</b>
Rupprecht, Christian, Rim S. J. Sarker, and Gerhard Rammes (2022). Morphological representation of C1q in the aging central nervous system. <i>Pharmacopsychiatry</i> 55: 203–210 (C. Rupprecht, Sarker, et al. 2022) (Reuse for doctoral thesis licensed under A.1)	1 Introduction 1.3 Morphology of C1q in the brain 2 Material and Methods 3.1 Morphology 4.1 Morphology
Rupprecht, Christian, Rainer Rupprecht, and Gerhard Rammes (2021). C1q, a small molecule with high impact on brain development: putative role for aging processes and the occurrence of Alzheimer’s disease. <i>European Archives of Psychiatry and Clinical Neuroscience</i> 271: 809–812 (C. Rupprecht, R. Rupprecht, et al. 2021) (Reuse for doctoral thesis licensed under "open access" publication)	1.4 Synaptic pruning via microglia 2 Material and Methods 3.2 The effect of age, Alzheimer’s disease and anesthetics on brain C1q 4.2 The influence of age and Alzheimer’s disease on C1q brain levels

**Table A.2:** Prepublication chapters

Prepublication	figures
<p>Rupprecht, Christian, Rim S. J. Sarker, and Gerhard Rammes (2022). Morphological representation of C1q in the aging central nervous system. <i>Pharmacopsychiatry</i> 55: 203–210 (C. Rupprecht, Sarker, et al. 2022) (Reuse for doctoral thesis licensed under A.1)</p>	<p>3.1B 3.2 3.3B 3.4 3.5 3.6 3.8 3.9 3.10 3.13B-D 3.14 3.17</p>
<p>Rupprecht, Christian, Rainer Rupprecht, and Gerhard Rammes (2021). C1q, a small molecule with high impact on brain development: putative role for aging processes and the occurrence of Alzheimer’s disease. <i>European Archives of Psychiatry and Clinical Neuroscience</i> 271: 809–812 (C. Rupprecht, R. Rupprecht, et al. 2021) (Reuse for doctoral thesis licensed under “open access” publication)</p>	<p>3.13A 3.15a 3.15b 3.16</p>

**Table A.3:** Prepublication figures



## B Publication

- 1.) **Rupprecht C**, Sarker RSJ, Rammes G (2022) Morphological representation of C1q in the aging central nervous system. *Pharmacopsychiatry* 55:203-210
- 2.) **Rupprecht C**, Rupprecht R, Rammes G (2021) C1q, a small molecule with high impact on brain development: putative role for aging processes and the occurrence of Alzheimer's disease. *Eur. Arch. Psychiatry Clin. Neurosci.* 271:809-812
- 3.) Rupprecht R, **Rupprecht C**, di Benedetto B, Rammes G (2022) Neuroinflammation and psychiatric disorders: relevance of C1q, translocator protein (18 kDa) (TSPO), and neurosteroids. *World J. Biol. Psychiatry* 23:257-263
- 4.) Rupprecht R, Pradhan AK, Kufner M, Brunner LM, Nothdurfter C, Wein S, Schwarzbach J, Puig X, **Rupprecht C**, Rammes G (2022) Neurosteroids and translocator protein 18 kDa (TSPO) in depression: implications for synaptic plasticity, cognition, and treatment options. *Eur. Arch. Psychiatry Clin. Neurosci.* 2022



## C Bibliography

- Afagh, A. et al. (1996). Localization and cell association of C1q in Alzheimer's disease brain. *Experimental Neurology* 138: 22–32.
- Banks, Paul, Nicholas P. Franks, and Robert Dickinson (2010). Competitive inhibition at the glycine site of the N-methyl-D-aspartate receptor mediates xenon neuroprotection against hypoxia-ischemia. *Anesthesiology* 112: 614–622.
- Benoit, Marie E., Michael X. Hernandez, et al. (2013). C1q-induced LRP1B and GPR6 proteins expressed early in Alzheimer disease mouse models, are essential for the C1q-mediated protection against amyloid- $\beta$  neurotoxicity. *Journal of Biological Chemistry* 288: 654–665.
- Benoit, Marie E. and Andrea J. Tenner (2011). Complement protein C1q-mediated neuroprotection is correlated with regulation of neuronal gene and microRNA expression. *Journal of Neuroscience* 31: 3459–3469.
- Bialas, Allison R. and Beth Stevens (2013). TGF- $\beta$  signaling regulates neuronal C1q expression and developmental synaptic refinement. *Nature Neuroscience* 16: 1773–1782.
- Brosnan, Heather and Philip E. Bickler (2013). Xenon neurotoxicity in rat hippocampal slice cultures is similar to isoflurane and sevoflurane. *Anesthesiology* 119: 335–344.
- Bürge, Martina et al. (2019). The anaesthetic xenon partially restores an amyloid beta-induced impairment in murine hippocampal synaptic plasticity. *Neuropharmacology* 151: 21–32.
- Cattano, Davide et al. (2008). Potential of xenon to induce or to protect against neuroapoptosis in the developing mouse brain. *Canadian Journal of Anaesthesia = Journal Canadien d'Anesthésie* 55: 429–436.
- Cattano, D. et al. (2011). Xenon exposure in the neonatal rat brain: effects on genes that regulate apoptosis. *Minerva Anestesiologica* 77: 571–578.
- Chung, Won-Suk, Nicola J. Allen, and Cagla Eroglu (2015). Astrocytes control synapse formation, function, and elimination. *Cold Spring Harbor Perspectives in Biology* 7:a020370.
- Chung, Won-Suk, Laura E. Clarke, et al. (2013). Astrocytes mediate synapse elimination through MEGF10 and MERTK pathways. *Nature* 504: 394–400.
- Dejanovic, Borislav et al. (2018). Changes in the synaptic proteome in tauopathy and rescue of tau-induced synapse loss by C1q antibodies. *Neuron* 100:1322–1336.e7.
- Diaz-Aparicio, Irune and Amanda Sierra (2019). C1q is related to microglial phagocytosis in the hippocampus in physiological conditions. *Matters*:e201904000013.

- DiMaggio, Charles, Lena S. Sun, and Guohua Li (2011). Early childhood exposure to anesthesia and risk of developmental and behavioral disorders in a sibling birth cohort. *Anesthesia and Analgesia* 113: 1143–1151.
- Dong, Yuanlin, Xu Wu, et al. (2012). Anesthetic isoflurane increases phosphorylated tau levels mediated by caspase activation and A $\beta$  generation. *PloS One* 7:e39386.
- Dong, Yuanlin, Zhipeng Xu, et al. (2011). RNA interference-mediated silencing of BACE and APP attenuates the isoflurane-induced caspase activation. *Medical Gas Research* 1: 5.
- Eckenhoff, Roderic G. et al. (2004). Inhaled anesthetic enhancement of amyloid-beta oligomerization and cytotoxicity. *Anesthesiology* 101: 703–709.
- Fan, Rong, Kelly DeFilippis, and William E. van Nostrand (2007). Induction of complement proteins in a mouse model for cerebral microvascular A beta deposition. *Journal of Neuroinflammation* 4: 22.
- Fonseca, Maria I., Shu-Hui Chu, Alisia M. Berci, et al. (2011). Contribution of complement activation pathways to neuropathology differs among mouse models of Alzheimer’s disease. *Journal of Neuroinflammation* 8: 4.
- Fonseca, Maria I., Shu-Hui Chu, Michael X. Hernandez, et al. (2017). Cell-specific deletion of C1qa identifies microglia as the dominant source of C1q in mouse brain. *Journal of Neuroinflammation* 14: 48.
- Györfy, Balázs A. et al. (2018). Local apoptotic-like mechanisms underlie complement-mediated synaptic pruning. *Proceedings of the National Academy of Sciences of the United States of America* 115: 6303–6308.
- Hammond, Jennetta W. et al. (2020). Complement-dependent synapse loss and microgliosis in a mouse model of multiple sclerosis. *Brain, Behavior, and Immunity* 87: 739–750.
- Harris, Katie et al. (2013). Neuroprotection against traumatic brain injury by xenon, but not argon, is mediated by inhibition at the N-methyl-D-aspartate receptor glycine site. *Anesthesiology* 119: 1137–1148.
- Haseneder, Rainer, Stephan Kratzer, Eberhard Kochs, Daniela Höfelmann, et al. (2009). The xenon-mediated antagonism against the NMDA receptor is non-selective for receptors containing either NR2A or NR2B subunits in the mouse amygdala. *European Journal of Pharmacology* 619: 33–37.
- Haseneder, Rainer, Stephan Kratzer, Eberhard Kochs, Corinna Mattusch, et al. (2009). Xenon attenuates excitatory synaptic transmission in the rodent prefrontal cortex and spinal cord dorsal horn. *Anesthesiology* 111: 1297–1307.
- Hashimoto, Tadafumi et al. (2020). Collagenous Alzheimer amyloid plaque component impacts on the compaction of amyloid- $\beta$  plaques. *Acta Neuropathologica Communications* 8: 212.
- Head, E. et al. (2001). Complement association with neurons and beta-amyloid deposition in the brains of aged individuals with Down Syndrome. *Neurobiology of Disease* 8: 252–265.

- Hecker, K., J. H. Baumert, et al. (2004). Xenon, a modern anaesthesia gas. *Minerva Anestesiologica* 70: 255–260.
- Hecker, K. and R. Rossaint (2001). Wirkmechanismen von Xenon und anderen volatilen Anästhetika. *Anesthesiologie, Intensivmedizin, Notfallmedizin, Schmerztherapie (AINS)* 36: 644–646.
- Henstridge, Christopher M., Bradley T. Hyman, and Tara L. Spires-Jones (2019). Beyond the neuron-cellular interactions early in Alzheimer disease pathogenesis. *Nature Reviews Neuroscience* 20: 94–108.
- Hofmann, Carolin et al. (2021). Inhalational anesthetics do not deteriorate amyloid- $\beta$ -derived pathophysiology in Alzheimer’s disease: investigations on the molecular, neuronal, and behavioral Level. *Journal of Alzheimer’s Disease* 84: 1193–1218.
- Hong, Soyon et al. (2016). Complement and microglia mediate early synapse loss in Alzheimer mouse models. *Science* 352: 712–716.
- Hosmer, David W., Stanley Lemeshow, and Rodney X. Sturdivant (2013). *Applied logistic regression*. Wiley series in probability and statistics. Hoboken, NJ: Wiley. 500.
- Iram, Tal et al. (2016). Megf10 Is a receptor for C1Q that mediates clearance of apoptotic cells by astrocytes. *Journal of Neuroscience* 36: 5185–5192.
- Istaphanous, George K. et al. (2013). Characterization and quantification of isoflurane-induced developmental apoptotic cell death in mouse cerebral cortex. *Anesthesia and Analgesia* 116: 845–854.
- Jiang, H. et al. (1994). Beta-Amyloid activates complement by binding to a specific region of the collagen-like domain of the C1q A chain. *Journal of Immunology* 152: 5050–5059.
- Jiang, Shanya and Kiran Bhaskar (2017). Dynamics of the complement, cytokine, and chemokine systems in the regulation of synaptic function and dysfunction relevant to Alzheimer’s disease. *Journal of Alzheimer’s Disease* 57: 1123–1135.
- Jin, Ming et al. (2011). Soluble amyloid beta-protein dimers isolated from Alzheimer cortex directly induce Tau hyperphosphorylation and neuritic degeneration. *Proceedings of the National Academy of Sciences of the United States of America* 108: 5819–5824.
- Kawai, Shintaro, Erkin Kurganov, and Seiji Miyata (2020). Transient increase of microglial C1q expression in the circumventricular organs of adult mouse during LPS-induced inflammation. *Cell Biochemistry and Function* 38: 392–400.
- Kishore, Uday et al. (2004). C1q and tumor necrosis factor superfamily: modularity and versatility. *Trends in Immunology* 25: 551–561.
- Knobloch, Marlen et al. (2007). Intracellular A $\beta$  and cognitive deficits precede beta-amyloid deposition in transgenic arcA $\beta$  mice. *Neurobiology of Aging* 28: 1297–1306.
- Lavaur, J. et al. (2016). Neuroprotective and neurorestorative potential of xenon. *Cell Death & Disease* 7:e2182.
- Lesné, Sylvain et al. (2005). NMDA receptor activation inhibits alpha-secretase and promotes neuronal amyloid-beta production. *Journal of Neuroscience* 25: 9367–9377.

- Li, Changsheng et al. (2014). The role of hippocampal tau protein phosphorylation in isoflurane-induced cognitive dysfunction in transgenic APP695 mice. *Anesthesia and Analgesia* 119: 413–419.
- Liang, Ge et al. (2010). Isoflurane causes greater neurodegeneration than an equivalent exposure of sevoflurane in the developing brain of neonatal mice. *Anesthesiology* 112: 1325–1334.
- Liang, Min, Fatin Ahmad, and Robert Dickinson (2022). Neuroprotection by the noble gases argon and xenon as treatments for acquired brain injury: a preclinical systematic review and meta-analysis. *British Journal of Anaesthesia* 129: 200–218.
- Liu, Jinping et al. (2019). The Role of NMDA Receptors in Alzheimer’s Disease. *Frontiers in Neuroscience* 13: 43.
- Longone, Patrizia et al. (2011). Neurosteroids as neuromodulators in the treatment of anxiety disorders. *Frontiers in Endocrinology* 2: 55.
- Loopuijt, L. D. and W. J. Schmidt (1998). The role of NMDA receptors in the slow neuronal degeneration of Parkinson’s disease. *Amino Acids* 14: 17–23.
- Lopez, Manuel E., Andres D. Klein, and Matthew P. Scott (2012). Complement is dispensable for neurodegeneration in Niemann-Pick disease type C. *Journal of Neuroinflammation* 9: 216.
- Luchena, Celia et al. (2018). Contribution of neurons and glial cells to complement-mediated synapse removal during development, aging and in Alzheimer’s disease. *Mediators of Inflammation* 2018: 2530414.
- Ma, Daqing et al. (2007). Xenon mitigates isoflurane-induced neuronal apoptosis in the developing rodent brain. *Anesthesiology* 106: 746–753.
- Mandrekar, Jayawant N. (2010). Receiver operating characteristic curve in diagnostic test assessment. *Journal of Thoracic Oncology* 5: 1315–1316.
- Matsuoka, Yasuji et al. (2001). Inflammatory responses to amyloidosis in a transgenic mouse model of Alzheimer’s disease. *American Journal of Pathology* 158: 1345–1354.
- Morgan, B. Paul (2018). Complement in the pathogenesis of Alzheimer’s disease. *Seminars in Immunopathology* 40: 113–124.
- Murphy, Kathy L. and Mark G. Baxter (2013). Long-term effects of neonatal single or multiple isoflurane exposures on spatial memory in rats. *Frontiers in Neurology* 4: 87.
- Naito, Atsuhiko T. et al. (2012). Complement C1q activates canonical Wnt signaling and promotes aging-related phenotypes. *Cell* 149: 1298–1313.
- Paolicelli, Rosa Chiara, Kanchan Bisht, and Marie-Ève Tremblay (2014). Fractalkine regulation of microglial physiology and consequences on the brain and behavior. *Frontiers in Cellular Neuroscience* 8: 129.
- Paolicelli, Rosa C. et al. (2011). Synaptic pruning by microglia is necessary for normal brain development. *Science* 333: 1456–1458.

- Park, Seong Ho, Jin Mo Goo, and Chan-Hee Jo (2004). Receiver operating characteristic (ROC) curve: practical review for radiologists. *Korean Journal of Radiology* 5: 11–18.
- Perucho, Juan, Maria J. Casarejos, et al. (2012). Trehalose protects from aggravation of amyloid pathology induced by isoflurane anesthesia in APP(swe) mutant mice. *Current Alzheimer Research* 9: 334–343.
- Perucho, Juan, Isabel Rubio, et al. (2010). Anesthesia with isoflurane increases amyloid pathology in mice models of Alzheimer’s disease. *Journal of Alzheimer’s Disease* 19: 1245–1257.
- Petanjek, Zdravko et al. (2011). Extraordinary neoteny of synaptic spines in the human prefrontal cortex. *Proceedings of the National Academy of Sciences of the United States of America* 108: 13281–13286.
- Pisalyaput, Karntipa and Andrea J. Tenner (2008). Complement component C1q inhibits beta-amyloid- and serum amyloid P-induced neurotoxicity via caspase- and calpain-independent mechanisms. *Journal of Neurochemistry* 104: 696–707.
- Presumey, Jessy, Allison R. Bialas, and Michael C. Carroll (2017). Complement system in neural synapse elimination in development and disease. *Advances in Immunology* 135: 53–79.
- Rainer Radtke (2019). Anzahl der Operationen vollstationärer Patienten in deutschen Krankenhäusern nach Altersgruppe im Jahr 2018. Ed. by Statistika. URL: <https://de.statista.com/statistik/daten/studie/29220/umfrage/krankenhaeuser-operationen-vollstationaerer-patienten/>.
- Reichwald, Julia et al. (2009). Expression of complement system components during aging and amyloid deposition in APP transgenic mice. *Journal of Neuroinflammation* 6: 35.
- Rodríguez, J. J. et al. (2009). Astroglia in dementia and Alzheimer’s disease. *Cell Death and Differentiation* 16: 378–385.
- Rohn, Troy T. (2013). The triggering receptor expressed on myeloid cells 2: ”TREM-ming” the inflammatory component associated with Alzheimer’s disease. *Oxidative Medicine and Cellular Longevity* 2013: 860959.
- Rupprecht, Christian, Rainer Rupprecht, and Gerhard Rammes (2021). C1q, a small molecule with high impact on brain development: putative role for aging processes and the occurrence of Alzheimer’s disease. *European Archives of Psychiatry and Clinical Neuroscience* 271: 809–812.
- Rupprecht, Christian, Rim S. J. Sarker, and Gerhard Rammes (2022). Morphological representation of C1q in the aging central nervous system. *Pharmacopsychiatry* 55: 203–210.
- Rupprecht, Tobias A. et al. (2007). Complement C1q and C3 are critical for the innate immune response to *Streptococcus pneumoniae* in the central nervous system. *Journal of Immunology* 178: 1861–1869.
- Sall, Jeffrey W. et al. (2009). Isoflurane inhibits growth but does not cause cell death in hippocampal neural precursor cells grown in culture. *Anesthesiology* 110: 826–833.

- Schafer, Dorothy P. et al. (2012). Microglia sculpt postnatal neural circuits in an activity and complement-dependent manner. *Neuron* 74: 691–705.
- Schäfer, M. K. et al. (2000). Complement C1q is dramatically up-regulated in brain microglia in response to transient global cerebral ischemia. *Journal of Immunology* 164: 5446–5452.
- Shi, Dai et al. (2023). The anaesthetics isoflurane and xenon reverse the synaptotoxic effects of A $\beta$ 1–42 on Megf10-dependent astrocytic synapse elimination and spine density in ex vivo hippocampal brain slices. *International Journal of Molecular Sciences* 24.
- Sim, Robert B. et al. (2007). C1q binding and complement activation by prions and amyloids. *Immunobiology* 212: 355–362.
- Sjöberg, Andreas P. et al. (2008). Native, amyloid fibrils and beta-oligomers of the C-terminal domain of human prion protein display differential activation of complement and bind C1q, factor H and C4b-binding protein directly. *Molecular Immunology* 45: 3213–3221.
- Stages of Alzheimer’s (2019). URL: <https://www.alz.org/alzheimers-dementia/stages> (visited on 10/22/2019).
- Stephan, Alexander H. et al. (2013). A dramatic increase of C1q protein in the CNS during normal aging. *Journal of Neuroscience* 33: 13460–13474.
- Stevens, Beth et al. (2007). The classical complement cascade mediates CNS synapse elimination. *Cell* 131: 1164–1178.
- Tacnet-Delorme, P., S. Chevallier, and G. J. Arlaud (2001). Beta-amyloid fibrils activate the C1 complex of complement under physiological conditions: evidence for a binding site for A beta on the C1q globular regions. *Journal of Immunology* 167: 6374–6381.
- Tao, Guorong et al. (2016). Isoflurane is more deleterious to developing brain than desflurane: The role of the Akt/GSK3 $\beta$  signaling pathway. *BioMed Research International* 2016: 7919640.
- Thielens, Nicole M. et al. (2017). C1q: A fresh look upon an old molecule. *Molecular Immunology* 89: 73–83.
- Tooyama, I. et al. (2001). Correlation of the expression level of C1q mRNA and the number of C1q-positive plaques in the Alzheimer Disease temporal cortex. analysis of C1q mrna and its protein using adjacent or nearby sections. *Dementia and Geriatric Cognitive Disorders* 12: 237–242.
- Vishal, Sharma, Aggarwal Sourabh, and Singh Harkirat (2011). Alois Alzheimer (1864-1915) and the Alzheimer syndrome. *Journal of Medical Biography* 19: 32–33.
- Wang, Zhi-Cong, Jie Zhao, and Shao Li (2013). Dysregulation of synaptic and extrasynaptic N-methyl-D-aspartate receptors induced by amyloid- $\beta$ . *Neuroscience Bulletin* 29: 752–760.
- Wei, Huafeng et al. (2005). Isoflurane and sevoflurane affect cell survival and BCL-2/BAX ratio differently. *Brain Research* 1037: 139–147.
- Wilder, Robert T. et al. (2009). Early exposure to anesthesia and learning disabilities in a population-based birth cohort. *Anesthesiology* 110: 796–804.

- Wolf, Yochai et al. (2013). Microglia, seen from the CX3CR1 angle. *Frontiers in Cellular Neuroscience* 7: 26.
- Wu, Tiffany et al. (2019). Complement C3 is activated in human AD brain and is required for neurodegeneration in mouse models of amyloidosis and tauopathy. *Cell Reports* 28:2111–2123.e6.
- Xie, Zhongcong, Deborah J. Culley, et al. (2008). The common inhalation anesthetic isoflurane induces caspase activation and increases amyloid beta-protein level in vivo. *Annals of Neurology* 64: 618–627.
- Xie, Zhongcong, Yuanlin Dong, Uta Maeda, Robert D. Moir, et al. (2007). The inhalation anesthetic isoflurane induces a vicious cycle of apoptosis and amyloid beta-protein accumulation. *Journal of Neuroscience* 27: 1247–1254.
- Xie, Zhongcong, Yuanlin Dong, Uta Maeda, Robert Moir, et al. (2006). Isoflurane-induced apoptosis: a potential pathogenic link between delirium and dementia. *Journal of Gerontology. Series A, Biological Sciences and Medical Sciences* 61: 1300–1306.
- Xie, Zhongcong and Zhipeng Xu (2013). General anesthetics and  $\beta$ -amyloid protein. *Progress in Neuropsychopharmacology & Biological Psychiatry* 47: 140–146.
- Zabel, Matthew K. and Wolff M. Kirsch (2013). From development to dysfunction: microglia and the complement cascade in CNS homeostasis. *Ageing Research Reviews* 12: 749–756.
- Zeiss microscopy, ed. (2020). Zeiss microscopy: Axio Observer.Z1. URL: <https://www.microshop.zeiss.com/en/no/system/axio+observer-axio+observer.z1-inverted+microscopes/10023/#variants> (visited on 09/20/2020).
- Zhang, Shuai et al. (2017). Isoflurane anesthesia promotes cognitive impairment by inducing expression of  $\beta$ -amyloid protein-related factors in the hippocampus of aged rats. *PloS One* 12:e0175654.
- Zhao, Xuli et al. (2013). Dual effects of isoflurane on proliferation, differentiation, and survival in human neuroprogenitor cells. *Anesthesiology* 118: 537–549.

